







Review

Zeolites: A Theoretical and Practical Approach with Uses in (Bio)Chemical Processes

Arthur Abinader Vasconcelos ^{1,*}, Thomas Len ^{2,*}, Alex de Nazaré de Oliveira ³, Ana Alice Farias da Costa ⁴, Allan Rodrigo da Silva Souza ⁴, Carlos Emmerson Ferreira da Costa ⁴, Rafael Luque ^{5,6}, Geraldo Narciso da Rocha Filho ⁴, Renata Coelho Rodrigues Noronha ⁷, and Luís Adriano Santos do Nascimento ^{1,4,*}

¹ Post-Graduation Program in Biotechnology, Federal University of Pará, Augusto Corrêa Street, Guamá 66075-110, PA, Brazil

² Department of Organic Chemistry, Universidad de Córdoba, Ctra Nnal IV-A, Km 396, 14014 Córdoba, Spain

³ Biocatalysis and Applied Organic Synthesis Group, Chemistry Course, Campus Marco Zero do Ecuador, Rodovia Josmar Chaves Pinto Km 02, Jardim Marco Zero, Federal University of Amapá, Macapá 68903-419, AP, Brazil

⁴ Post-Graduation Program in Chemistry, Federal University of Pará, Augusto Corrêa Street, Guamá 66075-110, PA, Brazil

⁵ Center for Molecular Design and Modern Organic Chemistry, Peoples Friendship University of Russia (RUDN University), 6 Miklukho Maklaya Str., 117198 Moscow, Russia

⁶ Departamento de Química Organica, Universidad ECOTEC, Km 13.5 Samborondón, Samborondón EC0922302, Ecuador

⁷ Laboratório de Citogenética, Centro de Estudos Avançados da Biodiversidade, Institute of Biological Sciences, Federal University of Pará, Augusto Corrêa Street, Guamá, Belém 66075-110, PA, Brazil

* Correspondence: arthurnadervas@yahoo.com.br (A.A.V.); qo2lelet@uco.es (T.L.); adriansantos@ufpa.br (L.A.S.d.N.)



Citation: Vasconcelos, A.A.; Len, T.; de Oliveira, A.d.N.; Costa, A.A.F.d.; Souza, A.R.d.S.; Costa, C.E.F.d.; Luque, R.; Rocha Filho, G.N.d.; Noronha, R.C.R.; Nascimento, L.A.S.d. Zeolites: A Theoretical and Practical Approach with Uses in (Bio)Chemical Processes. *Appl. Sci.* **2023**, *13*, 1897. <https://doi.org/10.3390/app13031897>

Received: 18 December 2022

Revised: 24 January 2023

Accepted: 26 January 2023

Published: 1 February 2023



Copyright: © 2023 by the authors. Licensee MDPI, Basel, Switzerland. This article is an open access article distributed under the terms and conditions of the Creative Commons Attribution (CC BY) license (<https://creativecommons.org/licenses/by/4.0/>).

Abstract: This review provides a state-of-the-art summary of distributed zeolite technology, as well as identifying strategies to further promote the absorption of these materials in various areas of study. Zeolites are materials that can be synthesized or found in natural rock deposits with a basic composition consisting in Al, Si, and O. Zeolite's consideration as a future material is due to many facile synthesis methods to obtain different structures with variations in pore size, surface area, pore volume and physical properties. These methods are developed using the control of relevant synthesis parameters that influences structure formation, such as crystallization temperature, time of aging and/or crystallization, stoichiometric relationships between components of synthesis gel, pH of the medium, and in some cases the type of structure-directing agent. Each method will lead to geometric changes in the framework formation, making possible the formation of typical chemical bonds that are the fingerprint of any zeolitic structure (O-Si-O and Al-O-Si), forming typical acid sites that give specificity in zeolite and allows it to act as a nanoreactor. The specificity is a characteristic that in some cases depends on selectivity, a fundamental property derived of the porosity, mostly in processes that occur inside the zeolite. In processes outside the structure, the surface area is the main factor influencing this property. Moreover, there are many natural sources with adequate chemical composition to be used as precursors. Some of these sources are waste, minimizing the deposition of potential hazardous materials that can be recalcitrant pollutants depending on the environment. Besides its uses as a catalyst, zeolite serves as a support for many bioprocesses; therefore, this review aims to explain relevant aspects in chemical nature, physical properties, main methods of synthesis, main precursors used for synthesis, and relevant applications of zeolites in chemical catalysis and biological processes.

Keywords: zeolite; synthesis; catalysis; biological applications

1. Introduction

Zeolites are products marketed in many countries, including China, India, South Korea, United States and Japan. These nations are leaders in shipments for zeolite exportation according to the website of Volza Grow Global. Shipments from China had reached 6360 as of November 2022, followed by India (4127) and South Korea (2852). The USA had 2861 shipments, while Japan had 1165. In monetary data, according to the website Expert Market Research, the market size of zeolites reached almost USD3.8 billion in 2020 and is expected to have a compound annual growth rate (CAGR) of 5.5%, reaching almost USD5.2 billion by 2026.

Zeolite's structure comprises a tridimensional framework, with atoms arranged in a tetrahedral geometric form. The general formula is TO_4 , where T atoms are a metal, bridged by oxygen atoms (O). The performance and properties of this material are determined by structural studies of pore volume, pore size, channel dimensionality and extra-framework species. The traditional chemical composition is similar to a typical aluminosilicate structure, where Al, Si and O are the main components. However, high or pure silica-based structures were recently synthesized. The Si atom may be changed (isomorphically substituted) by a heteroatom, likely Ge, B, Ga, Be, or P, to tune zeolite function. The charge is balanced by the presence of exchangeable extra-framework cations. There are several topologies available, varying in pore diameter, being small, medium, or large, pore systems with 1D, 2D, or 3D channels, and the presence of internal cages where compounds may react or be entrapped [1,2]. Some metal nanoparticles can be encapsulated in these channels as shown in Figure 1, according to [2].

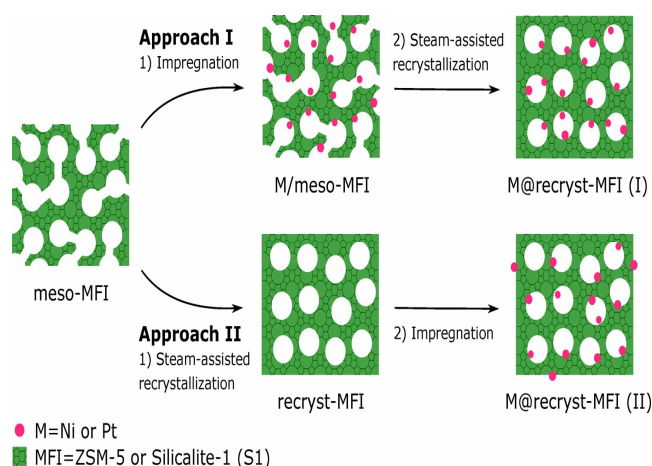


Figure 1. Metal nanoparticles encapsulated in MFI structure. Reproduced from [2]. Copyright ACS 2019.

Since a rise of interest in the 70s, the great necessity of zeolite's use, either in industry or in laboratories, led to the creation of new structures year after year. In this scenario, different structures were produced with the same framework but different names, synthesis conditions and chemical composition. The database of zeolite structures was created by the International Zeolite Association (IZA), with 248 known topologies up to 2020. In this amount, twenty different types are natural zeolites [3]. These structures are firstly identified by their pore size and dimensionality. In terms of pore size classification, the channel classification is determined by the number of T atoms delimiting the smallest pore opening, being small (8 T atoms ring), medium (10 T atoms ring) and large (12 T atoms ring) [1]. The zeolites may be classified according to their pore size, where those with diameter less than 2 nm are microporous. If the diameter is between 2 and 50 nm, the structure is mesoporous, and up to 50 nm it is classified as macroporous. The presence of mesopores could be beneficial to the catalyst lifetime (reducing the coke formation) and for the mass transmission [4]. The pore size of the structure determines how fast and efficient the physicochemical process is. Obviously, bulky molecules can enter the porous

structure only if the molecular size is smaller than the pore size. Increasing the molecular size or reducing the pore size would slow the diffusion rate until its total inefficiency. The molecular diffusion rate within the zeolite might be less than the Knudsen diffusion. Kim et al. [5] showed how pore size is important in characterization of mesoporous materials from silicate waste.

There are many applications of mesoporous ordered zeolites, for instance, for the adsorption of As (V) [6], the cracking of oil to produce liquid hydrocarbon fuel [7], for the valorization of agro-industrial waste [8], and the immobilization of enzymes for biocatalytic processes. For this purpose and an environmentally friendly production process, zeolite synthesis can be performed using wastes from different industrial sectors. Rice husk, electronic waste, fly coal ash and clay minerals such as smectite, sepiolite, kaolin, palygorskite, attapulgite, vermiculite and so on were all successfully applied to the synthesis of a wide variety of zeolitic materials. Other possibilities to be explored is the production of zeolite nanofibers [9].

Kaolin waste is a white material with a brown surface and a chemical composition of kaolinite ($\text{Al}_2\text{Si}_2\text{O}_5(\text{OH})_4$). Its theoretical composition is 46% silica (SiO_2), 39% alumina (Al_2O_3) and 14% water. Although the deposited and crystallographic properties are highly dependent on the source of extraction, one of the main configurations of kaolinite crystals is perfectly pseudohexagonal phases, but this can also occur in other phases, such as triclinic, pseudomonoclinic and polymorphic. The variation of Al amount from raw material allow the exploration of structures ranging its acidity [10]. The exploitation of kaolin generates a waste that—if not destined for an application—can cause great environmental damage, especially to water entities. In this context, there is the generation of two types of tailings, some rich in quartz and others formed by coarse kaolinite particles, occupying basins in large areas and with low toxicity, allowing their reuse as Longhi et al. [11] explored in production of geopolymers. During the transformation of raw kaolin into a commercial product, the first tailings are generated using high-iron-content kaolin obtained from mine exploration.

Coal ash has been used in obtaining molecular zeolitic sieves due to the existing environmental appeal for the reduction in deposits of this residue in the world. As an example, India reached 90 million tons generated annually and 65,000 acres of land are occupied as deposits. The ashes are composed of inorganic oxides from coal combustion, mainly SiO_2 and Al_2O_3 , varying infinitely with the nature of the coal used. These materials have a composition similar to volcanic rocks. The Na-A zeolite was produced from this raw material [12]. The synthesis process of zeolitic structures from this precursor is similar to the natural process of formation of it from volcanic rocks. The ashes, which are rich in aluminosilicate, become zeolites naturally, due to the influence of the percolation of water present in the environment, which can be converted into analcime and feldspar. This process can last from ten to a thousand years under natural conditions. The potential of volcanic ashes for zeolite synthesis is helpful to reduce contamination of environment [13].

Clays of natural origin, such as perlite and diatomite, have been used to obtain zeolitic structures such as A, X, HS, ZSM-5, ofretite and mordenite. This process has the drawback of a low degree of purity with respect to the structure obtained from pure reagents. For example, the presence of transition metal impurities in natural precursor can precipitate it heterogeneously in alkaline conditions [14]. The mineral clay precursors form the group of phyllosilicates, which are distinguished from lamellar structures, formed by tetrahedra of SiO_4 units linked to octahedral units of Al, Mg or Fe (O, OH). The formation of zeolitic structures using natural clays, such as chabasite and phyllipsite, was reported in experiments carried out at 175 °C. The incorporation of heteroatoms such as Mg and Fe as reported is another possible way to produce metal heteroatom-containing molecular sieves [15].

The zeolitic material synthesized from silica aluminous residue has great use as an adsorbent of cations such as Ni^{+2} , Cu^{+2} , Cd^{+2} , Pb^{+2} , Zn^{+2} , Ba^{+2} etc. This residue can be generated from the extraction of lithium from the mineral spodumene [16], oil shale

ash [17] and paper sludge ash [18]. Recently, there has been an appeal to minimize waste, so those that contain a large amount of Si and Al represent a low-cost alternative for obtaining catalytic materials. The use of slag from glass production, generated from the pyrometallurgical process, stands out notably due to its proportion of Si and Al as well as Ca and Mg. On the other hand, electric arc furnace slag has a more variable composition of silica and alumina e.g. the by-product from Ti extraction that generates the Ti-bearing electric arc furnace slag [19].

The formation of mesoporous zeolite structures may be accompanied by the development of microporous ones that make the diffusion of molecules into the structure difficult. At this point, new strategies for synthesis are proposed, such as leaching treatments by acid or alkali, dry-gel conversion for the transformation of amorphous mesoporous silica into zeolite and hard-template-directed synthesis. Some template methods offer crystalline and ordered zeolite structure with narrow pore sizes. Alternatively, the use of a mixture of templates can be applied, where two or more macromolecules are used to direct the structure's formation. In this process, the structure may be bulky with amorphous mesoporous material formed. An improvement is the use of organosilane and functionalized polymers that influence the crystal growth. Besides these experimental remarks, a computational screening is an approach that Blatov et al. [20] suggest to help the new zeolite developments.

The ordered mesoporous structure is a type of hierarchical zeolite structure that may be synthesized by a bottom-up method. This method occurs with the crystallization of aluminosilicate gel with the aid of mesoporous templates generating mesoporous channels. The mesoporous templates might be then removed by calcination. While the use of these substances is important to define the size and shape of mesoporous channels, their decomposition generates greenhouse gases at high temperatures. The green synthesis process may be classified into methods without template molecules or recyclable and renewable templates; methods using sustainable silicon or aluminum sources; solvent-free methods; and facile methods, such as the use of microwave to reduce the time of crystallization [21]. Figure 2 shows a template synthesis mechanism according with Li et al. [22].

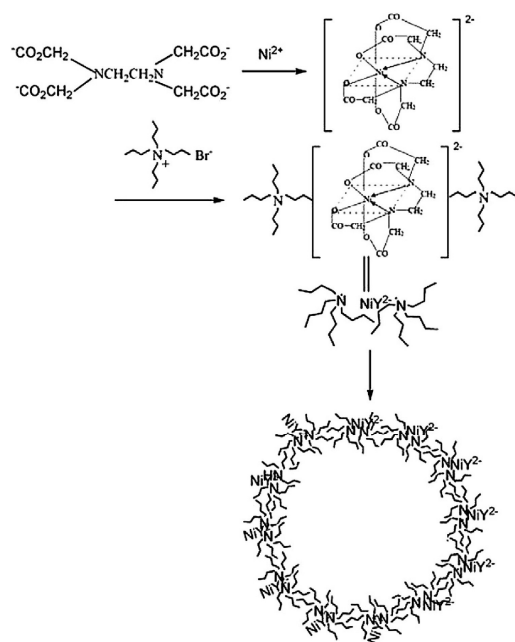


Figure 2. Template synthesis mechanism of zeolite Ni-MFI. Reproduced from [22]. Copyright Elsevier 2009.

The introduction of mesopores in zeolites makes the diffusion of bulky molecules inside their channels easier and decreases the intracrystalline diffusion length. The synthesis of mesoporous zeolites is adequate to obtain ultrafine structure not trespassing less than

100 nm of size. Postsynthesis treatments such as steaming, acid/base leaching and chemical treatment are eco-unfriendly and produce mesopores without good definition. Some other improved methods for mesoporous zeolite synthesis were proposed, including the aggregation of a metal in the structure, e.g., inimpregnation of Nb, Ta and Pd form a zeolite encapsulation system [23] and in incorporation of iron forming Fe-ZSM-5 zeolite [24]. Other methods are microwave-assisted single-surfactant templating [25] and pseudomorphic transformation [26]. A synthesis strategy using silica-carbon composites obtained by pyrolysis of carbonaceous gases in the presence of silica-gel was also described as useful for mesoporous zeolite production [27]. There are many possibilities of synthesis methods to obtain different zeolites structures with applications focusing on environmental protection, such as the removal of dyes, heavy metals, and other recalcitrant pollutants. The removal of greenhouse gases and catalytic reactions are other applications found in zeolite research. Figure 3 shows relevant publications involving zeolite synthesis and applications.

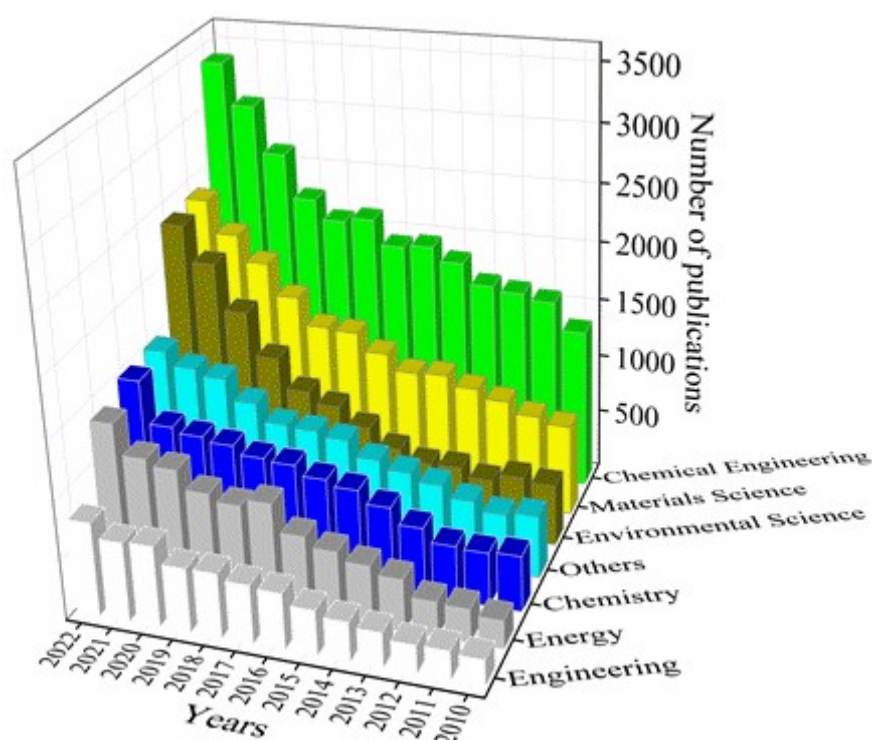


Figure 3. Evolution of the number of publications on zeolites obtained from the Web of Science database from 2010 to 2022.

This review aimed to explore the main aspects for the synthesis of zeolites, exploring factors such as the chemical nature of precursor, the chemical and physical properties of zeolites, the main precursor used for synthesis and the different applications in chemical processes, biochemical processes and the relevance of the material for environmental protection.

2. Zeolites

2.1. Remarks about Chemical Composition

Zeolites are crystalline solids with the general formula $M_2/nO, Al_2O_3, zSiO_2$, where “n” is the valence of the metal “M.” In these crystalline polymers composed of TO_4 tetrahedra (T = Al or Si), the stoichiometric ratio “z” can vary from 2 to infinity. According to Loewenstein’s rule, Al-O-Al bonds are not allowed in aluminosilicates, and thus an important parameter for obtaining a zeolitic structure is the Si/Al ratio [28]. The modification of chemical composition in zeolites lead to different properties, such as pore volume, channel dimensionality and framework density (FD). In framework composition, the Si/Al ratio is the main parameter that brings an identity for a particular structure: there are those

with high silica content ($\text{Si}/\text{Al} > 12$), e.g., the MFI structure ZSM-5 [29], intermediate Si/Al ratio between 1.2 and 3.0 [30], and same proportion of alumina and silica ($\text{Si}/\text{Al} = 1.0$), e.g., zeolite A [31]. The framework composition has an indirect effect on framework structure; therefore, zeolites with high silica content are rich in five-ring types [32]. Besides the framework chemical species, the extra-framework species are important for physicochemical properties such as ion-exchange capacity, catalytic selectivity, and adsorption.

The extra-framework species formation studied in the postsynthesis process called dealumination is generally used to obtain high-silica structures such as USY. The consequences of this process include changes in Si/Al ratio, structure, acidity, selectivity, reactivity and coking behavior for a certain catalytic reaction. Citric acid is one of the chemicals used to remove Al from zeolite [33]. The process of dealumination may increase the acidity by many factors, among which are revealing catalytic Lewis acid activity, stabilization of negative charge on the lattice after the removal of protons, and the synergism of Lewis and Brønsted acid sites due their proximity [34]. Some studies proved that the impact of EFAL (extra-framework aluminum) species on the effective size of supercage voids resulted in the confinement and stabilization of transition states [35,36].

The extra-framework cations (EFC) are Lewis acids, influencing the chemical and optical properties of adsorbing molecules as well as generating a strong electric field in comparison to the presence of protons (Brønsted acids). It is important to know the location and acidity of these extra-framework cations for a rational modification of acidity from zeolites. The acidity of these species can be evaluated through their interaction with a weak basic molecule such as CO. Effectively, its adsorption depends on the size of zeolite pore and channel, the zeolite topology, the cation size, and the Si/Al ratio [37]. The EFC influences the activity of aluminum extra-framework, and the Na^+ may influence the activation barrier of conversion reaction between the AlOH^{+2} and $\text{Al}(\text{OH})_2^+$ that are formed in the process of dealumination and are extra-framework aluminum species, together with Al^{+3} , AlOOH , $\text{Al}(\text{OH})_3$ and AlO^+ [35–38]. The increase and decrease in activation are a function of Na^+ coordination and the presence of other ions such as K^+ and Ca^{+2} , which are important for energy configuration of zeolite structure [34–39]. Another extra-framework cation is La^{+3} , present in structures such as zeolite L and may be hidden, altering ion exchange and thermodynamic properties [40]. Figure 4 shows the topology and location of extra-framework sites.

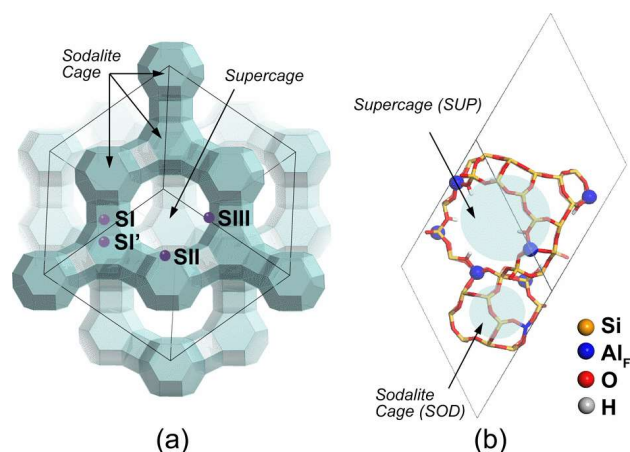


Figure 4. (a) Typical topology of faujasite zeolite and location of extra-framework aluminum active sites (S); (b) rhombohedral faujasite studied by [35]. Reproduced from [35]. Copyright 2015 ACS.

In the crystal structure of zeolite, Al^{3+} ions together with Si^{4+} arranged in tetrahedrons may generate an excess of negative unit charge. This charge can be compensated by Na^+ ions. The number of cations inside the structure is equal to the number of alumina units. The Na^+ ions can be partially replaced by protons (H^+) establishing between the Al-O-Si bonds, and thus the zeolitic structure can be configured as a large polyacid structure. In

that case, zeolite acts as a proton donor or a Brønsted acid at these sites. The acidic strength of a zeolitic structure depends on the amount of Al atoms present as well as the particular environment in which the proton is located. The acidity of media is important in the process of photooxidation of dyes and pollutants such as chlorophenols. The empirical rule describes it as possessing high acidity, with high formation of OH ionic radicals. In this process, the formation of molecular oxygen is a key factor for hydroxy and perhydroxy radicals [23] (p. 5). Studies report that some heteroatoms, such as Fe^{3+} , incorporated with different valences in zeolite structure may reduce the organic compound's oxidative capacity [24] (p. 5). The media acidity may be responsible for the increase in activity of materials [25] (p. 5). The presence of Al^{3+} cations is related to how intensive the acidity of the zeolite structure is, and depending on the media, it may have the behavior of a Brønsted acid site in the presence of water or may behave as a Lewis acid site in anhydrous conditions. Costa et al. [25] (p. 5) explored acid aspects of zeolite structures. In some cases, this property of zeolitic structure must be reduced. For this purpose, several methods are applied, such as modification with phosphorous, alkali treatment and exchange between alkali and metal. In this scenario, the dealumination is included in destructive methods together with desilication [26] (p. 5).

2.2. Isomorphic Substitution

According to Pang et al. [14] (p. 3), the presence of heteroatoms in an aluminosilicate framework increases material performance in catalysis, ionic exchange, and adsorption. The grafting of material with cation and anion modification has shown good catalytic activity due to better accessibility of its active sites. Xia and Mokaya [41] performed anion modification using NH_3 , bringing a partial substitution of oxygen atoms by nitrogen, at high temperatures, forming a web of oxynitrates and transforming the material in a basic catalyst. In general, the Al and Si atoms present in the zeolite structure can undergo an isomorphic substitution, i.e., replace another cation of similar size, by other tri- or tetravalent elements. As examples, the incorporation of Ge in thomsonite and the addition of Ga in zeolite A and faujasite can be mentioned. The incorporation of B makes possible the generation of a material with weak acid strength. Ti can be incorporated into an MFI structure, generating TS-1 zeolite. Isomorphic substitution has the likely function of stabilizing the secondary building units (SBUs), favoring the crystallization of zeolites, but making it difficult to obtain an aluminosilicate system. With this, there is the possibility of obtaining zeolites with low framework density, that is, the number of atoms in tetrahedral geometry per 1000 Å. Thus, the structures can have a high volume of micropores if the framework has a large number of three- and four-ring members, resulting in a structure with less stability than those with five- and six-membered rings. Moreover, the presence of specific heteroatoms can stabilize the three- and four-membered rings [42].

The formation of an SBU structure with four-membered double rings (D4R) can occur with the presence of Ge during the formation of zeolite. In this case, the insertion of more than three metal atoms can stabilize the D4R units, as the formation of a small mean angle of the Ge-O-Ge bond occurs, making the structure energetically stable [43]. The concentration of heteroatoms may be a parameter to measure the selectivity of a zeolitic material for a proposed catalytic conversion, such as in methanol to olefin reaction [10] (p. 3). In some studies, heteroatoms changing with Si and Al in the structure may cause the production of a large-pore framework, conferring dynamic flexibility in framework and enhancing the molecular diffusion in zeolite. It should be noted that the substitution of heteroatoms requires a charge compensation with extra-framework cations [44]. The amount and location of heteroatoms incorporated impact the chemical and physical properties [45]. The heteroatoms may be distributed in a zeolite framework to different degrees, as a full order or as a random order. Some computational studies have been done on heteroatom distribution and limitations in zeolites with high Si/Al ratio or small differences in energy for configurations [46]. While with high differences in energy configurations, the thermo-

dynamic factors will determine the distribution of heteroatoms and zeolite frameworks, a small difference leads to heteroatom distribution determined by synthetic conditions [47].

The isomorphic substitution of Si^{4+} atoms for trivalent cations such as Ga^{3+} , Fe^{3+} and B^{3+} changes the acid strength of a structure. The deprotonation energy (DPE) is the parameter that estimates the material strength [48]. As heteroatoms in structure may alter one of the main properties from zeolite (acid strength), the insertion of heteroatoms may increase the functionality of zeolites in a catalytic approach. Bian et al. [49] presented a new zeolite synthesis methodology called interlayer expansion reaction that may be made with insertion of heteroatoms such as Fe as Sn, generating materials with catalysis activity. Besides these metal species, Zn and Co may be used for this purpose.

In other works, in these molecular sieve structures called metal heteroatom-containing aluminophosphate occurs the incorporation of divalent heteroatoms, such as ions Mg^{+2} , Mn^{+2} , Zn^{+2} and Co^{+2} , which leads to Brønsted and Lewis acid sites after removal of the template, while the trivalent ions Co^{+3} and Mn^{+3} create redox sites [50]. The substitution of Al or P in AlPO by a heteroatom forms a MAPO structure. Among 201 zeotype structures, 48 are based on this composition [51], presenting a wide range of pore openings from six-ring to eighteen-ring and dimensionality from one- to three-dimensional. According to Li et al. [15] (p. 4) and Pang et al. [14] (p. 3), species incorporated include +1 valence (Li), +2 (Be, Mg, Ca, Zn, Mn, Fe, Co, Ni, Cu, Cd, Sr), +3 (Cr, Co, Fe, Ga, Mo), +4 (Ge, Ti, Sn, Zr, V), and +5 (As, V, Nb). There are three types of isomorphic substitution in AlPO framework: substitution of Al site, substitution of P site, and substitution of Al and P pairs. The first type is simple and occurs when heteroatoms with +1, +2 and +3 valences remove Al and form M-O-P bonds. The substitution of species with +4 and +5 valences is more complex and may involve one of these three types [15] (p. 4). The methodologies used for incorporation of heteroatoms are direct synthesis, postsynthesis, and improved direct synthesis [14] (p. 3). Figure 5 shows a structure with heteroatoms.

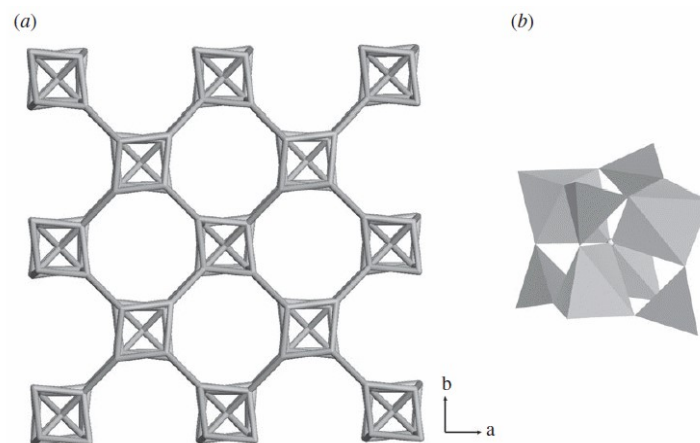


Figure 5. (a) Eight-ring channels in FeAPO-CJ66 structure along the [001] direction; (b) D4R unit from “Fe(Al)₄P₄.” Reproduced from [15]. Copyright 2012 The Royal Society.

2.3. Tetrahedral Geometry TO_4

The number of T atoms in zeolite framework has a crucial impact on many properties and different applications. This value is calculated by a quantity called framework density (FD), which lies qualitatively between low-density zeolites when the structure has 10 T-atoms per 1000 Å, e.g., CLO, IRR, ITV, IRR and IRY-type structures, up to 20–21 T-atoms per 1000 Å for high-density zeolites, e.g., CZP, JNP, PSI, VET and AEN-type zeolites [52]. Framework density is useful to distinguish zeolites from dense tectosilicates [53]. The characterization of structure based on FD exists as a numerical criterion called coordination sequences (CSs), a parameter that considers the number of neighboring T-atoms interconnected. In this way, a typical zeolite framework has four T-atoms connected to every single T-atom and each one has a maximum of three atoms connected to them. This

parameter is considered a fingerprint for zeolite structure, independently of unit cell and crystallographic symmetry and useful to identify and classify the zeolite framework. The FD is directly related to pore size in material: as a rule, wide-pore-size zeolites have low FD. Therefore, the formation of this structure is possible if average ring size on the surface is as close to four as possible, and so the presence of small rings on the structure determines the low FD value [54]. The distribution of FD in a structure is a function of the distribution of the smallest ring in the structure. Dense framework examples besides zeolites are the minerals quartz, cristobalite, petalite, feldspar, milarite, banalsite and scapolite. The size of the smallest ring is generally four-ring for a tetrahedral structure. Other structures have minimum sizes of rings of three and five [52] (p. 9). The FD may have some effects on properties in structures similar to silica-X structure: the high FD (about 22.0 T/1000 Å) renders negative thermal expansion and good ability to adsorb chemicals [55]. The variation in topological quantities rather than geometric quantities of a structure are responsible for variation in FD [56]. The FD may be related to enthalpy frameworks related to geometry in structure [57].

2.4. Physical Properties

Knowledge of zeolite properties is important in understanding the performance of the material, which depends on the dimension of its channels, the accessibility of pore volume, the diameter of the pore opening, and the number and location of extra-network species, that is, located outside the structure. Currently, the composition of zeolites has been replaced by heteroatoms, such as those with high silica content. The electronic structure of the component elements tends to affect the role of the counterions in counterbalancing the charges in the elementary mesh. For example, Al, which concentrates high electronic density, can be compensated by exchangeable extra-network cations [58].

The dimensionality in the zeolite structure is important to determine the ease of mobility of the reacting or adsorbed molecules in the pores, giving the molecular sieve character to the structure. Structures can be one-dimensional, two-dimensional, and three-dimensional, and the greater the dimensionality, the better the molecular mobility within the structure. Thus, it can also be an indication of the ease of deactivating the structure [59]. The International Union of Pure and Applied Chemistry determines the nomenclature of zeolites using three letters, regardless of chemical composition, and also determines that according to the size of the pores, they can be classified as small (<4 Å), medium (from 4 Å to 6 Å), large (from 6 Å to 8 Å), and super large (>8 Å) [53]. According to the pore size, a determined number of T-atoms define the smallest pore opening, channels delimited by 8 rings are small, 10 rings are medium and 12 rings are large, and an elevated number of ring members gives an extralarge pore opening. The rings may be distorted depending on the symmetry and T-atoms surrounding them. Moreover, the channel system is defined by channel directions relative to crystallographic axes [42] (p. 8).

Certain physicochemical properties may be achieved by structural and chemical modification, preserving the layer integrity. Among these properties, the increasing of surface area to ease molecular diffusion, transport, and access of substrates in active sites could be achieved with techniques such as swelling and pillaring. Many methods have been proposed for postsynthesis modification of interlamellar space in 2D zeolites. Among them are detemplation by thermal combustion and chemical extraction, intercalation into interlamellar space, delamination/exfoliation, and colloidal suspensions. The main property upgraded in modification of 2D zeolites is the increase in sorption capacities by the increasing of external surface area and presence of auxiliary mesoporosity [60]. Some examples that demonstrate the best values of external surface area may be unilamellar MFI (BET 710 m²·g⁻¹) and MIT-1 (BET 513 m²·g⁻¹). It is important to note the creation of mesopores influencing access to acid sites on the layer surface or inside micropores. The external surface has a high concentration of silanol groups in these conditions, bringing good hydrophilic interactions [54] (p. 9). The layered zeolites are 2D structures with silanol groups linked to each other with hydrogen bonding, making possible ionic/covalent

bonding between template molecules present in the interlayer space. In these structures, crystal growth in a third direction is constrained. An outstanding physical property of this structure is that the constructing layers is highly plastic [61,62].

The stacking mode of layers in postsynthesized materials has a great impact on the accessibility of layers [63]. In one of the most important zeolite structures for catalytic purposes (MFI), the layers may have the template as an integral part, so detemplation is crucial for further transformations of structure. In addition, the interlayer spacing is less visualized than other structures because of a lack of interlayer reflections. Layer thickness ranges from 1 to 1.5-unit cells, and layers isolated by exfoliation have a thickness of 3.5 nm or 1.5 unit cells. Some structures may be produced by bifunctional MFI templates, multilayered and monolayered, i.e., reaching the ideal increasing of interlayer spaces and accessibility [64]. One of the advantages in physical modification of layered zeolites in comparison to conventional unmodified zeolites is the accessibility of bulky molecules in micropores. In this way, the 2D structures increase the selectivity and reduce coke formation, making the access of reagents to active sites easier. These materials are hierarchical, i.e., they combine the microporosity with intracrystalline mesoporosity of pillared, self-pillared, and delaminated exfoliated forms. A parameter that quantifies the volume of micropores versus the surface area of mesopores is the hierarchical factor (HF), and 2D layer structures have large HF values, meaning mesopore surfaces are large and do not affect micropore volume [65]. The absence of Na^+ causes the formation of unilamellar nanosheets [66]. The delamination of a pillared structure allows it to incorporate different active sites and separate them at a controlled distance, leading to material with hydrothermal stability, typical of inorganic solids. The disordered characteristics of these materials do not mean that its structure is amorphous [67]. The profile of adsorption of 2D zeolites is more complex than 3D zeolites, and only fragments of adsorbate are incorporated with micropores [68].

Among the physical properties of great importance is adsorption. The adsorption process involves the fixation by a physical or chemical interaction of a solute in an interface of different natures. However, in zeolites, the process occurs between liquid–solid or gas–solid interfaces. In this process, the solute is selectively dispersed in the zeolitic material. The amount of solute capable of adsorbing on zeolite is small and in general demands high internal area per unit volume. Two types of adsorption phenomena are known, physical adsorption or physisorption, which involves van der Waals forces, and delaying chemisorption, which involves chemical bond formation. Exploration of these phenomena has shown great applicability in the processes of removal of pollutants from aqueous effluents or gases present in the atmosphere [69]. The textural properties are important in evaluating the capacity to undertake the adsorption process, and several methods may be used to determine the textural properties of zeolites, such as pore volume, surface area, and pore size. The ability of molecules to penetrate the pores at a certain speed helps in determining the pore size of the structure.

To obtain a precise value, it is important that the measurement temperature is close to the reaction process temperature [69]. The molecules must be inert during the process, so the use of unsaturated molecules such as olefins, which can isomerize or oligomerize on the surface of acidic zeolites, must be avoided. For interpretation of pore openings, Lennard-Jones kinetic diameters are usually used [69]. The presence of impurities in zeolite is one of the causes of decreased performance in terms of textural properties, allowing better adsorption. Postsynthesis base, acid, and hydrothermal treatments are performed to remove impurities. Some of these treatments use acids and remove the Al content, varying the acidity of material. Others uses a basic treatment to remove Si by hydrolysis in the presence of OH^- ions, altering specific surface area and pore size and generating mesoporosity for easy access of molecules and improving the adsorption capacity [70].

Al content may influence textural properties directly. The BET surface area and the micropore volume are parameters that translate this relationship. In some cases, the higher the Al content, the better the textural features that are reached, improving the performance of adsorbents. In the adsorption process, the time to reach the equilibrium and the amount

of adsorbate as the selectivity depends on textural features too. The great loss of micropores accompanied by mesopore formation may be seen at high levels of dealumination [71,72]. The use of different structure-directing agents (SDAs), such as ethylene glycol, pyrrolidine, isopropylamine, and N,N-dimethylformamide, may alter the microporous area of zeolitic structures, external areas, and micropore volume [73]. The incorporation of rare-earth elements in zeolite structures is a method of improving such properties as the acidity and catalytic activity. Differences in porosity may occur according to the loading of metal applied, allowing the formation of ink bottle-type pores, i.e., a change in the nature of pores depending on the balance between the number of acid sites and the rare-earth metal site requires a facile interaction between zeolite and metal. This implies that at lower rare-earth metal loading, a small number of acid sites are sufficient for this interaction and vice versa [74]. The cation exchange capacity (CEC) may increase with micropore texture, depending on total surface area, including external area. A molecule of ethylene glycol monoethyl ether may be used as adsorbate to verify the relationship of with CEC. The temperature influences on its adsorption in micropores and the CEC depends on the size of cations used in the exchange [75]. While zeolites may present textural properties with bottom qualities, MOFs present organic molecules as linkers in an inorganic framework [76].

2.5. Ion Exchange Process

The ion exchange process is established between a solid material and a fluid phase acting as the solvent. In the process, the exchange between fluid- and solid-phase ions occurs and vice versa. During this phenomenon, the ions are exchanged with other ions of the same nature of charge. In other words, positive ions exchange positive ions and negative ions exchange negative ions. The ion exchanger is linked to functional groups of different charges, for example, cation exchange resins usually have sulfonic groups attached to their structure. Less frequently, these groups can be carboxylic, phosphonic, phosphinic or others. Anionic resins, on the other hand, involve quaternary ammonium groups or amino groups [42] (p. 8). The ion exchange capacity of the structure is a function of the composition of the solid and fluid phases, as well as the concentration of the solution in which it is found. The exchange takes place between two or more phases, with the ions moving from one phase to the other and bonding relatively strongly. The quantity of ions exchangeable by the structure depends on the so-called ion exchange capacity, a property measured in meq/g. This process depends on the electroneutrality of the medium and the ion concentration in both phases [42] (p. 8). The capacity is related to the presence of extra-network cations, located in channels. In each type of zeolite structure, there is a cation capable of being exchanged, but this capacity depends on its position in the network and on the binding energy. The ion exchange can be complete or partial, and ions capable of being exchanged need to be compatible with the pore size and specific hydrophilic character [77].

An alternative method to facilitate the ion exchange of the structure is to carry out solid-state ion exchange [78]. In this process, the zeolitic structure is mixed with a salt containing the exchangeable cation. This mixture takes place in a solid medium and is followed by thermal dehydration. This method offers the following advantages: there is no need to handle large volumes of saline solutions; there is no disposal of the solution in the environment after the process; and the process is not limited by the solvation sphere of the exchangeable cation [79]. Zeolitic structures have great ion exchange capacity due to their thermal stability, stability to ionizing radiation and high adaptability to the environment, as they have no toxicity on it. Thus, these are ideal structures for catalytic processes, competing with ion exchange resins used in water purification. Much of the ion exchanging property of zeolites is due to the nature of their surface, with high reactivity and the presence of micropores [69] (p. 11). The porous structure of zeolites allows the incorporation of water and cations due to adjusted diameters through inlet ports in internal structure. The proportion of Na, K and Ca is higher than Mg, Ba, Sr, among others, since they are exchangeable with species aggressive to the environment, such as copper, cadmium, ammonium, and some radioactive species. CEC and selectivity are specific

according to the nature of zeolite [80], and the number of exchangeable positions and the Si/Al ratio are other factors involved.

The induction of an electric field using an electrokinetic system allows verification of the dependence of copper ions in the framework on the geometry, cavity dimensions, structural properties, and cation positions. The medium resistance for ions mobility is crucial in this process, the dynamic condition leading to as high a capture efficiency of metallic ions in zeolite as the concentration of H^+ in medium [81]. Some structures, such as Linde type and Na-P1 type, are strongly pH-dependent, even under weak acidity variation [82]. The CEC is the most important parameter to verify the zeolitization process, e.g., the use of some raw materials in agglomerate form may release some ions useless from a CEC perspective, leading to a decrease in yield of zeolite formation [83]. The main method for CEC determination uses an NH_4NO_3 solution following a determination of exchangeable NH_4^+ by Nessler's method using colorimetry. However, the use of NH_4^+ as exchanging agent is not useful for industrial application and may be underestimated, due its incapacity to remove some ions from the structure.

The ion exchange property of zeolites has been explored for inhibition of biofilm formation that is responsible for producing acids that generate secondary caries. In this scenario, EMT zeolites presenting silver ion exchange have been used for the inhibition of metabolism and growth of biofilm from *Streptococcus mutans*, *Streptococcus gordonii*, and *Streptococcus sanguinis*. Biofilm CFU was also revealed as an anti-caries material [83]. Another relevant application of ion exchange capacity from zeolites in odontology is in production of dental implants, where titanium substrates have been modified with Ca^{+2} -exchanged nanosized EMT zeolites, improving some undesirable characteristics of classic Ti implants, such as poor osteointegration leading to long treatment and implant failure [84]. The chemical and physical modification of structure may cause modification in cation exchange rates: in general, chemical modification generates higher cation exchange rates than physical modification. Chemical activation is achieved by acid washing the surface of the material, removing the impurities, and making the zeolite pore surface wider. Instead, the physical activation (modification) occurs by heating [85,86]. The synthesis parameters that may affect CEC are reaction temperature, liquid/solid ratio, NaOH concentration and reaction time. Its value may increase with temperature and the concentration of an alkali activator, affecting zeolite formation. The influence of CEC in open window size and pore structures has been verified in other types of structures, such as RHO, LTA, and FAU [87]. The increase in liquid/solid ratio following the increased CEC is justified for the improvement of zeolite formation. The same is observed in increased CEC with reaction time, related to the increase in zeolite content in the medium [88]. Some zeolites, such as chabazite, stilbite, and heulandite, have the capacity to adsorb radioactive metallic species such as ^{137}Cs . Correlating this property with the CEC, the differences in values are related to a multistep adsorption process [89]. Figure 6 shows an experiment developed to study the cation exchange capacity of a zeolite with an electrochemical approach.

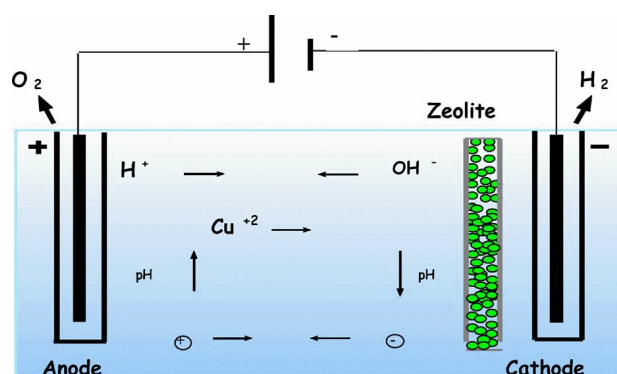


Figure 6. Ion Cu^{2+} migration under electric field toward electrodes and zeolite slice to trap them. Reproduced from [81]. Copyright 2006 Elsevier.

2.6. Crystallinity of Zeolites

The crystalline structure of zeolites is a remarkable characteristic of their properties, depending on the mechanisms involved in the crystallization process. The process of crystallization occurs in two steps: nucleation of discrete particles of the new phase and growth of zeolite crystals. In the nucleation stage, small particles called crystal nuclei represent a new crystalline phase formed. Crystal growth is depicted by the crystallization curve, which shows the process from gel diffusion to equilibrate composition, followed by nucleation and polymerization, and finally crystal growth [90]. However, the synthesis temperature and the time of reaction have great influence in zeolite crystallization, due to the metastable nature of material [91]. Other important factors are the purity and reactivity of raw materials (precursors), agitation of the system, order of mixing, and aging [92]. The initial mixtures have gel-like viscosity because of the amorphous aluminosilicate gel particles suspended in the basic medium [93].

The temperature is directly related to the contact time in synthesis and therefore with degree of crystallization for interconversion between zeolitic phases, e.g., zeolite A to S. The formation of a given zeolite depends on solubility at a certain temperature and equilibrium between the liquid phase and gel [94]. Changes in zeolite structure occur depending on reaction time, since, e.g., the sodalite may be formed in 2–3 h at boiling temperature, while being transformed into zeolite A after 9 h [95]. Figure 7 shows the influence of temperature in a constant time of 2 h in zeolite crystallinity to obtain NaA zeolite, based on [91].

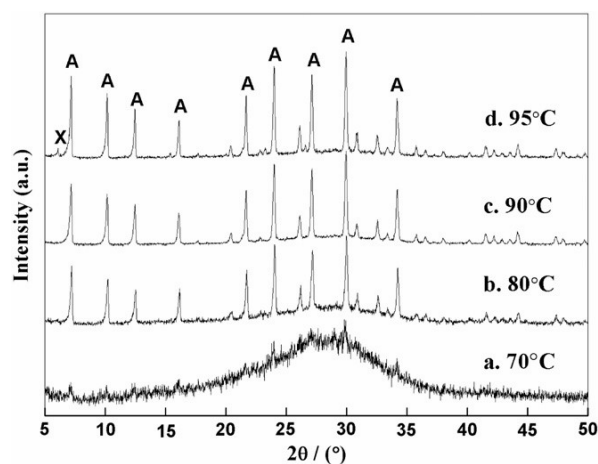


Figure 7. XRD patterns of products synthesized at different crystallization temperatures. Reproduced from [91]. Copyright 2013 Elsevier.

The maximum degree of crystallinity may be controlled with H_2O/Na_2O ratio, which is very dependent on the solution's pH and strongly influences the kinetics of structure formation [96]. Studies show that the precipitation of zeolite from the mother solution is increased with high alkalinity and is the first step of crystallization; therefore, pH is an important parameter for this goal [97]. The Si/Al ratio in some cases may influence induction time less [98], defined as the time that the gel precursors are forming and rearranging to make viable the crystal growth from the nuclei, i.e., this is a step before the crystallization [42] (p. 8).

The aging time has a great influence on the growth process and alters the crystal size, affecting also the appearance of another phase, such as in synthesis of Y-type zeolite, where the aging time of 72 h is enough to generate a zeolite P phase. The average crystal diameter may be changed by prolonged aging and crystallization times. The agglomeration of small crystals formed in a synthesis is dependent on the Al_2O_3 content and the alkalinity, that is, the small crystals formed in low alumina content may agglomerate significantly, as the alkalinity of the mixture is high. As the Al_2O_3 increases, the crystal size and reaction time decreases; therefore, the Al provides a site of nucleation and so the nucleation

accelerates with increase in alumina content. The elevated alkalinity values make difficult the incorporation of tetrahedrally coordinated Si in the framework because of the high solubility in this condition [99]. This can change the Si/Al ratio in the crystallized material and even affect performance during its application.

The Si/Al ratio is a fundamental parameter to determine thermal and acid stability, and affects both the crystallization behavior and application performance. The alkalinity may generate a structure of low density, with value above 0.82, and the aluminosilicate layers tend to aggregate, forming another phase. The reduction in OH⁻ concentration in the synthesis medium leads to lower monotonic zeolite growth and crystallinity [100]. Studies have shown that the amount of synthetic powder and water content in synthetic powder increases the crystallization rate, and the amount of NaOH may change the morphology as well [101,102]. The use of a structure-directing agent represents a change in topology of crystals by the use of an organic molecule that modifies bond lengths and bond angles [103].

2.7. Mechanical Properties

The mechanical properties of porous materials are another relevant issue in physical properties of zeolites, together with adsorption properties [104], as evident in such phenomena as clay swelling [105], breathing of structures [106], adsorption-induced phase transitions [107], pressure-induced amorphization, or hydration [108]. Microporous zeolites may have a great relationship between adsorption and mechanical properties, allowing one to focus on the effect from adsorbates on compressibility of the crystalline phase and reversible pressure-induced amorphization [109]. The presence of organic molecules on the framework generates an MOF structure, which is a porous material too. The framework exhibits a transition between two distinct regions of near-linear compressibility, being incompressible at low pressure before compressing rapidly beyond a threshold pressure. In this process, change in space group symmetry does not occur [110]. The pressure-induced amorphization is a phenomenon where a material may be amorphized reversibly under pressure, returning to its original crystalline structure and orientation when pressure decreases [111]. The presence of nondeformable units is essential for this reversibility, acting as a template and restoring the original structure [112].

X-ray diffraction is the main method of gaining evidence of a change in structure crystallinity, showing the formation of a high-density amorphous phase. Synchrotron X-ray diffraction has been applied for this purpose. An FT-IR study of stretching modes on a zeolite framework found a shift of bands to high energy values with increasing pressure. The occurrence of T-O asymmetric stretching mode is evidence that the crystallinity of zeolite decreases as the pressure is increased. The vibrational mode related to the double four-membered rings (D4R) may become very weak with the increased pressure being able to disappear, indicating that the structure is amorphous [113]. The decrease in pressure may bring back the D4R band, showing the reversibility of the process. The mechanical stresses and strains are critical to reach practical implementation. Good stiffness and robustness are important in retaining structural integrity under high-pressure environments, e.g., in sorption applications. Excessive structural distortion and framework collapse may be averted. The stiffness and hardness properties are important in ZIF structures, i.e., a zeolitic imidazolate framework, and they have influence in sterically bulky imidazolate-type linkages [114]. The elastic properties, measured by elastic constants, may be elucidated by computational tools such as DFT (density functional theory), which gives a better understanding of the origin of the elastic anisotropy. The stiffness may also influence bond distances and angles [115].

The elastic modulus of zeolitic and other porous materials is the measure of the material's resistance to elastic deformation: if its value is low, the material stretches a lot and vice versa. This parameter was measured to confirm a relationship with the topology, which may play a bigger role in elastic response [116]. The topology, pore geometry, and size define the mechanical strength, where the pore shapes (cubic, cylindrical, spherical, tetrahedral, and octahedral) contribute to structural performance under load [117]. Some

mechanical properties of dense polymorphs of silica are important for sodalite, chabazite and mordenite structures. These properties may be described by an elastic tensor using Hooke's law [118]. In these structures, the cohesive energies are almost independent of structure and the important variation in Si-O-Si angle distribution has a great influence [119]. According to Astala et al. [118], the bulk modulus, i.e., the pressure required to cause a unit change in volume, is dependent on network constraints and space group symmetry. Some zeolites may present an auxetic property, i.e., having a behavior similar to auxetic polymers, getting fatter when stretched and thinner when compressed. This physical property has importance in application of these materials on such catalytic processes as pelletization or extrusion steps [120]. Figure 8 shows a molecular perspective of mordenite's four-ring behavior when it is compressed [118].

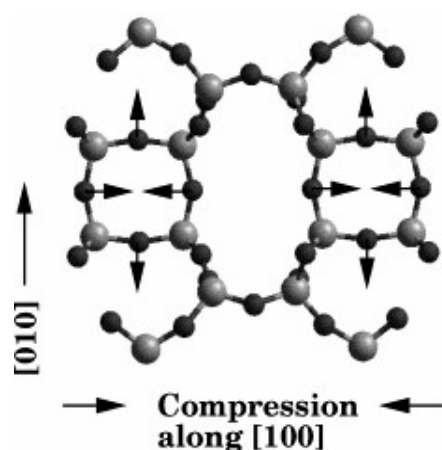


Figure 8. Pattern of relaxation process in compression of mordenite along [100] axis. Reproduced from [118]. Copyright 2004 ACS.

2.8. Thermal Conductivity

The thermal conductivity of zeolites is a key factor controlling the transport of energy. Measuring this property in a dense bulk zeolite is difficult because of little sinterability. For measures done on zeolite resin composites, the heat capacity reflected the relative density, suggesting that the pores have an influence on the heat capacity [121]. Other parameters to take into consideration are the thermal diffusivity and thermal conductivity, which may be slightly influenced by porosity. Thermal diffusivity is the capacity to conduct thermal energy relative to capacity to store energy by the material. High values of this parameter mean that heat transfers rapidly, increasing with decreasing temperature [122]. Negative thermal expansion is a phenomenon in the zeolitic framework related to the prevalence of low-frequency acoustic modes of vibrations being the major contributor to thermal conductivity. A measurement of this parameter is a way to separate contributions of different vibrational modes, providing a microscopic insight into thermal properties of framework silicates [123]. The removal of crystalline powder may be performed to determine thermal conductivity based on three principal contributors: heat transfer through the gas, radioactive heat transfer, and conduction through the solid sample. Thermal conductivity has relevance in zeolites also, because it uses a catalytic reaction where chemical reactions release heat either inside the structure or at surfaces due to adsorption of molecules [124].

Some authors used a computational technique called nonequilibrium molecular dynamics (NEMD), an approach to thermal conductivity determination inducing a thermal gradient by moving kinetic energy between different parts of the simulation box. Verifying the thermal gradient is a path to ascertain thermal conductivity in materials [125]. This property allows the use of zeolites as electric insulators, with a low dielectric constant and transporting heat away from electric components [126]. The high-silica zeolites satisfy the conditions for this characteristic. The direction of the crystallographic axis in the zeolite

framework is another factor relevant for thermal conductivity. In some cases, as in FER zeolites, the property is three times higher in the z-direction than in the x-direction. Moreover, the high framework density in general is related to high conductivity.

Thermal stability of zeolites is an important parameter to understand in which range of temperature the structure maintains its properties. It is important to verify if the temperature is near or beyond the point of dehydration and does not significantly affect the degree of structural order. In terms of this aspect, the geometry of the crystal lattice plays a large part in stability [127]. For this purpose, Castro et al. [128] screened thermal stability using DRX. An FAU structure was subjected to different temperatures—200 °C, 400 °C, and 600 °C—which did not change the diffraction peak pattern at 2θ : 10.11 (220), 23.58 (533), or 31.31 (751). The collapse of structure occurs at 800 °C, elevating at 850 and 880 °C, the formation of nepheline and mullite phases is observed, and the higher the silica content, the higher the thermal stability. Although this relationship exists, the Si/Al ratio is not the only parameter that determines stability. The degree of structural order (crystallinity) of the zeolites is another characteristic, depending on the synthesis conditions. The morphology may also change according to temperature. The capacity of a zeolite to be stable at high temperatures considering changes in its structure during the process has great relevance in applications of these structures in pyrolysis processes, e.g., the use of ZSM-5 for fast pyrolysis of cellulosic and algal biomass to phenolic and aromatic hydrocarbons [129]. In narrow temperature variations, such as 50 to 100 °C, some structures may show an altered crystalline system, e.g., a reversible phase transition from monoclinic to orthorhombic in all MFI zeolites, well reported in several works [130,131]. These transitions depend on the elemental composition, defect density, and nature/amount of adsorbed molecules, and small changes in siloxane bond angles and distances are associated with this process. The structure may show a continuous negative volume expansion due to the slight volume reduction with increasing temperatures in the range of 100–300 °C. In high temperatures between 1000 and 1200 °C the zeolitic structure becomes amorphous silica–alumina, occurring because of the abandonment of Al atoms from its tetrahedral sites by dehydroxylation, collapsing the crystal structure. However, according to studies, in intermediate temperatures (300–1000 °C) the changes are related to the calcination process [126]. Figure 9 shows the percentage of Brønsted acid sites remaining with heating, determined by different analysis methods [132].

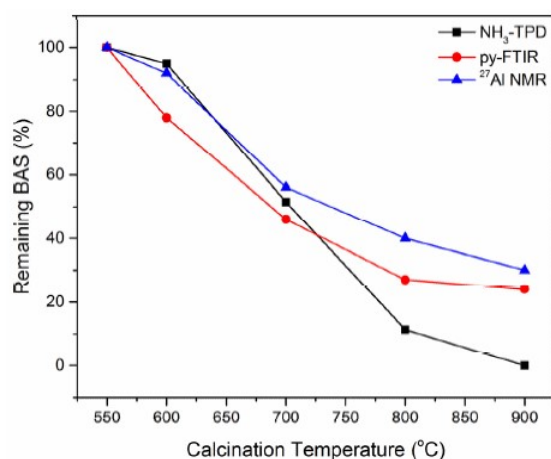


Figure 9. Brønsted acid sites (BAS) after different calcination temperatures determined by three methods. Reproduced from [132]. Copyright 2016 ACS.

2.9. Synthesis Methods

2.9.1. Hydrothermal

The hydrothermal process of preparation of zeolites involves two main processes: the dissolution of Si and Al and the nucleation and growth of crystals for the formation

of zeolite [133]. Hydrothermal synthesis is a multiphase process involving a crystallization reaction, comprising a liquid phase and a solid phase, which can be amorphous and become crystalline. Some authors define the process as in situ reactions that occur at a temperature above the ambient temperature in an aqueous medium and at a pressure of about 14.5 psi [134]. The advantages of using this process include the low energy consumption involved, the high reactivity of the reagents used, the impossibility of environmental pollution, and the formation of metastable phases [135]. In the work of Hartati et al. [136], synthesis in the hydrothermal condition must occur through reagents containing Si and Al being mixed with a cation source of basic character. The reaction must occur in a closed flask in an autoclave at a temperature above 100 °C. During the synthesis, the structure of the Si and Al sources is amorphous and the obtaining of crystalline zeolite depends on passing through the induction period.

The initial function of used alkali (NaOH) is to supply hydroxyl ions for the process of dissolution of Si and Al, thus acting as a mineralizer. This can be evidenced by the disappearance of quartz peaks in a diffractogram as the amount of sample inserted is increased, as Si becomes more available in the mother solution [137]. Some authors also note the effect on the crystallization process, supplying sodium ions that improve the crystallinity of the structure zeolite [133]. In the synthesis process, Cundy and Cox [138] showed that the induction period is between the beginning of the reaction and the observation of the first formation of crystalline material. In the synthesis process, the amorphous phase is considered constant. This phase is responsible for releasing soluble species and is called the “primary amorphous phase,” forming as the reagents are mixed, forming a gel, which can also be called “clean solution” when it has a colloidal form, being translucent. The primary amorphous phase is formed by the immediate appearance of the product, existing in an unbalanced condition, and as a heterogeneous system, which may contain aluminosilicate precipitates, coagulated silica, and precipitated alumina or untransformed reagents [139]. However, the formation of the secondary amorphous phase occurs under conditions of medium heating and formation of a pseudo-transition-state intermediate, which follows the reaction path involving silicates and aluminosilicates, monitoring the pH of the medium, and at the end of the process, the formation of crystalline zeolitic product [138].

According to Abdullahi et al. [134], the complexity of the hydrothermal synthesis process exists due to the different factors that can affect it, among which the following stand out: impurities from the starting materials, the composition of the synthesis gel, the pH of the medium, time and temperature of the calcination and crystallization steps, the formation of intermediate metastable phases, the Si/Al ratio, the water content used, the alkalinity, the use of organic drivers, and the nucleation and growth steps of more stable phase crystals in digestion conditions. In accordance with the studies by Hartati et al. [136] (p. 18), the presence of impurities in the starting material can influence the crystallization of the zeolite structure. One of the impurities that fulfills this role are the Fe atoms present as oxides or not. The reactivity in the presence of this element is influenced by temperature. The removal of impurities can be carried out with a dispersing agent. However, this decreases the SiO₂ content and increases the Al₂O₃ content. In this regard, the composition of the synthesis gel is influenced by kinetic and thermodynamic parameters during the nucleation process [140]. Thus, the Si/Al ratio of zeolite tends to be a factor that influences the synthesis, as it determines the need to add reagents to the precursor, such as zeolite with LTA structure, which does not require addition of the Si source when the precursor is kaolinite or metakaolin, as it has the same Si/Al ratio. Another important parameter in the synthesis is digestion, which comprises the time elapsed between the formation of the gel of known composition and crystallization, thus affecting the nucleation and crystal growth [141]. At this stage, the agitation of the system is important to maintain the uniformity of the mixing gel and selectivity for the formation of different phases of the material [142].

Finally, Abdullahi et al. [134] (p. 18) observed in their studies that the temperature and time of synthesis must be within a defined range, defining the type of zeolite to be formed

and maintaining a direct relationship between structure crystallization, crystallization time, and particle size. Other studies have shown that gradually, the amorphous material is replaced by the crystalline zeolitic material [143]. Studies have been carried out on the effect of temperature varying between 120 and 190 °C for 48 h, and the time has varied from 24 to 96 h [144]. The increase in temperature enabled amorphous crystalline–quartz material transition [145]. While studies have reported that an increase in reaction time at a temperature of 150 °C leads to the formation of crystalline zeolitic material, the increase in time at 120 °C leads to the transformation of quartz to crystalline material [136] (p. 18). Figure 10 shows a general scheme of hydrothermal synthesis.

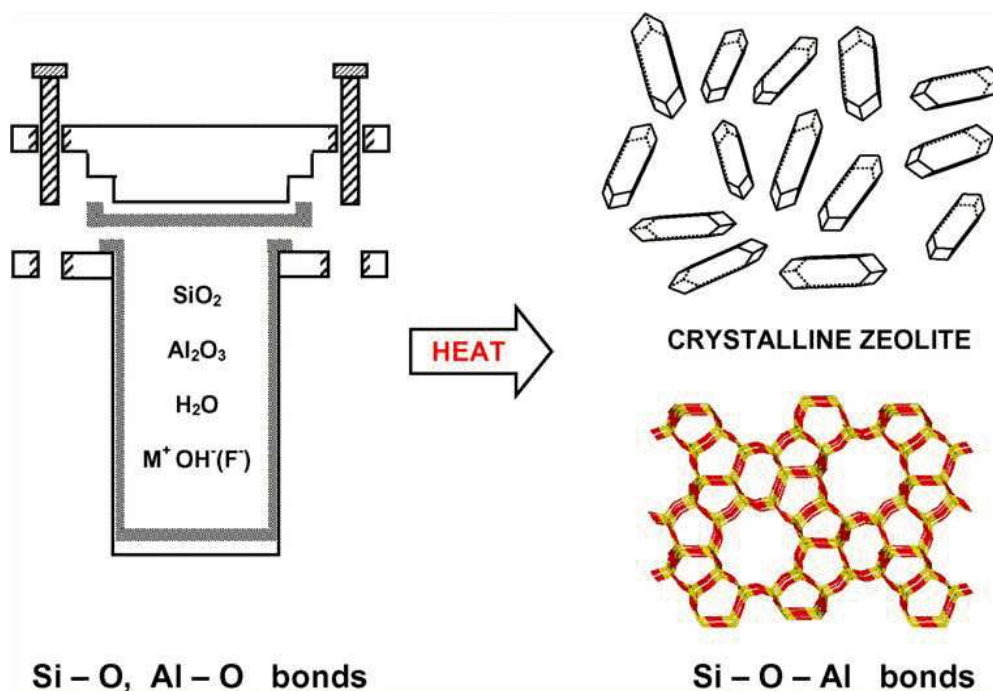


Figure 10. General scheme of hydrothermal synthesis. Reproduced from [138]. Copyright 2005 Elsevier.

2.9.2. Fusion

The hydrothermal synthesis method can be preceded by a process of fusing the starting material with the alkali necessary to carry out the zeolitization of the material. According to the literature, the foundation of the method is based on mixing the precursor with the alkali and melting the system, allowing the crystalline phases of Si and Al present in the material to decompose, thus forming sodium silicates and aluminates with high reactivity and water solubility and enabling the formation of the zeolitic product that must be formed in the hydrothermal process carried out later. This method more specifically directs the synthesis to a certain type of zeolite through the variation of activation parameters in hydrothermal treatment. Compared to the hydrothermal method, that involving pre-alkaline fusion of the precursor enables an improvement in the zeolitization process and the crystallinity of the product. While the hydrothermal method without fusion generates products with structural heterogeneity and poor ion exchanger properties [146], in the fusion process, as the sodium hydroxide, the main alkali used, is introduced, the sodium ions act as stabilizers for the zeolite crystal structure construction subunit, increasing the amount of zeolite formed over a long synthesis. In this regard, Dere Ozdemir and Piskin [147] investigated the use of microwaves and ultrasound to assist the synthesis, and found them useful tools to minimize the reaction time while maintaining a high content of formed zeolite. The sonication process assisting the fusion can be applied for only 10 min, generating positive aspects regarding the reaction speed [148]. According to Naghsh and Shams [149] the process of improving the melting method allows the generation of a product with a wider

range of applicability, as in the removal of water hardness by geopolymers, which fixed the melting time at 14 h and the optimum melting temperature between 500 and 700 °C.

The characterization of the products obtained by the fusion method is important for comparing the degree of similarity of the product obtained with a natural zeolite through X-ray diffraction [150]. Ayele et al. [151] observed that this increase in crystallinity is important in aluminosilicate precursors such as kaolin, as it is the result of its activation and dissolution in the synthesis medium. In addition, Deng et al. [150] described that thermal analysis allows the comparison of the stability of products obtained by hydrothermal process and fusion, where greater stability of the hydrothermal method product was found in relation to the fusion product. In addition to the high crystallinity that can reach more than 80% in some types of zeolites, the synthesis method can provide good cation exchange capacity [151]. To improve the results of the products, fusion methods with desilicification with NaOH and fusion with hydrothermal reaction with Na₂CO₃ have been introduced. With these methods, Lee et al. [152] applied control of the NaOH/precursor ratio, which has been of great importance in ensuring the percentage of crystallinity of the zeolitic product at high values, as well as the size of the particles formed, which decreases with the increase in alkali in the medium.

2.9.3. Molten Salt Method

This method is an alternative to the zeolitization process with high mass yield, thus improving synthesis processes that demand high solution/solid ratios and give low yield in volume relative to the ratio of the weight of zeolite to the reaction volume. These processes can also be accompanied by a large generation of liquid effluent, low purity of the material obtained, and structural heterogeneity, which limit material applications [153]. Thus, for Park and Choi [154] the development of this method was based on the formation of zeolitic structures containing a salt or a base at temperatures above 250 °C with salts of specific natures being occluded in the pores of the structure. The characteristics of this method are the simplicity and versatility of execution, good cost–benefit ratio for obtaining pure products in a single phase, and low temperatures. In addition, the synthesis time is shorter than other frequently used methods described in some papers. Interestingly, in the work of Zhang et al. [155], it was also noted that this does not use water and thus avoids the generation of alkaline liquid waste, which is a positive aspect of the method. However, this may lead to insufficient contact between the components in the crystallization process, and thus the rate of conversion of the precursor to the product can be slow, making the morphology of the zeolite irregular.

In another study led by Zhou et al. [156], it was observed that in the process, the precursor material is initially mixed with a salt or a eutectic mixture of salts, such as NaCl/KCl. The temperature then increases to a level above the melting temperature of the salts, allowing for a flow and diffusivity of the salt, forming a molten stream, thus leading to the dispersion and rearrangement of precursor components in the saline environment. After this process, with the increase in temperature, a nucleation process starts to occur followed by a growth step depending on the chemical nature of the salts, the amount of salt present, the temperature and the reaction time. In work by Miao et al. [153] (p. 20), it is reported that applications of the method may involve helping to dissolve minerals such as vanadium slag and chromite minerals at ambient pressure. In this context, medium conditions such as high alkalinity and high boiling point contribute to good fluidity of the reaction medium. Mass transfer and product conversion increase as temperature decreases. The use of so-called molten salt reactors was reported by Riley and colleagues, who made use of this method to aid in energy generation, being another application in addition to the synthesis of zeolitic materials [157]. Regarding applications, in the work by Yang et al. [158] the use of a sub-molten salt method for the depolymerization of aluminosilicate structures in silicon and aluminum species in mesoscale structures stands out. Figure 11 shows the steps of this synthesis method.

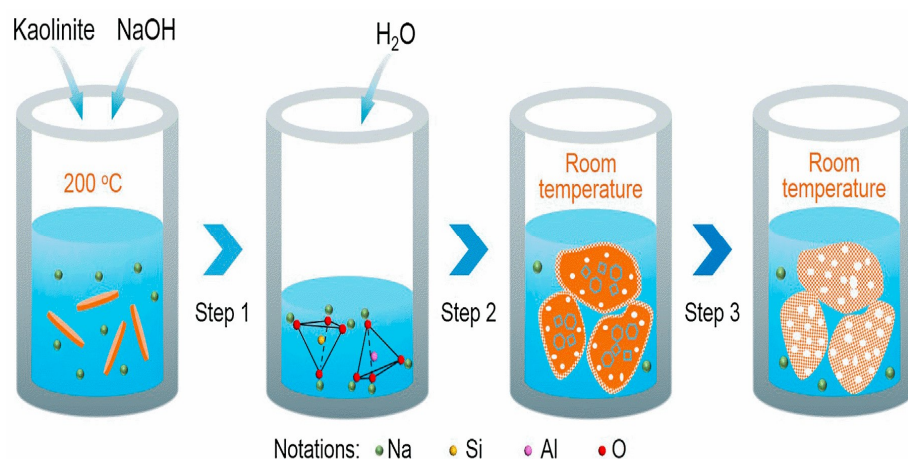
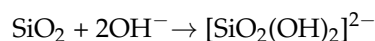


Figure 11. Sub-molten salt method for synthesis of hierarchical sodalite. Reproduced from [158]. Copyright 2020 Elsevier.

2.9.4. Alkaline Activation

The synthesis method with alkaline activation is mainly applied to obtain geopolymers, which can be derived from the same precursor as zeolites, a source of Si and Al. These are polycondensed aluminosilicate amorphous structures. The alkaline activator is a concentrated alkali that can be a hydroxide, silicate, carbonate or sulfate [159]. However, it has been used to obtain zeolitic structures [160–164]. Alkaline activation is a hydration reaction of aluminosilicates with alkaline and alkaline earth substances. The mechanism of the process is complex, involving reactions of dissolution, coagulation, condensation and crystallization, the first step being the breaking of Si-O-Si and Al-O-Si covalent bonds, occurring when the pH of the solution increases, transforming itself into a colloidal solution. After this process, the cleaved structures unite with time, forming a coagulated structure and thus generating a condensed structure in which—as time progresses and temperature varies—a crystallization process can develop [165]. The initial phase consists of silica dissolution, followed by the transport and polycondensation phase. Studies show that the dissolution of aluminosilicates present in the alkaline medium is the primordial and fundamental step for its realization; thus, hydrolysis reactions are those that occur more frequently and according to the following reactions [166].



The literature shows that the presence of hydroxyl ions reveals that alkalinity plays an important role in the reaction. In addition, temperature and reactivity of the raw material play a fundamental role. The solubility of SiO_2 grows as the pH of the medium increases, while Al_2O_3 has high solubility in extreme pH conditions (acid and basic). Alkaline attack releases silicate and aluminate ions in the medium, with the Al atoms changing from coordination 5 or 6 to coordination 4. Because they have faster release, the Al atoms react with any silicate present in the activating solution, forming oligomers. Thus, the use of sodium silicate (Na_2SiO_3) as an activator allows the generation of a product with greater mechanical resistance than those formed only by the use of NaOH [167].

Several works report that in the condensation step, there is a nucleophilic substitution reaction between the species $[\text{Al}(\text{OH})_4]^-$ and $[\text{SiO}(\text{OH})_3]^-$, forming an intermediate complex from the attraction of OH^- groups and Al^{+3} ions. This step is accompanied by dehydration to form the aluminosilicate network. In the process, cations with a smaller radius form a less ordered system accompanied by greater condensation than those with a larger radius [167]. In general, many works report that in the synthesis process, alkali

metal hydroxides or a mixture of these with an alkali metal silicate are used. Alkali metal cations play a fundamental role in controlling synthesis steps, such as hardening and crystal formation [168]. Silicate allows the generation of a product with higher Si content and greater mechanical strength. According to Severo et al. [167], mixtures activated from the combined use of alkali silicate with alkali metal hydroxide allow the reaction to progress to a greater degree, as silicate silica reacts before precursor silica.

Temperature and time of alkaline activation can determine proportions of zeolitic products, and the formation of polymorphic structures of NaAlSiO_2 can be observed. In a study by Monzón et al. [161] (p. 21), the purity of a zeolitic product formed in a hydrothermal process depended on the activation employed, and Na_2CO_3 could be used in addition to hydroxides. In the work by Palomo et al. [169], they established that the conditions of the alkaline-activated products are important for its resistance. In this regard, long curing and high temperature are fundamental conditions for the formation of an aluminosilicate matrix, improving the product's mechanical properties. In kinetic terms, the lower the reaction speed, the lower the curing temperature and the greater the amount of aluminum incorporated in the product. The textural properties of the product can be modified by varying the type of alkaline activator and postsynthesis conditions. Optimal conditions of mechanical strength and pore distribution can be achieved by using H_2O_2 in the mixture with the activator. In an investigation by Tisler [170], the modified chemical and thermal properties of zeolitic products allowed the control of their acidic properties, such as strength and number of sites. Regarding the activation of metakaolin, this process is exothermic, with the formation of an amorphous inorganic polymer responsible for the increase in its mechanical resistance. In this material, alkaline hydrothermal activation has been an alternative to the traditional calcination process [159–171].

2.9.5. Microwave-Assisted Synthesis

The process of obtaining a porous material from the use of microwaves brings numerous unique synthesis characteristics. Among them is the reduction in process time to develop and the production of products with a distribution of sizes and pores more uniform. These characteristics can extend both to the nucleation step and to the growth of formed crystals. In obtaining zeolites, the process occurs for a great range of Si/Al ratios, highlighting the possibility of incorporating metals in zeolite structures [172,173]. Studies always emphasize that improvement in the synthesis of nanoporous materials by microwaves may be due to the following factors: heating by radiation increases the rate of temperature rise of the medium; radiation leads to greater uniformity of heating in the synthesis medium; there is a change in association between species in the medium; hot spots are created in the reaction mixture; and radiation enables the ideal dissolution of the precursor gel [173,174]. Empirically, there have been some findings in obtaining zeolites. The beginning of the application of this method is in its synthesis, and a patent from the company Mobil verified that the crystallization processes can be similar to the use of the traditional method of synthesis. Furthermore, the particle size distribution of the product is greater than that for the use of a hydrothermal method [175].

Other developments in the method lie in obtaining zeolite A after 12 min of synthesis, studying the effect of digestion on the formation of this structure [176]. Synthesis of faujasite zeolites is capable of being completed in a short period of time at temperatures close to 150 °C. Faujasites with high Si content can be obtained by assisting the use of microwaves with optimal characteristics for use in catalysis, such as high selectivity, activity, and stability, at a reduced reaction time from 48 h to 30 min compared to the conventional process [175]. In obtaining the Y type, the advantages of the method lie in maintaining the characteristics of those structures obtained industrially. The evolution of the products obtained as temperature advances can be amorphous phase, zeolite Y, and zeolite P2. Moreover, among the phenomena that can explain the synthesis process in this method, the interaction that water molecules promote with radiation and dispersion of the aluminosilicate gel in the medium should be noted [177,178].

Studies show that microwave-assisted synthesis can be used in the so-called dry synthesis and in the method of growth on surfaces (membranes), both efficiently [175]. In obtaining zeolitic membranes, three strategies can be combined with the use of microwaves: in situ hydrothermal synthesis, secondary growth synthesis, and vapor transport synthesis. Among the zeolite structures obtained in the form of membranes by these methods assisted with microwaves are LTA, MFI, AFI, FAU, SOD and ETS-4 [174]. In addition to these, MOF zeolitic structures can be obtained by the microwave method and solvothermal synthesis [179]. Some authors demonstrated that the synthesis of NaP zeolite from NaY gel can occur with the use of microwaves, generating pure products that can go through a recrystallization process, and the synthesis can be composed of crystallization and rapid cooling in the microwave chamber, with wave digestion at room temperature and crystallization at a temperature higher than the first step, since the temperature reached in the system allowed the network density to vary [180]. Figure 12 shows differences in zeolite morphology obtained by a microwave-assisted method.

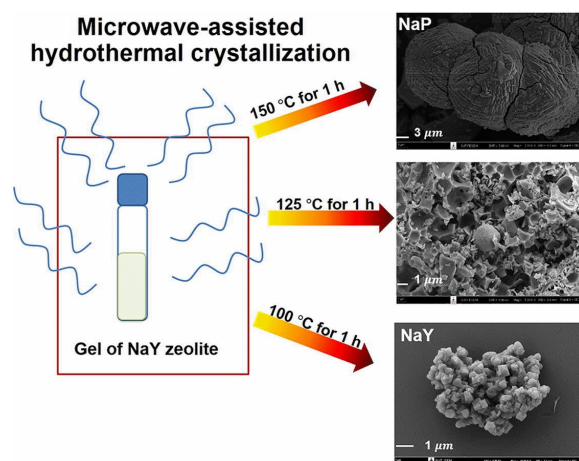


Figure 12. Microwave-assisted synthesis method and differences in product morphology. Reproduced from [177]. Copyright 2020 Elsevier.

2.9.6. Methods for Heteroatom Zeolite Synthesis

These methods are perfectly described by Pang et al. [14] (p. 3). The heteroatom zeolites have received increased attention for the development of synthesis methods, mostly due to changes in such characteristics as microporous structure, particle size and surface acidity. One of the methods involved to obtain this framework is direct synthesis [181]. This process is conducted as a traditional hydrothermal synthesis where the heteroatom is inserted and directly adding a metal salt solution or a metal organic [182]. The hydrolysis of heteroatom precursors occurs simultaneously with the addition of silicon/aluminum sources, giving the formation of a homogeneous sol alkaline or neutral, crystallized into the heteroatom zeolite at a certain temperature, performing the uniform insertion of plenty of heteroatoms in the zeolite framework during the crystallization [183]. The function of heteroatoms is to substitute silicon or aluminum and to form a new framework with connection by SiO_4 tetrahedrons. When the execution of this method occurs under alkaline conditions, there is the possibility of hydroxides forming from the transition metals used, resulting in an inhomogeneous distribution of heteroatoms on the surface and in the channels of zeolite that may block the micropores [184]. The production of Ga-ZSM-5 zeolite by this process gives the advantage of reducing the decomposition of the structure at the temperature necessary to remove the template. The acidity required for some catalytic processes increases, such as the insertion of Ga as of Fe in this MFI structure [185].

TS-1 is another type of structure with insertion of Ti atoms forming the peroxotitanate species and replacing the aluminum atoms. The experimental procedure for the production of TS-1 zeolite has two steps: the mixing of alkoxides with solutions of TPAOH, TEOS

and TEOT suffering a hydrolysis and the dissolution of titanium mixing TEOT in water and then hydrogen peroxide, after which the system is cooled, forming the clear orange solution of peroxotitanic acid, and then inserting aqueous solution of TPAOH, forming a yellow solution of peroxotitanate. The process is finished by adding colloidal SiO₂ with mild heating. The use of F⁻ as mineralization agent helps Ti atom incorporation in the framework, producing a Ti-β zeolite with high hydrophobicity and selective oxidation for organic substrates with H₂O₂. The formation of TS-1 is highly dependent on the pH of the synthesis medium, which influences the number of Ti atoms per unit cell. If the pH is near 7.0, there are near 2.3 atoms/unit cell and the anatase phase may be formed. As the pH values increase, the anatase phase extinguishes with increased unit cell volume. The direct method to heteroatom zeolite production is readily applicable in industrial scaling up, with the product showing high crystallinity, and control of heteroatom content, topology, morphology, and particle size. Nevertheless, some deficiencies related to the mismatching of transition metals in hydrolysis rate relative to Al/Si ions as well as the radius differences are present in this method. Other inconvenient features include the long reaction time for crystallization, partial incorporation of heteroatoms in alkaline conditions, facile formation of extra-framework heteroatoms, severe and narrow synthesis conditions, and in some cases metal agglomeration [186].

Another type of pathway to obtain heteroatom zeolites is the postsynthesis method, which incorporates the metal in the zeolite framework of as-synthesized zeolites in liquid–solid, solid–solid, and gas–solid systems combining the dealumination and desilication with isomorphic substitution of framework atoms under specific conditions [187]. When the Si and Al leave the structure, voids are formed, making the introduction of metal complexes easy, giving a more efficient method than direct synthesis, doping transition metal heteroatoms with much larger radii than Si or Al atoms such as Ti, Sn and Zr, resulting in no formation of extra-framework species or bulk oxides, i.e., a zeolite structure with high metal loading [188]. In a study by Pang et al. [14] (p. 3), the synthesis of Ti β-zeolite by gas–solid isomorphic substitution is reported. This occurs firstly with the removal of B atoms from the B-β zeolite structure, with acid treatments generating lattice vacancies in framework. Then, H-B-β zeolite is treated in titanium chloride vapor at 300 °C, replacing the boron atoms with titanium atoms at tetrahedral sites in framework. Another procedure adopted to obtain Ti-β zeolite is the dealumination of H-β zeolite in concentrated nitric acid, making Si/Al > 1800 and generating vacant T sites with silanol groups. In sequence, the dry impregnation with mechanically grinding Si-β and organometallic precursor follows calcination at 800 °C. In recent years, some improvements in heteroatom zeolite synthesis have been achieved by researchers based on better uses and green principles, such as the change in use of aggressive sources of transition metal and organic templates by a special ionic complex such as template and metal sources and dry gel conversion.

The described methods have common characteristics that reflect in energy consumption, chemical consumption, time to complete the process, and the purity of zeolite formed. Some ideal characteristics of performance shown by a specific structure in pure form in some cases can be observed in a heterogeneous product containing concurrent zeolitic phases. The quality of experimental conditions for a method's development is also determined by the fulfillment of all steps involved in the chemical system where the reactions of zeolitization occur. Therefore, the choice of a method should consider energy efficiency in heating the system, the use of diluted solutions causing less damage in environment when unit operations are made, such as the wash of product formed and even the cleaning of apparatus used, and the absence of organic molecules, such as structure-directing agents. Thus, the hydrothermal method is the best alternative, with the possibility of using microwave assistance to reduce the time of induction and crystallization depending on the properties desired in future applications.

3. Wastes in Zeolite Synthesis

3.1. Kaolin Waste

The production of kaolin has a long background of almost 150 million years, being an important clay with industrial value and consumption, mostly by the paper industry, representing 40% of production. In this field, it is used to fill the cellulose fibers and as coating agent for production of high-gloss paper with good printability [189]. It is useful in clay-based ceramics [190] and refractories [191], fireglass, fillers, and extenders in rubber [192], paint [193], and plastic and adhesives [194]. Other uses include pesticide and herbicide carrier [195], manufacturing of zeolites [196], catalyst support, and cosmetics [197]. Other applications are in plastics production [198] as antiblocking for infrared radiation absorption in agriculture, and the hydroxyl groups present on surface of calcined kaolin may improve its heat resistance [199]. This aluminosilicate mineral is found in sedimentary deposits. The main mineralogical content is kaolinite ($\text{Al}_2\text{Si}_2\text{O}_5(\text{OH})_4$), occurring with feldspar, mica, quartz, illite, montmorillonite, ilmenite, bauxite, zircon, kyanite, silliminate, graphite, atapulgite, halloysite, and oxides such as hematite and rutile. The process of formation is by rock weathering, a process called kaolinization. With plate-like morphology, its characteristics include refractory capacity, highly stable chemical structure, and being a good raw material for ceramic production [199,200]. Industrial kaolin waste is produced from beneficiation being deposited in open-pit lagoons. Its use as an aluminum and silicon source is a highlight due to low operational cost and the great amount generated, where each ton of kaolin produces 9 tons of waste [201]. Actually, the recycle and reuse of wastes reduce production costs, giving alternative materials for many sectors.

There are two types of kaolin waste generated. The first results from the separation of sand from ore, i.e., rich in quartz. The second is from the wet sieving process, separating the finer fraction to obtain a pure kaolin. This second residue has optimal characteristics for production of metakaolinite with high reactivity because of its extremely fine particles. Kaolinite is present in high quantity in this second compound [202]. One compound that gives great performance in synthesis of materials from kaolin waste is mullite ($2\text{Al}_2\text{O}_3 \cdot 3\text{SiO}_2$) because of its unique composition of stable Si and Al. Its properties comprise high melting point, low coefficient of thermal expansion, great strain resistance, and supporting high temperatures with great chemical stability [203]. Besides this, the formation of metakaolinite from dehydroxylation of kaolinite enables a facile route for zeolite synthesis, generating different types of zeolitic structures for each starting material. The use of kaolinite to be attacked with NaOH gives hydroxysodalite as the main product. Nonetheless, when metakaolinite is used, zeolite A is formed significantly [204].

Kaolin waste has been used for faujasite zeolite synthesis with thermal activation of material by calcination at 700 °C. The ideal conditions to obtain optimal crystallinity involve a molar composition of $7\text{Na}_2\text{O}-\text{Al}_2\text{O}_3-3\text{SiO}_2-\text{H}_2\text{O}$. The zeolitization reaction occurs at 90 °C in 48 h without aging [205]. Wastes from two different regions of kaolin exploration in Brazil (Rio Capim and Jari) were used to obtain sodalite under equal conditions of Bayer process, verifying that the waste from Jari region was more reactive for sodalite formation, presenting less crystallinity and increased reactivity. The experimental conditions reached for zeolite synthesis were 150 °C and $\text{Na}_2\text{O}/\text{Al}_2\text{O}_3 = 2.0$, which gave a partial reaction of kaolinite for product generation. An increase in temperature to 200 °C enabled the complete reaction of kaolinite and the parameter $\text{Na}_2\text{O}/\text{Al}_2\text{O}_3$, with values above 2.0 allowing the complete reaction of precursor and total formation of sodalite [206].

The gismondine (GIS) zeolite can be synthesized from wastes extracted in Seridó in northeastern Brazilian, refined by mechanical milling and thermally activated. This product was applied in photocatalytic degradation of an azo dye, being useful for effluent treatment. Another product obtained from a zeolite synthesized from kaolin waste is ultramarine pigments using zeolite Na-A [207]. The cation exchange in zeolite NaA obtained from Rio Capim and Jari in Brazil were studied in the production of zeolites KA, CaA and MgA and demonstrated the possibility of pore variation in structures [208]. The synthesis of a hybrid structure of zeolite A-LDH was made from mineral wastes from kaolin processing

and copper concentrate production for application as adsorbent in dye removal [209]. The gibbsite–kaolinite waste obtained from bauxite washing was used to obtain a FAU zeolite, with experiments for optimization of synthesis parameters, among them alkalinity, time, and Si/Al ratio. Besides this, calcination favors structure formation, avoiding sodalite formation [210].

3.2. Coal Fly Ash

This material is often used for zeolite synthesis and comes from the burning of pulverized coal, having the physical aspect of powder. The process of its generation involves the combustion of pulverized coal, generating a dry ash. A great amount of ash leaves the furnace as fly ash, entraining in the gas flow. This process occurs in a dry-bottom boiler [211]. Other types of precursor material are generated using the wet-bottom or slag tap furnace, with which 50% of the ashes remain in the furnace and the other 50% is left with gas flow [212]. The cyclone furnace uses between 70% and 80% as boiler slag, while 20–30% is left in gas flow as dry ash. There are high numbers for coal fly ash generation just in the USA, according to the Federal Highway Administration. In 1996, the electrical utility industry generated approximately 53.5 million metric tons of coal fly ash. According to this report, from 1977 to 1996, this generation was constant, varying from 42.9 to 49.7 million metric tons [213]. In a survey done in 2019 about the worldwide production of coal combustion products published on the Coltrans Conferences website (<https://www.coaltrans.com> (accessed on 23 October 2022)), in 2010, this number was approximately 780 million metric tons, and in 2017 reached 1.1 billion metric tons. This includes the use of ashes in concrete applications [214], road construction [215], and filling applications [216], besides soil amendment and zeolite synthesis [217]. Adequate disposal and use of the waste is important to reduce the pollution of water and soil, disruption of ecological cycles, and environmental hazards. Generally, its disposal is into ash ponds, landfills and lagoons [218].

The chemical composition of coal fly ash is complex, with almost 316 individual mineral and 188 mineral groups identified [219]. In addition to metallic oxides such as SiO_2 , Al_2O_3 , Fe_2O_3 , CaO , MgO and K_2O , the unburnt carbon is also present and may be determined by loss on ignition [220]. Some trace elements may be present, such as Cr, Pb, Ni, Ba, Sr, V and Zn [221]. Some important physical properties are the particles, with an average size of $< 20 \mu\text{m}$ and low bulk density ranging from 0.54 to 0.86 g/cm^3 , surface area from 300 to $500 \text{ m}^2/\text{kg}$, and light texture [199] (p. 25). Its acidity is weak; therefore, a majority of ashes are alkalis, where the molar ratio Ca/S determines pH in a water–ash system [222]. Thus, it is possible to classify the materials as strongly alkaline (pH 11–13), mildly alkaline (pH 8–9) and acid ash [223]. The morphology is spherical, consisting in cenospheres, solid spheres, irregularly shaped debris and porous unburnt carbon [218] (p. 26). The mineral composition of coal fly ash includes quartz and mullite, as well as amorphous glass phases, hematite, and magnetite [224]. The large amount of amorphous phase is dissolved in alkaline media, promoting geopolymerization reactions. This may be better as the waste is treated with NaOH at high temperatures [225]. The transformation in geopolymers is favorable to change in the structure of a zeolitic framework under adequate conditions, giving more organization in structure, and useful for a remediation process for soil pollution called “solidification/stabilization” (S/S) [226].

“Fly ash zeolites” (FAZ) have been used to compose in situ chemically reactive barriers or in situ treatment zones in water pollution remediation. This technology is based on permeable zones placed within the aquifer reacting with contaminants in the flow of water [227]. The main phenomena involved are sorption and precipitation for retention of contaminants [228]. In the process of fly ash zeolitization, the partial transformation of the precursor in zeolite P and the use of hydroxysodalite of an alkali medium are reported. During this process, slow dissolution of quartz and stabilization of mullite occurs. The main zeolites obtained by fly ash zeolitization are zeolite P, X, A and hydroxysodalite in NaOH medium, preparing a high-capacity cation exchanger. The presence of each

zeolite phase depends on kinetic factors and seeding that enables the change of each phase proportion [229].

The main method used to produce zeolites from fly ash is hydrothermal and the adsorption property of fly ash is described as similar to 13X zeolite structure. Another method, applying fusion after hydrothermal synthesis, enabled the obtaining of low-silica NaX zeolite. The fused alkali–fly ash mixture easily makes Na-aluminate and silicates highly active, with great solubility in water and good properties for zeolite formation. The optimal pH for zeolite synthesis using fly ash is alkaline, as proved in tests using different alkaline activators (NaOH and KOH) for NaP1 and NaP [230].

3.3. Rice Husk

Rice husk (RH) is a spinoff of rice production and originates in the milling process for separation of the husk and bran from the edible part. The global production of RH per annum is estimated as 10 million tons, in most cases burnt to produce reek for machinery work [200] (p. 25). Other uses are feedstock for bioethanol production and additive in materials demanding high siliceous content or as fertilizer [231]. The global annual production estimated by husk paddy ratio (HPR) is 120 million tons with China contributing 29%, following by India (21%), Indonesia (8.8%), Bangladesh (6.4%), Vietnam (5.8%), Thailand (4.4%), Myanmar (3.9%), the Philippines (2.3%), Brazil (1.9%), and Japan (1.8%) [232].

The chemical composition of RH is based on cellulosic sugars and its nature is lignocellulosic, with lignin representing up to 20% of husks [233]. The rice husk ashes are produced by gasification of RH and contain considerable amounts of silica (SiO_2) varying from 15.30% to 24.60% [232–234]. The silica may be pyrolyzed at elevated temperatures or extracted as sodium silicate using solvent extraction. Rice husk ash (RHA) has better characteristics for applications than rice husk and represents an ideal form of environment-friendly application, due to its burnt waste origin [232].

The uses of RHA include soil ameliorants, breaking up clay soils and improving soil structure, besides its use as insulator in the steel industry and as pozzolan in the cement industry. In zeolite synthesis, this material may present crystalline tridymite and α -cristobalite, allowing the synthesis of BEA and ZSM-5 [235]. Zeolite synthesis is one of the most important applications [232,235–238]. The zeolite NaY was synthesized using RHA waste as source of silica after acid leaching of husks. In this process, zeolite NaP was obtained also [239]. The products presented such characteristics as uniform distribution of particle size, surface area depending on synthesis method, and the presence of another phase obtained (zeolite P) [232].

The acid leaching in RHA may not be used for the synthesis process as in ZSM-5 zeolite preparation using the solvent-free method by mixing solid raw materials such as solid waste RHA, NaAlO_2 , $\text{Na}_2\text{CO}_3 \cdot 10\text{H}_2\text{O}$ and TPABr with optimum molar ratios TPABr/ SiO_2 , $\text{Na}_2\text{CO}_3 \cdot 10\text{H}_2\text{O}/\text{SiO}_2$ and synthesis time [240]. The solvent-free method presents great recovery rate of Si and Al with respect to the hydrothermal method [236]. The micropore and mesopore surface areas of material reached adequate values and the method without the use of solvent and using RHA as precursor represents a sustainable alternative [236].

The zeolite SUZ-4, a new synthetic zeolite, may be obtained by use of RHA as raw material. This process is described as occurring with hydrothermal conditions in the presence of tetraethyl ammonium hydroxide as template. The properties obtained from RHA waste in comparison with products from pure silica sol are: the needle-shape crystals from pure silica sol reach a smaller diameter than those obtained from RHA, which were larger, increased crystallite size, and generation of higher-purity zeolite using just 50% RHA in comparison to 100% pure silica sol [237].

Zeolite A was synthesized from RHA at low temperatures using NaOH as activator to dissolve the silicate ion from RHA that reacts with aluminate in solution to form an aluminosilicate structure for zeolite formation. In this process, there are three steps in the synthesis: the dissolution of Si from the precursor, the gelation among Si and Al to form

the aluminosilicate gel, and finally the crystallization of gel to yield the zeolitic structure, which can reach high crystallinity [238].

Rice husk in the form of rice husk ash appears to be a cheap alternative to synthesis of other porous materials that require synthetic and expensive Si sources, such as tetraethyl orthosilicate (TEOS) and tetramethyl orthosilicate (TMOS). In this scenario, the mesoporous molecular sieves from the M41S family, such as PABA-MCM-41, present hexagonal mesostructure and high surface area [241]. Hierarchical porous carbon materials have been obtained, applying RHA as carbon precursor and used as capacitor in electrode materials [242].

3.4. Sediments

The use of sediments for zeolite synthesis involves working with different samples in nature and geographic location; however, the chemical composition might be similar to a viable use, mostly relative to the presence of Si and Al. The dam sediments of sand mine located in southern Brazil were used with alkaline fusion. Sediments were illite, kaolinite, vermiculite, quartz and K-feldspar. The NaOH/sediment ratio was tested, as well as the temperature and fusion time. The quartz was the only mineral not solubilized for the formation of faujasite. The low NaOH/sediment ratio was responsible for the low amounts of zeolite formed, verifying that kaolinite and vermiculite presented better solubilization in media, favoring zeolite formation [243].

Thermal treatment guarantees the ex situ decontamination of heavily polluted sediments and soils [244]. The main disposal of these sediments is landfill, which may return to its source in rivers, harbors and estuaries [245]. According to Wu et al. [133] (p. 18), the reuse of this material includes application in asphalt, road beds, building foundation support, filling and grading. There are some physical, chemical and mineralogical similarities between this material and coal fly ash. Thermally treated sediment found in Suzhou Creek, Shanghai, China was used to obtain zeolites Na-P1, Na-X, hydroxysodalite, F linde A and FAU. Among the important parameters to successfully prepare these structures, the cation exchange capacity and specific surface area are highlighted. The type and the crystallinity were influenced by Si/Al of the starting material, NaOH/sediment ratio and the liquid/solid ratio.

Dredged sediments originated mostly in China, due to black odorous water phenomena, compromising almost 1197 waterbodies; therefore, the disposal of these sediments might be reduced by using them as a precursor for zeolite synthesis for adsorption uses in the removal of heavy metals such as Cd (II) [246].

4. Applications of Zeolites in Catalysis, Bioprocesses, and Environmental Remediation

4.1. Production of Light Olefins

Light olefins are important substances that are building blocks of derivative substances from the petroleum industry, such as polyethylene and polypropylene [247]. The main compounds in the light olefin family are ethylene, propylene and butene, which have been of great importance for the petrochemical industry. The global demand for these products is higher than other petrochemical products. As an example, the demand for propylene was 82 million tons in 2010 and is expected to reach 165 million tons by 2030 [248]. For this production, fractions of gasoline and gas are used and the main process is the catalytic cracking of vacuum gas oil. An example is the propylene production that accounts for 81% of the yield (50% from steam cracking and 31% from FCC). The nature of feedstock used influences this quantity: heavy feed produces high propylene content, while lighter feed is produces low propylene content. Alternative feedstocks such as natural gas, coal, and biomass (a carbon-neutral feedstock) can be used, as well as other related feedstocks, such as vegetable oils in pyrolysis and thermal cracking. The bio-oil obtained from woodworking (sawdust) pyrolysis, a lignocellulosic biomass, is useful for light olefin production in spite of some difficulties faced, such as the coking property. The use of Fischer–Tropsch synthesis may be helpful for olefin production from synthesis gas, a better process to transform

biomass, but nonetheless there is high greenhouse gas generation in the form of methane and carbon dioxide. Another approach is the MTO (methanol to olefins) reaction [247–249]. Crude oil is another feedstock highlighted for light olefin production [250].

The fluid catalytic cracking (FCC) method is the main catalytic conversion process used with lower CO₂ generation and higher energy economy, using much lower temperature in operation than steam cracking. The innovation in process development is reached because of high capacities of the cracking unit; therefore, the redesign of the unit improves the olefin production. Two of these innovations are the catalytic pyrolysis process (CPP) and deep catalytic cracking process (DCC) [251]. The increase in light olefin production is achieved by reaching severe conditions in the FCC process with higher reaction temperature or ratio catalyst/oil. This leads to excessive dry-gas (C₁ and C₂) production and higher hydrogen transfer activity. The severity of process conditions and the adequate design of catalysts have fundamental roles in optimal light olefin generation. FCC catalysts are responsible for decreasing the activation energy for breaking the C–C bonds while the temperature decreases. The adequate selectivity for desired products is a function of the catalyst, where the coke may be removed by regeneration or decoking. The main types of catalysts used are acids, basics and transition metal oxides. Proton donor catalysts such as zeolites are solid acid catalysts and highly active in cracking hydrocarbons [247–251].

The conversion of syngas into light olefins (STO) has been used with catalytic support of zeolitic structures. The direct conversion was made using Fisher–Tropsch (FT) catalysts, because the introduction of a second zeolite phase to the conventional FT catalysts may optimize the hydrocarbon distribution [252]. The use of bifunctional catalysts such as Zr/Cr oxide and SAPO-3 zeolite allows the direct synthesis of light olefins from syngas with 80% selectivity [253]. The conversion of CO or CO₂ to light olefins by SAPO zeolites is reported in use of other bifunctional systems, such as ZnZr/SAPO-34, ZnAl/SAPO-34, MnO_x/SAPO-34 and InZr/SAPO-34 [254].

The use of ZSM-5 zeolite, with strong acidity, in reaction with STO results in the initial formation of paraffins or aromatics [255]. The reduction in Si content in a zeolite structure enables a olefin/paraffin ratio of <6 in STO reaction and the CO conversion reaches 11%. This is tailoring the structure. Moreover, the acidity of zeolites in bifunctional catalysts in STO reactions improves CO conversion and olefin selectivity [256]. The use of SAPO-34 zeolite to produce light olefins is due to the facile diffusion of olefins in its channel structure, presenting eight-membered ring channels [254]. In ZSM-5, used in catalytic cracking of gasoline to generate C₂–C₄ olefins, this process occurs at the expense of gasoline yield due to preferential cracking of low-octane gasoline with linear olefins on its internal acid sites [257]. The bimolecular hydrogen transfer reaction decreases in a medium with ZSM-5, thereby contributing to the formation of light olefins [42] (p. 8).

MFI zeolites are usually added in the FCC process, increasing either the production of light olefins or the gasoline octane number [258]. The stability of the H-MFI structure is guaranteed by phosphorous impregnation and high yields of products [259]. The dual additives MFI and BEA zeolites may improve the production of light olefins, mostly after treatment of acid activation with phosphoric acid. Moreover, the dual additives do not impact the quality of naphtha in comparison with just one structure-based additive (e.g., MFI) [260].

The catalytic process to obtain olefins from CO₂ to MeOH conversion and then MeOH to olefins demands high temperature control using several oxides, such as In₂O₃, ZnGa₂O₄, ZnZrO, and others as catalysts. To complete this MTO (methanol to olefins) reaction, many zeolites have been used to produce light olefins from CO₂ hydrogenation, such as SAPO-34, SSZ-13 and ZSM-5. The degree of proximity and distance of two catalysts involved, metal oxide/zeolite mass ratio, and the operating conditions are relevant to reach a good yield of C₂–C₄ olefins [261].

The conventional zeolites that are made with microporous channels impose the restriction of bulk molecule diffusion and frequently yield coke, besides side reactions. Therefore, the hierarchical zeolites composed of mesopores and macropores in the same structure

come to give a solution for this problem in light olefin synthesis under a zeolite structure used as catalyst [262]. These structures include MFI, MEL, CHA, FER, FAU, BEA and MTW, exhibiting high olefin selectivity, high conversion, and long lifetimes [263]. The reactions applied for these structures range from MTO and CO₂/CH₄ conversion and factors such as increase in external surface areas, decrease in diffusion path length, accessibility of guest molecules to acid sites, and low coke formation, are relevant for this application and suppressed if a heteroatom is inserted in the framework, modifying the acidity of the material [264]. A simulation of an increase in light olefins from MTO reaction using H-ZSM-5 has been reported [265].

Large-pore zeolites may increase the yields of light olefins such as ethylene and mostly propylene. With a combination of ZSM-5 and a large-pore zeolite, optimal conditions were obtained in Daqing heavy oil cracking. Good product yields were reached when the combination of the same MFI structure was made with RE-USY and AT-H β -4 was employed, with increased yields when pore size increased [262]. Figure 13 shows the application of Y/ZSM-5 zeolites to obtain light olefins from Fischer–Tropsch synthesis.

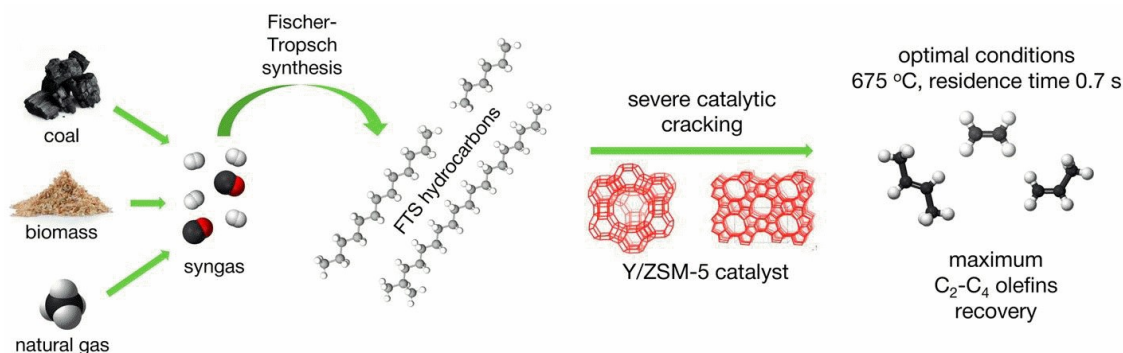


Figure 13. Scheme of light olefin formation using zeolites as heterogeneous catalysts. Reproduced from [249]. Copyright 2020 ACS.

4.2. Production of BTX Aromatics

The compounds known as BTX have three identities—“B” from benzene, “T” from toluene and “X” from xylene—and are all aromatic compounds. They are derived from oil thermal cracking and naphtha reforming [266]. The use of light cycle oil (LCO), a middle distillate from FCC process, is also useful to obtain these aromatics, which may contain up to 90% of mono-, di- and triaromatic compounds. In BTX production, hydrotreating (HDT) and hydrocracking (HCK) procedures are achieved with catalysts with important roles in hydrogenation in naphthalene structure and selective cracking of naphthalenic structures, resulting in one-ring aromatic hydrocarbons with alkyl chains. The MTA (methanol to aromatics) reaction has been another process of BTX production, mostly due to the development of coal-, shale gas-, and biomass-derived methanol using the syngas route [267,268].

BTX synthesis from syngas can reach good selectivity using a dual bed of MnCrO_x-ZSM-512-MR zeolites. Silica modification of external acid sites and the topology of zeolites determine BTX selectivity. The presence of 12-membered rings in zeolite structures such as USY enhance the product formation. Thus, it has been used to design a catalyst for a one-step synthesis reaction of BTX using syngas [269].

Bifunctional catalysts are important in improving the production of these compounds, ideally with acid nature acting as a support and with a metal for hydrogenation–dehydrogenation steps following the HDT and HCK reactions before BTX production [270]. In this process, the strong acidity and excess of hydrogenation activity may crack molecules generating gaseous light hydrocarbons and become sensitive to coke formation [271]. In this scenario, zeolites are important as catalyst support, mostly because of their stronger acidity, great thermal and hydrothermal stability, higher resistance in the presence of sul-

fur and nitrogen compounds, reduced tendency for coke formation, and great capacity of regeneration [266]. Other characteristics include shape selectivity allowing the occurrence of specific reactions influenced by distribution of microporous Brønsted acidity [272]. A catalyst composed of Ni, CoMo, NiMo, and NiSn when supported over zeolite H-beta presented good BTX yields that may be improved by adding ZSM-5 zeolite in combination with H-Y. This effect was ascribed to large pores of FAU zeolite used becoming an easy medium for tri-ring aromatic molecules [266].

The zinc phosphate groups can be anchored in the channel system of HZSM-5 zeolite, enhancing the hydrogen transfer pathway, essential for high BTX selectivity and avoiding the methylation of these compounds generating heavy aromatics [267]. Nonetheless, the application of mesoporous zeolites is limited because of such structural factors as poor hydrothermal stability and weak acidity. Therefore, hierarchical structures can be used because they combine good structural aspects of microporous and mesoporous zeolites, such as large surface area and better metal or acid/base dispersion, in comparison to amorphous silica–alumina supports. Modification of these structures, such as using ZSM-5/SBA-15 with a heteroatom, decreases acid generation and increases aromatic hydrocarbon formation. As an example, modification with Ga atoms gives high BTX catalytic selectivity [268].

The intensity of zeolite acidity (Brønsted sites) is important to drive the glycerol conversion in aromatics. The yield of aromatics is also very dependent on Si/Al ratio, the high Al content (low Si/Al ratio) leading to higher aromatic production. The alternative addition of bentonite in catalyst support can increase selectivity for benzene. The coke formation is a drawback in this process that can be removed by calcination. During the regeneration step, the bentonite structure collapses and reduces the acid strength. The modification of zeolitic structure by a metal has such effects as decreased aromatic yield, the changes in main reactions catalyzed avoiding the aromatization. Using glycerol as reactant, the nature of metal determines the performance in scission of C–O bonds, and the temperature is important for conversion of glycerol to aromatics [273].

The modification of H-ZSM-5 with Zn allows the formation of binuclear $[ZnOZn]^{+2}$ species, acting as strong Lewis acid sites, improving dehydrogenation activity in the aromatization of 1-hexene. The presence of heteroatoms has good characteristics to obtain products from BTX reactions. These characteristics are high surface area, small particles, and weakness of Brønsted acid site with good stability due to short diffusion paths and more channel mouths, diffusing the aromatics and not allowing coke formation [274]. It is important to highlight other features, such as optimal porosity to allow the removal of aromatics in different medium, e.g., Na-P1 and Na-X from fly ash [275,276]. It is also important to highlight the complexity of structures used to obtain BTX molecules, such as nanosized sulfide Ni–W catalysts based on zeolite [277] and the ZSM-5/silicalite-1 core–shell zeolite catalyst [278]. Figure 14 shows a mechanism for BTX formation.

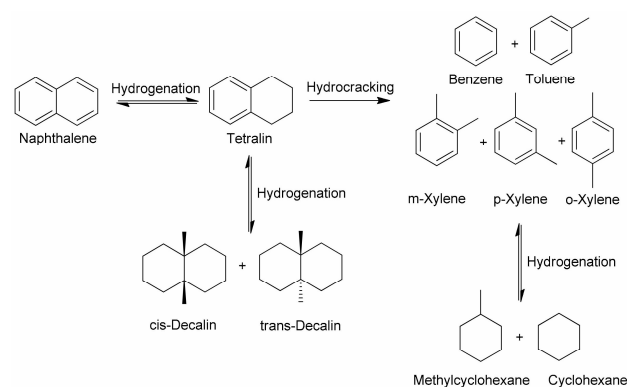


Figure 14. Mechanism of BTX production from hydrocracking of pyrolysis fuel oil components. Reproduced from [277]. Copyright 2020 MDPI.

4.3. Processes with P-Xylene

Para-xylene is a volatile organic compound (VOC), easily becoming a gas molecule at room temperature, undesirable in the environment, and coming mainly from automobiles. The adsorption of this molecule is one of the main approaches to remove it from the air [279]. The main source of xylenes is naphtha reforming and pyrolysis of gasoline, where the compound exists in an equilibrium proportional to the other two isomers (meta- and ortho-xylene). P-xylene is much in demand in the plastic industry for the production of terephthalic acid and dimethyl terephthalate, intermediates in PET production (polyethylene terephthalate). However, the separation from isomers mixture is very important to obtain pure p-xylene. The reactions involved in this process are the isomerization of C₈ aromatics and the disproportionation and transalkylation of toluene. Alkylation of toluene with methanol is used in the same manner [42] (p. 8).

The separation of p-xylene with usual methods, such as distillation, is difficult because its isomers have similar molecular structures and close boiling points. To make this process easier, zeolites are used to promote adsorption processes alongside the fractional crystallization method. These processes demand a great amount of energy and batch operations. In this context, polycrystalline MFI zeolites have been used to separate p-xylene by pervaporation and vapor permeation processes. The physical and structural characteristics of MFI-type zeolites allow the diffusion of p-xylene molecules, such as straight channels in b directions and sinusoidal channels in a direction. The shape selectivity is the main property that enables this separation. The decrease in xylene adsorption level improves this property for isomer separation [280]. The form of zeolites used for this operation is membranes using ferrite (FER) zeolites as MFI zeolites. Therefore, the presence of pinholes as large as 1 nm makes the separation of p/m xylenes difficult, so the presence of narrow pores is undesirable, and the temperature is crucial for separation of binary mixture such as p/o xylene [281].

The zeolite SSZ-35 is used as catalyst for reaction of p-xylene alkylation with isopropyl alcohol. This zeolite has a 10-ring channel system and shallow cavities with 18-ring cages. Chemical modification with acidic treatment results in decreased void volume, such as the concentration of acid sites located in external surface. Desilication of the structure can increase the selectivity of the desired product (2,5-dimethylcumene), leading to the formation of a hierarchical structure [282]. Besides reactions of transformation p-xylene, there are chemical processes for production of this molecule using biomass-derived dimethylfuran, involving H-beta zeolite [283] and beta zeolite with nanosponge-like morphology [284], ZSM-5 and Y zeolites [285].

Sustainable processes of p-xylene production avoid the traditional obtainment from the petrochemical industry. One of these routes is based on the use of a biomass-derived compound called 2,5-dimethylfuran (DMF), producing a biobased p-xylene by Diels–Alder cycloaddition of DMF and ethylene followed by dehydration process of an intermediate. For this process, a beta zeolite with a nanosponge-like morphology was obtained from multi-ammonium surfactants as a meso–micro dual structure-directing agent, composed of ultrathin zeolitic nanocrystals with intracrystalline mesopores and a large number of Brønsted sites, both externally and in micropores. Mesopores in addition to acid sites make access easier for reactant molecules and void the coke formation [284].

The application of zeolites beta, ZSM-5 and Y in continuous flow synthesis presents better catalytic performance, acrylic acid and DMF being used in the process. The Si/Al ratio determined the complete conversion of DMF, with yield of 83% p-xylene. The optimum factors that guaranteed optimal catalytic activity in reaction were the combination of high specific surface area and medium to high acid density allowing the occurrence of two reactions (Diels–Alder cycloaddition and decarboxylation), as well as suppressing alternative self-condensation reactions [285]. The Al-rich H-beta zeolite presented its catalytic activity dependent on Si/Al in this conversion, using ethylene and DMF, mostly the Si/Al ratio equaling 22, giving 97% p-xylene yield [283]. A computational study was done on this reaction with this type of zeolite, analyzing the free energies. The secondary addition

can be eliminated with n-heptane as inert solvent, decreasing the loading of DMF or using weak Brønsted acid sites that facilitate the dehydration of Diels–Alder product [286]. The electronic structure calculations to investigate catalytic activity of HY and alkali-exchanged Y zeolites in this reaction showed a bidirectional electron flow mechanism [287]. The Figure 15 shows a reaction of p-xylene formation in three proposed processes [285].

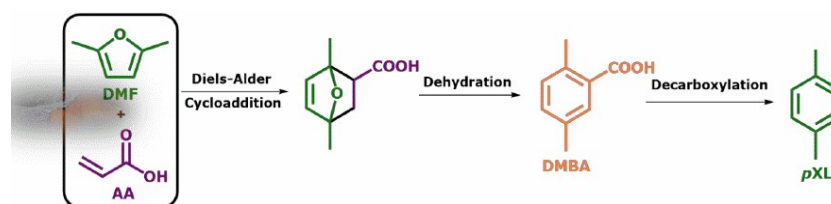


Figure 15. Proposed three-in-one continuous reaction of 2,5 dimethylfuran (DMF) and acrylic acid (AA) to produce p-xylene (pXL) and 2,5 dimethylbenzoic acid (DMBA). Reproduced from [285]. Copyright 2020 Royal Society of Chemistry.

4.4. Microbial Immobilization

The use of porous materials as supports for immobilization of distinct microorganisms (MOs) is increasingly used to solve industrial problems. There are some processes that use anaerobic routes for different functions, such as wastewater and solid waste treatment [288,289], biodegradation of pollutants [290], alcohol fermentation [291], mineral self-healing concrete [292] and anaerobic treatment of agricultural wastes [293]. The physical properties and structure of zeolites, mostly the channel and pore cavities, minimum diameter pores, average surface area of 24.9 m²/g, low bulk density, high cation exchange capacity and adsorption make this material useful for biological processes. Moreover, the wastewater biological treatment has been a highlight, reducing inhibitory substances in feedstock such as ammonia [288].

In this context, anaerobic remediation has many good characteristics, such as the high degree of purification in loco even possessing high organic feeds, low nutrient requirements, small amount of excess sludge produced in the process, and the production of renewable biogas, enabling recovery of energy instead of just saving it and reducing costs in comparison with aerobic process [294].

When anaerobic digestion is achieved in the absence of a support for immobilization of a microorganism, there are some drawbacks: long processing, requiring a large reactor volume, and the possibility of washout of the microorganism due the high substrate loading rate, reducing the reactor performance. With porous solid materials as support for anaerobic microorganisms, there is an ideal environment, e.g., the bacterial growth that is increased by the porosity of material. Moreover, the chemical oxygen demand (COD) is reduced, preventing biomass loss at high loading rates [288].

The sorbent property for microbial immobilization is reported to be presented by clay rocks and has been used for oil-oxidizing microorganisms such as *Pseudomonas yamanorum*, *Rhodotorula glutinis* and the microalgae *Chlorella vulgaris*, acting as biogeo-sorbents that increase the efficiency of cell immobilization, preserving viability and biochemical activity. The sorbents act as transport bases for Mos, allowing up to 10 years of anabiosis, i.e., reduction of metabolism. The zeolites analcime, clinoptiolite and glauconite have been found to be great biogeo-sorbents in tests of hydrocarbon oxidation with the capacity of holding volatile low-molecular-weight alkanes [290]. Natural and modified zeolites have been also used for immobilization of the strain of *Trichoderma viride* SL-45 with success [295].

The immobilization of cells for ethanol fermentation is an important line of work using zeolites. *Saccharomyces cerevisiae* has been immobilized with a natural zeolite and the system presented 3.6·10⁸ cells/mL in carrier capacity, reaching that required for immobilization and alcohol fermentation twofold higher than glass beads and being stable for 21 days without the loss of carrier. The immobilization of cells increases the reaction

rates, enzyme productivities, and cell densities [291] (p. 34). A synthetic zeolite was used in the fermentation process of lactic acid production by immobilization of *Lactobacillus rhamnosus*, where the simple cell separation from fermentation media and their reuse in repeated batch cycles were achieved with success [296]. In the process of ethanol fermentation, by-products are generated, such as in the corn ethanol industry, where thin stillage is generated. Thus, the nature of reactor used for this waste treatment has great importance, an anaerobic fluidized bed reactor generally being applied. Using zeolite in this reactor achieved 88% COD removal efficiency in some works, showing the importance of supporting the MO for this process in all steps until in waste treatment [289] (p. 34). The anaerobic fluidized bed reactor was studied for treatment of vinasses using natural zeolite mainly composed of clinoptilolite, mordenite and montmorillonite. The microbial communities with great predominance were *Methanosaeta* and *Methanosarcinaceae*, besides sulfate reducing bacteria. The physical characteristics of zeolite promoted good media for immobilization with high organic removal efficiency, the irregular surfaces of the material being the factor responsible for this. A large accumulation in the interior of ruggedness and in superficial zones of support was observed [289] (p. 34).

Zeolites have high importance in immobilization of Mos. A porous ceramic carrier made from fly ash was made for wastewater treatment for the purposes of nitrogen removal [292–297]. Figure 16 shows the immobilization of a colony on a zeolite structure.

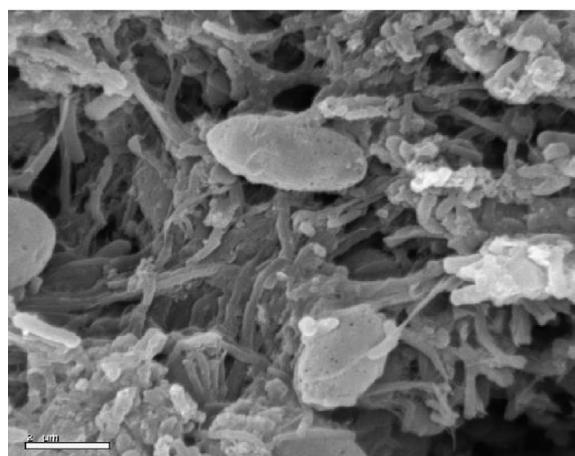


Figure 16. Micrography of zeolite with a microorganism immobilized. Reproduced from [293]. Copyright 2007 Elsevier.

4.5. Biomass Conversion

Global concerns about new forms of production of useful products for society such as fuels and chemical compounds (platform molecules) have been in the focus of industry and research entities. In this scenario, processes involving biomass conversion have great importance, e.g., for biofuel production, which may replace a great quantity of fossil-derived fuels, allowing the generation of advanced biofuels, also called second- and third-generation biofuels, replacing the widely used ethanol (first-generation) [42] (p. 8). For zeolite utilization in biofuel production, hydrolysis, esterification–transesterification, isomerization, condensation, pyrolysis, and upgrading bio-oil can be performed [298].

The use of zeolites in biomass conversion to transportation fuels has been a great alternative use of catalysts with sustainability because some zeolites are formed from natural precursors or biomass wastes, e.g., coconut shell and lignocellulosic residues, and are the most abundant bioresource available composed of cellulose, hemicellulose, and lignin. Lignocellulosic biomass is used in pyrolysis oil to produce biomolecules, food aroma, pesticides, and biofuels. This process heats the material in the absence of oxygen, transforming it into an oil with fewer problems in processing. In this process, the zeolite bed converts the vapors of pyrolysis oil in hydrocarbons, H_2O , CO_2 and coke [299].

In catalytic processes, for conversion of lignocellulosic matrices, the transport of heavy molecules through the zeolite pores is cumbersome and faces mass transport limitations. The interactions between biomass components and zeolites are different and not only based in carbocation-like active centers. One highlighted process involved the conversion of oxygen from biomass-derived products in hydrophobic molecules with good chemical and combustion properties. The hydrophilic substrates begin to present more of a hydrophobic nature, with changes in interactions with active centers along the course of the reaction. Reactions of dehydration and hydrogenolysis can form water in medium that can act as a poison for active sites. In addition, polymeric molecules react with external surface sites with continuation at the internal active sites [300].

One of the main goals in biomass conversion, including in triglyceride conversion (e.g., oils obtained from vegetables matrices), is the reduction of molecular mass; therefore, Brønsted acid sites might enable the cracking and upgrading of biomass components [301]. Oleic acid (cis-9-octadecenoic acid) is a component of a large number of biomass matrices, being the main fatty acid in olive oil pressed from the ripe fruit of the olive (*Olea europaea*) [302]. This compound can undergo acid-catalyzed isomerization, forming a mono-branched-chain unsaturated fatty acid. In this reaction, the zeolites give considerable yields in comparison to clays. Their relatively small channels and pores are responsible for this. In the beginning of this process, coke formation with isomerization limited to the micropores occurs. The size and geometry of pores determine the type of compound formed that can be methyl mono-branched-chain unsaturated fatty acid or ethyl and propyl mono-branched-chain unsaturated fatty acid [301]. The effect of desilication of MOR zeolite on esterification of oleic acid as a model reaction has been investigated. The generation of mesoporosity in the structure increased the conversion of biomass and maximized the life of the catalyst [303].

The types of zeolites used for biomass conversion include ZSM-5, beta zeolite, Y zeolite, mordenite, silicoaluminophosphate and other porous materials. The shape selectivity of these materials is one of the factors in the behavior in formation of mono-branch-chain unsaturated fatty acid. This factor in processes of biomass conversion using zeolites, was studied closely because of little understanding about it, and the reaction was the conversion of glucose to aromatics by catalytic fast pyrolysis. Studying the kinetic diameters of reactants and products and the occurrence of reactions inside the pores as in external surface verified that aromatic products and reactants occurred inside the pores in medium-and large-pore zeolites, while in smaller pore structures the locale was the external surface [304].

The use of beta zeolite for biomass conversion processes is the most highlighted. This structure can be modified with the introduction of heteroatoms to increase the Lewis acidity, improving the conversion. One main structure used is the Sn β zeolite, constructed in an ordered 3D network of SiO₂ and presenting some Si atoms replaced by Sn atoms. The high activity as a catalyst is evidenced in sugar isomerization or epimerization, production of lactates from carbohydrates, Baeyer–Villiger oxidation, and Meerwein–Ponndorf–Verley reactions. In this structure, there is a combination of Brønsted and Lewis acidity, giving suitable conditions for biomass conversion reactions, such as conversions from carbohydrates to chemicals, for instance, the conversion of glucose in 5-hydroxymethylfurfural (HMF), where the Lewis sites catalyze the conversion of glucose to fructose and the Brønsted sites catalyze the dehydration for 5-HMF formation [305]. The production of furfural, a compound derived from lignocellulosic biomass with more than 200,000 annual tons produced, has been achieved by applying H-beta zeolite as catalyst, presenting a bifunctional nature, such as those structures with Sn in the framework. In this case, the isomerization reaction was in xylose and arabinose before the dehydration. Depending on the composition of biomass feedstock for this purpose, H-beta can be used together with H-mordenite if the presence of xylose is high in hemicellulose fraction [306]. The acidity in zeolite structure is improved by metal clusters and nanoparticles, making the biomass processes conversion better, solving problems as metal coalescence, sintering and leaching [307]. Figure 17 shows pathways to obtain a product from carbohydrates.

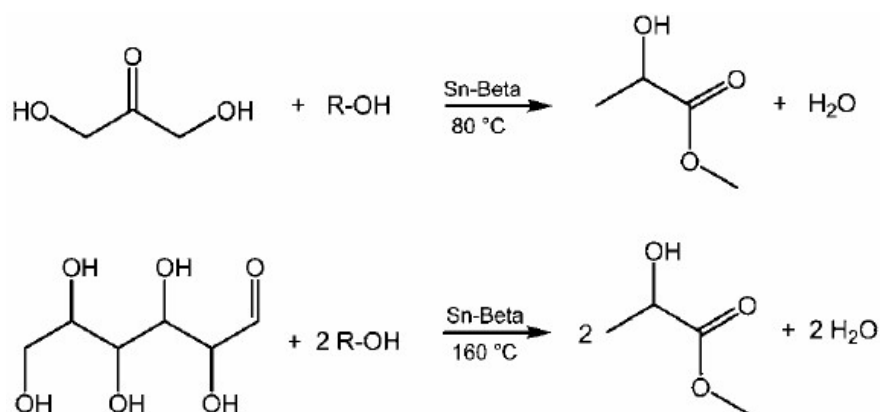


Figure 17. Lewis acid zeolite Sn-Beta catalyzing the formation of methyl lactate from a triose and hexose. Reproduced from [299]. Copyright 2011 Royal Society of Chemistry.

4.6. Enzyme Immobilization

The high applicability of enzymes in industrial processes and their favorable characteristics for processes, such as low toxicity, high conversion rate in ambient production conditions, high selectivity and high specificity, have been decisive in the improvement of their use in the pharmaceutical and textile industries, food and paper production, and water treatment [308]. Some aspects of the use of enzymes as biocatalysts for industrial purposes include the improvement of their stability under conditions of pH, use of organic solvents, temperature and pressure. Their high solubility in aqueous media leads to a difficult separation from reaction medium. The conventional use of enzymes can cause their loss from the process, even if it presents high activity, requiring the insertion of more enzymatic load in the process, burdening it [309]. The immobilization methods employed influence the specificity, selectivity and activity of the enzymatic molecules. As they are fixed to a solid material, their removal from the medium is facilitated, minimizing contamination and inhibition of the final product, enabling its recovery, minimizing aspecific adsorption and microbial contamination [310,311].

The immobilization consists of the confinement of the enzymatic structure in a different phase from the one that the substrate and the products are presented. This phase is called matrix or support, which can be zeolitic structures [312], and must be inert, have high physical resistance, stability, regenerability, ability to improve activity, and enzymatic specificity [313].

There are factors that can influence the performance of immobilized enzymes, such as the hydrophobic partition, the microenvironment in which the support is found, the presence of several binding points, the possibility of immobilization of different types of enzymes, diffusion constraints and the presence of substrates or inhibitors [314]. Other factors include the porosity of the support, the modes of enzyme–support binding and the physical nature of the support [311].

Among the characteristics of zeolites that provide utility for this process are their mechanical strength, enabling their resistance to different pressures and experimental conditions [315], and the possibility of surface modification, allowing the insertion of compounds that facilitate the binding of the enzyme [316]. The possibility of synthesizing these supports with ideal characteristics such as morphology, porosity and presence of micropores allows better interaction between the enzyme and the substrate [317]. The mechanical stability and chemical inertia of the support, in addition to its ecologically favorable and nonpolluting nature, close the useful characteristics of these materials to immobilization [318]. Figure 18 shows the types of enzyme immobilization on carriers such as zeolites.

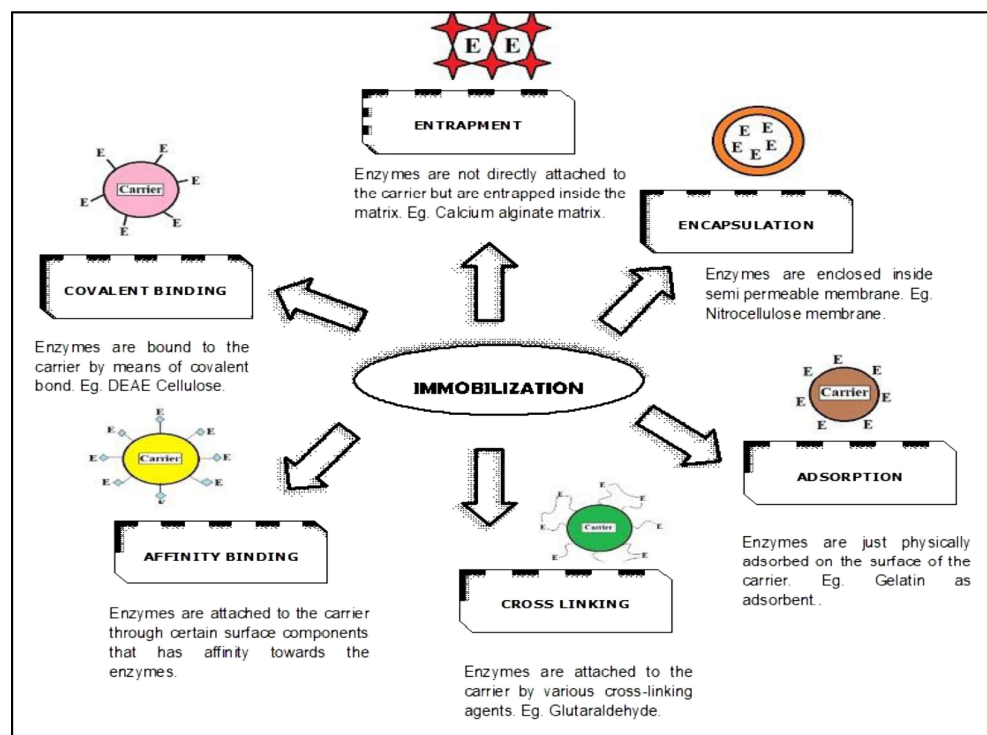


Figure 18. Methods of immobilization of enzymes onto carriers. Reproduced from [316]. Copyright 2020 Elsevier.

Adsorption or physisorption is the simplest and least expensive method, occurring due to aspecific weak-force interactions such as van der Waals interactions, hydrogen bonding, electrostatic interactions and hydrophobic interactions [319]. Because these interactions are weak, the enzyme can easily undergo a desorption process as a result of environmental parameters such as pH, ionic strength, temperature and pressure [320]. Such weak interactions do not change the structure of the enzyme, preserving its active site and maintaining its activity [321]. Protein adsorption has occurred in mesoporous silicates with narrow pore distribution range. In these porous materials, the presence of silanol groups is essential to effect adsorption by hydrogen bonding [311] (p. 37). There is good stability of the lipase enzyme against factors such as pH and temperature when immobilized by physical adsorption with respect to its free form. This immobilization protects its structure when changes in pH and temperature occur, delaying its denaturation [309] (p. 37).

In zeolitic structures, adsorption can generate heterogeneous catalysts with high activity due to the presence of Si-OH groups, allowing catalysis of a reaction in a considerable number of cycles [322]. The Si/Al ratio is one of the determining properties of enzymatic adsorption, as this parameter determines surface properties as well as hydrophilicity/hydrophobicity and ion exchange capacity. This effect could be evaluated in the immobilization of pancreatic porcine lipase. The presence of heteroatoms in structures such as Fe in ZSM-5 has promoted improvement in immobilization.

Immobilization of enzymes on the support through covalent bonding occurs due to the presence of amino acid side chains such as lysine, arginine, aspartic acid, cysteine, glutamic acid and histidine via their functional groups such as carboxyl, sulfhydryl, hydroxyl, imidazole, amino, epoxy, thiol and phenol [323]. The enzyme-support interaction is strong and generally requires activation of the support through Schiff bases and carbodiimide, where glutaraldehyde and glyoxal are the main groups used, as well as spacers in the structure, offering simplicity and enzyme preparations with stability [309–311] (p. 37). Zeolitic supports have been used for this immobilization, such as nanoporous zeolite, used in the immobilization of α -amylase, resulting in an increase in stability and a decrease in denaturation [324].

Glutaraldehyde has been the most used ligand in the immobilization of enzymes in zeolitic structures of different topologies, namely, glucose oxidase@MFI, amylase@LTA, laccase@SOD, lipase@MFI, lipase@GIS/LTA/BEA/FAU. In addition to this, other binding agents used are glyme and ethylenediamine. Sometimes metallic ions and metallic nanoparticles can be used as ligands according to their affinities. The formation of enzyme-zeolite composites can occur by the fusion of terminal carbon and terminal nitrogen of enzymes producing fused bifunctional proteins.

The enzyme immobilization process by entrapment and encapsulation are irreversible processes in which the macromolecule is in physical confinement in the support structure. The entrapment matrix, composed of several subunits of the immobilized enzyme, differs from the encapsulation that consists of a support unit with the catalyst inside [325]. In this process, there is no chemical interaction between the enzyme and the support and thus it does not undergo structural modification [326]. These forms of immobilization can make the interaction of the enzyme with the substrate more difficult due to mass transfer limitations. Thus, the material must have adequate morphology and porosity to allow the passage of substrate and products through the pores and retention of the enzyme. Both forms of immobilization guarantee an increase in the mechanical strength of the system [309] (p. 37).

The use of zeolitic supports in the encapsulation and entrapment of enzymatic macromolecules has occurred in ZIF-8 structures. This is an MOF-like structure with isomorphism to a zeolitic structure, presenting imidazolate structures in the network [327]. In this structure, the lipase enzyme could be encapsulated, modulated by a surfactant, showing good thermal stability in the range of 50 to 70 °C, good storage stability (20 days) and catalyst recovery in six cycles, and stability to solvent denaturation [325]. The use of this structure can occur in the encapsulation of the HRP enzyme and can also form a hybrid HRP@ZIF-8/DNA system [328].

In the cross-linking method, an agent containing functional groups is used for the interaction between enzymes or in the formation of the enzyme–support complex. This method can be used in combination with others with lower immobilization efficiency, such as adsorption, improving the stability of the macromolecule [329]. This method can be used in the formation of enzymatic aggregates forming structures called CLEA (cross-linked enzyme aggregates), allowing the retention of high activity in the biocatalyst, in addition to high stability and recycling [330]. Its formation process involves mixing an aqueous solution of proteins with organic solvents, salt anions or polymeric structures [309,310] (p. 37). The use of zeolites as a support for this type of immobilization is not much explored; however, the use of ZSM-5 structures to incorporate the pectinase stands out, verifying that the bifunctional catalyst obtained was ultraefficient in the catalysis of the hydrolysis of bonds of β -glycosidics, with good thermal stability and good reusability [331].

FAU Zeolites as Support for Peroxidase Enzymes

Most of the need for production of FAU (faujasite) zeolites is aimed at its use in adsorption of NH_3 [332], as catalyst for hydrogenation of 1,4-bis(phenylethynyl) benzene [333], as catalyst–adsorbent for desulfurization of fuel oil [334], as a model by Monte Carlo molecular simulation in removal of ethyl mercaptan traces from natural gas [335], as catalyst for the synthesis of coumarins [336], in separation of $\text{CO}_2/\text{N}_2\text{O}$ gases [337], and as a precursor of hierarchical zeolite used for fatty acid isomerization [338]. One of the most important characteristics of these structures is biocompatibility, allowing its use in biological systems and giving affinity in contact with the biological molecules of peroxidase. Therefore, FAU zeolites offer an alternative to peroxidase immobilization and may be used in future applications optimizing its functions as biocatalyst support, such as high sensitivity to environmental conditions, low storage stability, and low reusability. This increase in enzyme-supported performance allows better applications in oxidation of phenols, amines and aromatic compounds, often present as environmental pollutants [339].

In this scenario, the FAU zeolites offer adequate properties for immobilization of these macromolecules. There are two main possibilities for the construction of this hybrid system or enzyme–support complex. One possibility is due to the high specific surface area of most types of FAU structures, reaching values ca. $600\text{ m}^2/\text{g}$ compared to other structures commonly used in many research fields, including enzyme immobilization, and MFI structures that reach specific surface areas of ca. $300\text{ m}^2/\text{g}$, these studies about the surface area are useful for strategies of zeolite modification with chemical modifiers [340,341]. The large specific area allows an adsorption of the molecule in an adequate microenvironment for accommodation of its high molecular volume. The high framework density of 13.3 atoms T per 1000 \AA and the wide ring forming the alpha cavity makes the enzyme entrapment easier than other zeolites, increasing the stability of the immobilized biocatalyst. The second possibility for protein immobilization is the functionalization of the structure with consolidated substances that can bind covalently with amino acid residues from enzyme. Moreover, the FAU structures can be modified with good acceptability with aminosilanes such as 3-aminopropyltriethoxysilane (APTES), aminopropylmethyl-diethoxysilane (APMDES) and 3-aminopropyl-dimethyl-diethoxysilane (APDMES) [342]. This modification of FAU zeolites allows great stability of immobilized protein because of the formation of chemical bonds between the support and the biocatalyst with the chemical modifier in the interface. The Figure 19 illustrates this process.

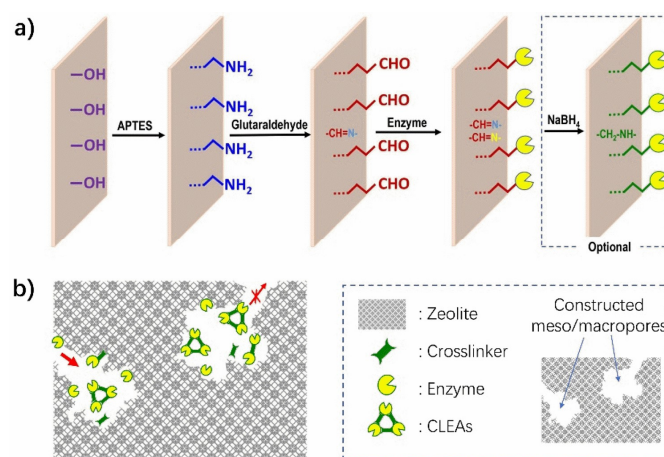


Figure 19. Schematic diagram of enzyme immobilization on zeolite through chemical methods. (a) Using glutaraldehyde for covalent anchoring; (b) entrapment of enzyme aggregates in mesoporous structure. Reproduced from [340]. Copyright 2021 Elsevier.

These two possibilities to use this consecrated structure as support for peroxidase immobilization are validated by the adequate properties of FAU zeolites. Once formed, the immobilized peroxidase can catalyze many important chemical processes, such as the hydroxylation of aromatic compounds in biotransformations [343], the soil detoxification and bioremediation of water bodies containing phenols, cresols and chlorinated phenols [344], with possible use in different reactions routes as showed for peroxygenase by Pellegrini et al. [345], in biotechnological processes such as in the development of diagnostic kits for the quantification of uric acid, glucose, cholesterol and lactose [346].

In the bioremediation of water bodies, the supported enzyme has potential use in the degradation of dyes acting in the degradation of anthraquinone dye. The removal of aromatic compounds in effluents has involved HRP and LiP enzymes, which once immobilized can be easily used in the treatment of contaminants such as anilines, hydroxyquinolines, benzidines and naphthylamines. The mineralization of recalcitrant aromatic compounds and oxidation of polycyclic aromatic compounds are other possibilities. With regard to the soil detoxification process, the immobilized enzymes can be useful in the biotransformation of atrazine herbicides such as diethylatrazine and hydroxyatrazine [344].

In the degradation of mycotoxins, peroxidases show activity against aflatoxins B1 and M1, deoxynivalenol, ochratoxin A and zearalenone. In the food industry, they stand out as indicators of the efficiency of thermal processing of fruits and vegetables due to their relatively high thermal stability, a feature that have better behavior when the enzyme is stabilized in a support [346].

Application in biotechnological processes demands knowledge of zeolite's properties, such as the low water solubility of substrates of interest, which has been remedied using hydrophobic matrices acting as a reservoir for substrates and products. The high temperature is a limiting factor for its activity. Such characteristics are considered in the elaboration of diagnostic kits in which peroxidase is very useful for generating chromogenic products at relatively low concentrations and good stability [346] (p. 40). The physical or chemical attachment of protein in FAU zeolites can maintain the low solubility because of the Si content presented in some types of zeolites with this structure such as NaY. The thermal stability offered by zeolite structure can avoid the temperature effects in enzyme optimizing its use.

The FAU zeolites are structures that deserve more attention to increase the lifetime and the activity of peroxidase enzymes through immobilization. Other research fields might develop besides the actual ones used where the product (zeolite) is just synthesized and chemically modified as in insertion of a strong acid behavior as in the use of some transition metal for incorporation of its structure. These most used applications have a limited field of study, exploring just the material properties for physicochemical processes. This structure is known to be obtained by natural precursors, e.g., wastes, increasing the value as an eco-friendly material and the incorporation of a biocatalyst, that can be obtained from natural sources as well, represents a sum of two possibilities for production a new material with wide range of applications and with less cost in comparison to the synthetic routes using organic solvents and other chemicals that offer great risk for the production process.

4.7. Zeolites in Environmental Remediation

The global changes in environment is an actual concern of many international institutions working with the screening of factors that turn ecosystems in hard conditions, such as the increase in deposition of heavy metals in water bodies, accumulation of organic compounds that offers deleterious effect for many organisms e.g., the herbicides and general pesticides disposed on soil and water and the gas evolution that gives undesirable effects for the global temperature and for the life quality of people from many cities.

Zeolite production on an industrial scale is the beginning of the discussion on the role of these products in environmental protection. Industrial interest for zeolite production began in 1954, and year by year the amount of produced material increases by hundreds of thousands of tons. The production process in scaling up is the first contribution of the material for environmental protection, because there is a necessity for aluminosilicate hydrogels or clay minerals, i.e., sources found in many natural environments requiring less use of hazardous chemicals as precursor. The temperature employed contributes to energy efficiency because low temperatures are used, another relevant contribution of zeolites for direct development of ecofriendly industrial processes. Indirectly, its production is useful for the production of fine chemicals and is part of clean technological steps used in industry, converting raw materials in more than 70,000 everyday products and as a product protagonist for biomass conversion, fuel cell development, thermal energy storage, carbon dioxide adsorption and wastewater treatment [347–349].

The amount of biomass generated in different sectors of human activity is around 100 billion tons annually, comprising energy in form of organic chemical compounds derived from the photosynthesis process in plants, although there is biomass from animals, but in less quantity. The zeolite assumes its role as catalyst when the biomass might be transformed in other types of products where the main aggregate value is the generation of energy as biofuels or compounds from fine chemistry sector, produced from a renewable source and reducing the accumulation of biomass in environment. Therefore, in this

regard, zeolites are one of the main agents to promote biomass valorization, accelerating the reactions involved and promoting less energy use in production. Biomass conversion in fuels needs two characteristics of zeolites as catalysts—acid/base catalyst or a single multifunctional catalyst—allowing the structure to convert oxygenate compounds that can generate biofuel additives and intermediates of biofuel additives as well. It is important to highlight the development of hierarchical zeolites, i.e., structures with auxiliary mesoporosity and macroporosity, increasing the performance in reactions involved [350]. In research, there are tools to make a systematic study of a particular zeolitic structure for biomass valorization as biofuel, such as the use of oleic acid as a molecule for esterification study [351]. In this scenario, computational simulations are helpful to verify the relevant structural aspects, allowing the use of the lab scale for a previous study of the viable use of a determined structure. The microalgal biomass is a promising source of hydrocarbons useful for production of biofuels and has been applied in the aviation sector. Not a complex method to cultivate, rapid growth and facile harvest with the zeolite H-ZSM-5 is used as catalyst for cracking of molecules found in this source [352].

The development of fuel cells, namely, hydrogen fuel cells, is a modern development that shows how zeolites can act in eco-friendly processes, since zeolites are used to construct fuel cells. A fuel cell can be highlighted as one of the most important products of modern era. These devices use molecules of hydrogen gas for an oxidizing process with molecular oxygen, producing water in vapor form. The advantage offered is the high energy generation by weight in comparison with batteries. Zeolites have been taking part in the development of proton exchange membrane fuel cell, (PEMFC), better in energy efficiency than diesel and gas engines, without generation of pollution or toxic by-products. The application of a composite membrane using sulfonic acid functionalized zeolites plays an essential role stabilizing the dimension and proton conductivity of membranes [353]. In this scenario, the zeolite A-supporting noble metals have helped in the purification of the hydrogen used in this type of cell [354]. Microbial fuel cells have been developed with zeolitic structures associated. These convert organic or inorganic waste in electricity with microorganisms as catalysts decomposing a determined biomass. The eco-friendly aspect involved in this device is the hydrolyzation and oxidation of a liquid waste by bacteria without emission. For this process, the anode material determines the performance of electron transfer and a zeolitic material has been focused to compose it [355].

There are other strategic research areas involving zeolites for processes focusing on environmental protection highlighting energy (thermal energy storage), adsorption of greenhouse gases such as CO₂, and water treatment. Table 1 shows some works on these topics with relevant information to match zeolites with environmental protection.

Table 1. Uses of zeolites for environmental protection in different approaches.

Approach	Zeolite Type	Main Considerations	Reference
Energy storage	13X (FAU)	A mobile thermal energy storage system was developed reducing greenhouse gas emissions.	[356]
	13X (FAU)	A process of drying was evaluated in relationship with thermal storage energy increasing the performance in 1.6 times.	[357]
	13X (FAU)	The modeling based in TES (thermal energy storage) was created varying zeolite properties with success.	[358]
	13X (FAU) with MgSO ₄ impregnated	Generation of a TES that contributes for renewable energy production with thermal and electrical energy driven with reasonable feature.	[359]

Table 1. Cont.

Approach	Zeolite Type	Main Considerations	Reference
Gas adsorption	5A (LTA)	Separation of propane and propylene, saving energy consumption involved in distillation process.	[360]
	ZK5 (KFI)	The structure synthesized by ultrasound assisting hydrothermal method showed good separation of CO ₂ /CH ₄ and CH ₄ /N ₂ mixture.	[361]
	ZSM-5 (MFI)	Good selective adsorption capacities due internal electrostatic fields in structure. Adsorption of CO ₂ with dependence of temperature.	[362]
	NaX (FAU) and CaA (LTA)	NaX presented high separation for mixture CO ₂ /CO and CaA presented high separation stability for the same mixture.	[363]
Water treatment	LTA and FAU	The mechanism of absorption of nickel metal ions was strongly related to the architecture of the pores, while the exchange of copper and lead was related to the cation exchange properties of the zeolite structure.	[364]
	A (LTA) and X (FAU)	The selectivity sequence of cation adsorption can be given as Pb ²⁺ > Cd ²⁺ > Cu ²⁺ > Zn ²⁺ > Ni ²⁺	[365]
	LTA	The adsorption of cyanide anion was tested. The cyanide loading was a maximum of 24 mg/g of zeolite and the ideal solution pH was 7 or less	[366]
	NaP (GIS) and 4A (LTA)	Structures useful in adsorption of dyes. The mechanism of the adsorption processes was controlled by three successive stages, i.e., internal diffusion, external diffusion and pore diffusion processes	[367]

5. Conclusions and Outlook

Materials science offers a large range of different crystalline structures that may present a simple chemical composition, such as the molecular sieves discussed called zeolites. These structures are obtained by various methods: high energy consumption processes due to heating and long reaction with either stirring or static conditions, or the so-called facile route of synthesis, using microwave and ultrasound to minimize reaction time, leading to energy saving. The use of mineralizer agent of an alkaline nature is necessary and influences the size of the formed particles. Other parameters such as aging, temperature, crystallization time, the use of an amorphous seed, and the use of a synthetic precursor are also of critical importance in zeolite properties.

The incorporation of heteroatoms in structures is important to improve catalytic activity by combining the (photo)catalytic property of some metals and the shape selectivity of zeolite pores. Thermal and mechanical resistance in various reaction conditions is commonly reached for these materials. As an example, the addition of zeolites to waste precursors in petroleum industry processes are necessary in order to shift to an eco-friendlier position.

The aggregation of other materials that are used as synthesis precursors to compose the zeolite framework is advantageous in the recovery of waste. Therefore, zeolite synthesis accomplishes the features of a green material, using wastes as precursors, minimizing energy costs through facile synthesis routes, and allowing the incorporation of biomolecules in microorganisms as well as catalyzing the conversion of biomass in useful molecules. These products could act as platform molecules in different applications in the pharmaceutical, food, and cosmetics sectors.

Zeolites are often called “zeozymes” because of their high specificity, even in reactions involving huge molecules. This property and other factors make them potential material for specific enzyme immobilization. Incorporating the increase in features found in these macromolecules that exists to a huge extent in the variety of zeolite structure would lead

to potential applications in biofuel production or biocatalysis. The large variety of zeolitic structures might be explored together with the large variety of enzymes from different sources to explore new potentialities. In terms of environmental protection, strategic areas have been studied, but using a restrict group of zeolite structures. Thus, the exploration of as many zeolitic structures as possible to compare performance and explore new fields would be beneficial. Other areas to consider would be the use of zeolites for environmental problems, e.g., the removal of plastics from oceans, remediation of oil leaks in different ecosystems, and reduction in NO₂ emissions from agricultural activities in order to fight against the greenhouse effect and global warming.

Author Contributions: Conceptualization, A.A.V., T.L., L.A.S.d.N. and R.L.; methodology, A.A.V., A.A.F.d.C., T.L., A.R.d.S.S. and A.d.N.d.O.; resources, L.A.S.d.N., R.C.R.N., R.L. and C.E.F.d.C.; writing—preparation of original draft, A.A.V., T.L., A.A.F.d.C. and A.d.N.d.O.; writing—proofreading and editing, G.N.d.R.F., R.C.R.N., C.E.F.d.C. and L.A.S.d.N.; visualization, R.C.R.N., R.L., G.N.d.R.F. and L.A.S.d.N.; supervision, R.L., C.E.F.d.C., G.N.d.R.F. and L.A.S.d.N.; project management, R.C.R.N., R.L. and L.A.S.d.N.; acquisition of financing, R.L., R.C.R.N., G.N.d.R.F. and L.A.S.d.N. All authors have read and agreed to the published version of the manuscript.

Funding: This work was supported by CNPQ, grant 315279/2021-4 (LASN grant) and CAPES (AAFC doctoral grant). This publication was supported by the RUDN University Strategic Academic Leadership Program (R. Luque).

Institutional Review Board Statement: Not applicable.

Informed Consent Statement: Not applicable.

Data Availability Statement: Not applicable.

Acknowledgments: The authors thank LAPAC and PROPESP/UFPA for their support.

Conflicts of Interest: The authors declare no conflict of interest.

References

1. Fu, W.; Shen, R.; Bai, E.; Zhang, L.; Chen, Q.; Fang, Z.; Li, G.; Yi, X.; Zheng, A.; Tang, T. Reaction Route and Mechanism of the Direct N-Alkylation of Sulfonamides on Acidic Mesoporous Zeolite β -Catalyst. *ACS Catal.* **2018**, *8*, 9043–9055. [[CrossRef](#)]
2. Rasmussen, K.H.; Goodarzi, F.; Christensen, D.B.; Mielby, J.; Kegnæs, S. Stabilization of Metal Nanoparticle Catalysts via Encapsulation in Mesoporous Zeolites by Steam-Assisted Recrystallization. *ACS Appl. Nano Mater.* **2019**, *2*, 8083–8091. [[CrossRef](#)]
3. Verboekend, D.; Keller, T.C.; Milina, M.; Hauert, R.; Pérez-Ramírez, J. Hierarchy Brings Function: Mesoporous Clinoptilolite and L Zeolite Catalysts Synthesized by Tandem Acid–Base Treatments. *Chem. Mater.* **2013**, *25*, 1947–1959. [[CrossRef](#)]
4. Cai, R.; Pei, X.; Pan, H.; Wan, K.; Chen, H.; Zhang, Z.; Zhang, Y. Biomass Catalytic Pyrolysis over Zeolite Catalysts with an Emphasis on Porosity and Acidity: A State-of-the-Art Review. *Energy Fuels* **2020**, *34*, 11771–11790. [[CrossRef](#)]
5. Kim, J.H.; Kim, M.; Yu, J.-S. Recycle of Silicate Waste into Mesoporous Materials. *Environ. Sci. Technol.* **2011**, *45*, 3695–3701. [[CrossRef](#)]
6. Sivalingam, S.; Sen, S. Sono-Assisted Adsorption of As(V) from Water by Rice-Husk-Ash-Derived Iron-Modified Mesoporous Zeolite Y: A Cradle-to-Cradle Solution to a Problematic Solid Waste Material. *Ind. Eng. Chem. Res.* **2019**, *58*, 14073–14087. [[CrossRef](#)]
7. Li, L.; Quan, K.; Xu, J.; Liu, F.; Liu, S.; Yu, S.; Xie, C.; Zhang, B.; Ge, X. Liquid Hydrocarbon Fuels from Catalytic Cracking of Waste Cooking Oils Using Basic Mesoporous Molecular Sieves K₂O/Ba-MCM-41 as Catalysts. *ACS Sustain. Chem. Eng.* **2013**, *1*, 1412–1416. [[CrossRef](#)]
8. Gomes, J.F.; Sachse, A.; Gregório, J.R.; Bernardo-Gusmão, K.; Schwanke, A.J. Sustainable Synthesis of Hierarchical MWW Zeolites Using Silica from an Agro-Industrial Waste, Rice Husk Ash. *Cryst. Growth Des.* **2020**, *20*, 178–188. [[CrossRef](#)]
9. Anis, S.F.; Khalil, A.; Saepurahman; Singaravel, G.; Hashaikeh, R. A Review on the Fabrication of Zeolite and Mesoporous Inorganic Nanofibers Formation for Catalytic Applications. *Microporous Mesoporous Mater.* **2016**, *236*, 176–192. [[CrossRef](#)]
10. Deimund, M.A.; Harrison, L.; Lunn, J.D.; Liu, Y.; Malek, A.; Shayib, R.; Davis, M.E. Effect of Heteroatom Concentration in SSZ-13 on the Methanol-to-Olefins Reaction. *ACS Catal.* **2016**, *6*, 542–550. [[CrossRef](#)]
11. Longhi, M.A.; Rodríguez, E.D.; Bernal, S.A.; Provis, J.L.; Kirchheim, A.P. Valorisation of a kaolin mining waste for the production of geopolymers. *J. Clean. Prod.* **2016**, *115*, 265–272. [[CrossRef](#)]
12. Hong, J.L.X.; Maneerung, T.; Koh, S.N.; Kawi, S.; Wang, C.H. Conversion of Coal Fly Ash into Zeolite Materials: Synthesis and Characterizations, Process Design and its Cost-Benefit Analysis. *Ind. Eng. Chem. Res.* **2017**, *56*, 11565–11574. [[CrossRef](#)]

13. Belviso, C.; Abdolrahimi, M.; Peddis, D.; Gagliano, E.; Sgroi, M.; Lettino, A.; Roccaro, P.; Vagliasindi, F.G.A.; Falciglia, P.P.; Di Bella, G.; et al. Synthesis of zeolite from volcanic ash: Characterization and application for cesium removal. *Microporous Mesoporous Mater.* **2021**, *319*, 111045. [[CrossRef](#)]
14. Pang, T.; Yang, X.; Yuan, C.; Elzatahry, A.A.; Alghamdi, A.; He, X.; Cheng, X.; Deng, Y. Recent Advance in Synthesis and Application of Heteroatom Zeolites. *Chin. Chem. Lett.* **2021**, *32*, 328–338. [[CrossRef](#)]
15. Li, J.; Yu, J.; Xu, R. Progress in Heteroatom-Containing Aluminophosphate Molecular Sieves. *Proc. R. Soc. A* **2012**, *468*, 1955–1967. [[CrossRef](#)]
16. Xing, P.; Wang, C.; Zeng, L.; Ma, B.; Wang, L.; Chen, Y.; Yang, C. Lithium Extraction and Hydroxysodalite Zeolite Synthesis by Hydrothermal Conversion of α -Spodumene. *ACS Sustain. Chem. Eng.* **2019**, *7*, 9498–9505. [[CrossRef](#)]
17. Bai, S.; Zhou, L.; Chang, Z.; Zhang, C.; Chu, M. Synthesis of Na-X zeolite from Longkou oil shale ash by alkaline fusion hydrothermal method. *Carbon Resour. Convers.* **2018**, *1*, 245–250. [[CrossRef](#)]
18. Wajima, T.; Haga, M.; Kuzawa, K.; Ishimoto, H.; Tamada, O.; Ito, K.; Nishiyama, T.; Downs, R.T.; Rakovan, J.F. Zeolite synthesis from paper sludge ash at low temperature (90 °C) with addition of diatomite. *J. Hazard. Mater.* **2006**, *132*, 244–252. [[CrossRef](#)]
19. Li, Y.; Peng, T.; Man, W.; Ju, L.; Zheng, F.; Zhang, M.; Guo, M. Hydrothermal synthesis of mixtures of NaA zeolite and sodalite from Ti-bearing electric arc furnace slag. *RSC Adv.* **2016**, *6*, 8358–8366. [[CrossRef](#)]
20. Blatov, V.A.; Blatova, O.A.; Daeyaert, F.; Deem, M.W. Nanoporous Materials with Predicted Zeolite Topologies. *RSC Adv.* **2020**, *10*, 17760–17767. [[CrossRef](#)]
21. Zeng, X.; Hu, X.; Song, H.; Xia, G.; Shen, Z.Y.; Yu, R.; Moskovits, M. Microwave synthesis of zeolites and their related applications. *Microporous Mesoporous Mater.* **2021**, *323*, 111262. [[CrossRef](#)]
22. Li, X.; Li, B.; Mao, H.; Shah, A.T. Synthesis of Mesoporous Zeolite Ni-MFI with High Nickel Contents by Using the Ionic Complex [(C₄H₉)₄N]⁺+2[Ni(EDTA)]²⁻ as a Template. *J. Colloid Interface Sci.* **2009**, *332*, 444–450. [[CrossRef](#)] [[PubMed](#)]
23. Reddy, G.R.; Balasubramanian, S.; Chennakesavulu, K. Zeolite Encapsulated Active Metal Composites and Their Photocatalytic Studies for Rhodamine-B, Reactive Red-198 and Chloro-Phenols. *RSC Adv.* **2015**, *5*, 81013–81023. [[CrossRef](#)]
24. Aziz, A.; Park, H.; Kim, S.; Kim, K.S. Phenol and Ammonium Removal by Using Fe-ZSM-5 Synthesized by Ammonium Citrate Iron Source. *Int. J. Environ. Sci. Technol.* **2016**, *13*, 2805–2816. [[CrossRef](#)]
25. Costa, M.J.; Marszewska, J.; Gonçalves, A.A.S.; Souza, L.K.C.; Araújo, A.S.; Jaroniek, M. Microwave-assisted single-surfactant templating synthesis of mesoporous zeolites. *RSC Adv.* **2016**, *6*, 54956–54963. [[CrossRef](#)]
26. Einicke, W.-D.; Uhlig, H.; Enke, D.; Gläser, R.; Reichenbach, C.; Ebbinghaus, S.G. Synthesis of hierarchical micro/mesoporous Y-zeolites by pseudomorphic transformation. *Colloids Surf. A Physicochem. Eng. Asp.* **2013**, *437*, 108–112. [[CrossRef](#)]
27. Singh, B.K.; Kim, Y.; Kwon, S.; Na, K. Synthesis of Mesoporous Zeolites and Their Opportunities in Heterogeneous Catalysis. *Catalysts* **2021**, *11*, 1541. [[CrossRef](#)]
28. Larin, V.A. The Loewenstein rule: The increase in electron kinetic energy as the reason for instability of Al-O-Al linkage in aluminosilicate zeolites. *Phys. Chem. Miner.* **2013**, *40*, 771–780. [[CrossRef](#)]
29. Gou, Y.; Xiao, L.; Yang, Y.; Guo, X.; Zhang, F.; Zhu, W.; Xiao, Q. Incorporation of Open-Pore MFI Zeolite Nanosheets in Polydimethylsiloxane (PDMS) to Isomer-Selective Mixed Matrix Membranes. *Microporous Mesoporous Mater.* **2021**, *315*, 110930. [[CrossRef](#)]
30. Si, D.; Zhu, M.; You, R.; Li, Y.; Wu, T.; Gui, T.; Hu, N.; Kumakiri, I.; Chen, X.; Kita, H. Influences of Alkali Metal Fluoride and Si/Al Ratio on Preparation Aluminum-Rich ZSM-5 Zeolite Membrane without Organic Template. *Microporous Mesoporous Mater.* **2021**, *324*, 111286. [[CrossRef](#)]
31. Mahima Kumar, M.; Irshad, K.A.; Jena, H. Removal of Cs⁺ and Sr²⁺ Ions from Simulated Radioactive Waste Solutions Using Zeolite-A Synthesized from Kaolin and Their Structural Stability at High Pressures. *Microporous Mesoporous Mater.* **2021**, *312*, 110773. [[CrossRef](#)]
32. Wang, B.; Ren, L.; Zhang, J.; Peng, R.; Jin, S.; Guan, Y.; Xu, H.; Wu, P. Ultrafast Synthesis of High-Silica Beta Zeolite from Dealuminated MOR by Interzeolite Transformation for Methanol to Propylene Reactions. *Microporous Mesoporous Mater.* **2021**, *314*, 110894. [[CrossRef](#)]
33. Pu, X.; Liu, N.; Shi, L. Acid Properties and Catalysis of USY Zeolite with Different Extra-Framework Aluminum Concentration. *Microporous Mesoporous Mater.* **2015**, *201*, 17–23. [[CrossRef](#)]
34. Rybakov, A.A.; Larin, A.V.; Zhidomirov, G.M. Influence of Alkali Cations on the Inter-Conversion of Extra-Framework Aluminium Species in Dealuminated Zeolites. *Microporous Mesoporous Mater.* **2014**, *189*, 173–180. [[CrossRef](#)]
35. Liu, C.; Li, G.; Hensen, E.J.M.; Pidko, E.A. Nature and Catalytic Role of Extraframework Aluminum in Faujasite Zeolite: A Theoretical Perspective. *ACS Catal.* **2015**, *5*, 7024–7033. [[CrossRef](#)]
36. Pidko, E.A.; Hensen, E.J.M.; van Santen, R.A. Self-Organization of Extraframework Cations in Zeolites. *Proc. R. Soc. A* **2012**, *468*, 2070–2086. [[CrossRef](#)]
37. Meeprasert, J.; Kungwan, N.; Jungsuttiwong, S.; Namuangruk, S. Location and Reactivity of Extra-Framework Cation in the Alkali Exchanged LTL Zeolites: A Periodic Density Functional Study. *Microporous Mesoporous Mater.* **2014**, *195*, 227–239. [[CrossRef](#)]
38. Yi, X.; Liu, K.; Chen, W.; Li, J.; Xu, S.; Li, C.; Xiao, Y.; Liu, H.; Guo, X.; Liu, S.-B.; et al. On the Origin and Structure Characteristics of Tri-Coordinated Extraframework Aluminum Species in Dealuminated Zeolites. *J. Am. Chem. Soc.* **2018**, *35*, 4819. [[CrossRef](#)]
39. Channon, Y.M.; Catlow, C.R.A.; Jackson, R.A.; Owens, S.L. A Computational Investigation into the Effect of Extra Framework Cations on the Structural Composition of Heulandite-Type Zeolites. *Microporous Mesoporous Mater.* **1998**, *24*, 153–161. [[CrossRef](#)]

40. Lozinska, M.M.; Miller, D.N.; Brandani, S.; Wright, P.A. Hiding Extra-Framework Cations in Zeolites L and Y by Internal Ion Exchange and Its Effect on CO₂ Adsorption. *J. Mater. Chem. A* **2020**, *8*, 3280–3292. [[CrossRef](#)]
41. Xia, Y.; Mokaya, R. Highly Ordered Mesoporous Silicon Oxynitride Materials as Base Catalysts. *Angew. Chem.* **2003**, *42*, 2639–2644. [[CrossRef](#)] [[PubMed](#)]
42. Čejka, J.; Morris, R.E.; Nachtigall, P. *Zeolites in Catalysis Properties and Applications*; Royal Society of Chemistry: London, UK, 2017; ISBN 978-1-78262-784-5.
43. Zhang, J.; Yue, Q.; Mazur, M.; Opanasenko, M.; Shamzhy, M.V.; Čejka, J. Selective Recovery and Recycling of Germanium for the Design of Sustainable Zeolite Catalysts. *ACS Sustain. Chem. Eng.* **2020**, *8*, 8235–8246. [[CrossRef](#)]
44. Yabushita, M.; Osga, R.; Muramatsu, A. Control of Location and Distribution of Heteroatoms Substituted Isomorphously in Framework of Zeolites and Zeotype Materials. *CrystEngComm* **2021**, *23*, 6226–6233. [[CrossRef](#)]
45. Bregante, D.T.; Tan, J.Z.; Sutrisno, A.; Flaherty, D.W. Heteroatom Substituted Zeolite FAU with Ultralow Al Contents for Liquid-Phase Oxidation Catalysis. *Catal. Sci. Technol.* **2020**, *10*, 635–647. [[CrossRef](#)]
46. Li, L.; Slater, B.; Yan, Y.; Wang, C.; Li, Y.; Yu, J. Necessity of Heteroatoms for Realizing Hypothetical Aluminophosphate Zeolites: A High-Throughput Computational Approach. *J. Phys. Chem. Lett.* **2019**, *10*, 1411–1415. [[CrossRef](#)] [[PubMed](#)]
47. Arce-Molina, J.; Grau-Crespo, R.; Lewis, D.W.; Ruiz-Salvador, A.R. Screening Heteroatom Distributions in Zeotype Materials Using an Effective Hamiltonian Approach: The Case of Aluminogermanate PKU-9. *Phys. Chem. Chem. Phys.* **2018**, *20*, 18047–18055. [[CrossRef](#)]
48. Trachta, M.; Bulánek, R.; Bludský, O.; Rubeš, M. Brønsted acidity in zeolites measured by deprotonation energy. *Sci. Rep.* **2022**, *12*, 7301. [[CrossRef](#)]
49. Bian, C.; Wang, X.; Yu, L.; Zhang, F.; Zhang, J.; Fei, Z.; Qiu, J.; Zhu, L. Generalized Methodology for Inserting Metal Heteroatoms into the Layered Zeolite Precursor RUB-36 by Interlayer Expansion. *Crystals* **2020**, *10*, 530. [[CrossRef](#)]
50. Montejo-Valencia, B.D.; Pagán-Torres, Y.J.; Martínez-Iñesta, M.M.; Curet-Arana, M.C. Density Functional Theory (DFT) Study To Unravel the Catalytic Properties of M-Exchanged MFI, (M = Be, Co, Cu, Mg, Mn, Zn) for the Conversion of Methane and Carbon Dioxide to Acetic Acid. *ACS Catal.* **2017**, *7*, 6719–6728. [[CrossRef](#)]
51. Kang, J.H.; Alshafei, F.H.; Zones, S.I.; Davis, M.E. Cage-Defining Ring: A Molecular Sieve Structural Indicator for Light Olefin Product Distribution from the Methanol-to-Olefins Reaction. *ACS Catal.* **2019**, *9*, 6012–6019. [[CrossRef](#)]
52. Brunner, G.O.; Meier, W.M. Framework density distribution of zeolite-type tetrahedral nets. *Nature* **1989**, *337*, 146–147. [[CrossRef](#)]
53. Jensen, Z.; Kim, E.; Kwon, S.; Gani, T.Z.H.; Román-Leshkov, Y.; Moliner, M.; Corma, A.; Olivetti, E. A Machine Learning Approach to Zeolite Synthesis Enabled by Automatic Literature Data Extraction. *ACS Cent. Sci.* **2019**, *5*, 892–899. [[CrossRef](#)] [[PubMed](#)]
54. Hyde, S.; Ninham, B.W.; Andersson, S.; Larsson, K.; Landh, T.; Blum, Z.; Lidin, S. The Lessons of Chemistry. In *The Language of Shape*; Elsevier: Amsterdam, The Netherlands, 1997; pp. 43–85. ISBN 978-0-444-81538-5.
55. Marler, B.; Krysiak, Y.; Kolb, U.; Grafweg, C.; Gies, H. Two New Members of the Silica-X Family of Materials: RUB-5, a Silica Zeolite with a Very High Framework Density and RUB-6, a Hydrous Layer Silicate. *Microporous Mesoporous Mater.* **2020**, *296*, 109981. [[CrossRef](#)]
56. Stixrude, L. Rings, Topology, and the Density of Tectosilicates. *Am. Mineral.* **1990**, *75*, 11.
57. Zwijnenburg, M.A.; Bell, R.G. Absence of Limitations on the Framework Density and Pore Size of High-Silica Zeolites. *Chem. Mater.* **2008**, *20*, 3008–3014. [[CrossRef](#)]
58. Styczeń, J.; Barnat-Hunek, D.; Panek, R.; Franus, W. The Microstructural and Physical Properties of Renovation Renders with Clinoptilolite, Na-P1 and Na-X Zeolites. *Constr. Build. Mater.* **2020**, *261*, 120016. [[CrossRef](#)]
59. Luna, F.J.; Schuchardt, U. Modificação de zeólitas para uso em catálise. *Quím. Nova* **2001**, *24*, 885–892. [[CrossRef](#)]
60. Mahoney, L.; Emdadi, L.; Leff, A.C.; Tran, D.T.; Wu, W.; Cheng, S.; Liu, D.; Nguyen, C.K.; Lee, I.C. Influences of Metal-Modification and Lamellar Zeolite Structure on Ethylene to Liquid Aromatics Conversion Reaction Using MFI Catalysts. *Fuel* **2019**, *256*, 115953. [[CrossRef](#)]
61. Xu, L.; Choudhary, M.K.; Muraoka, K.; Chaikittisilp, W.; Wakihara, T.; Rimer, J.D.; Okubo, T. Bridging the Gap between Structurally Distinct 2D Lamellar Zeolitic Precursors through a 3D Germanosilicate Intermediate. *Angew. Chem.* **2019**, *131*, 14671–14675. [[CrossRef](#)]
62. Chen, Y.; Cong, S.; Wang, Q.; Han, H.; Lu, J.; Kang, Y.; Kang, W.; Wang, H.; Han, S.; Song, H.; et al. Optimization of Crystal Growth of Sub-Micron ZSM-5 Zeolite Prepared by Using Al(OH)₃ Extracted from Fly Ash as an Aluminum Source. *J. Hazard. Mater.* **2018**, *349*, 18–26. [[CrossRef](#)]
63. Xu, L.; Wu, P. Diversity of Layered Zeolites: From Synthesis to Structural Modifications. *New J. Chem.* **2016**, *40*, 3968–3981. [[CrossRef](#)]
64. Emdadi, L.; Liu, D. One-Step Dual Template Synthesis of Hybrid Lamellar-Bulk MFI Zeolite. *J. Mater. Chem. A* **2014**, *2*, 13388. [[CrossRef](#)]
65. Shamzhy, M.; Gil, B.; Opanasenko, M.; Roth, W.J.; Čejka, J. MWW and MFI Frameworks as Model Layered Zeolites: Structures, Transformations, Properties, and Activity. *ACS Catal.* **2021**, *11*, 2366–2396. [[CrossRef](#)]
66. Xu, H.; Wu, P. New Trends in Layered Zeolites. In *Zeolites—New Challenges*; Margeta, K., Farkaš, A., Eds.; IntechOpen: London, UK, 2020; ISBN 978-1-78985-469-5.
67. Díaz, U. Layered Materials with Catalytic Applications: Pillared and Delaminated Zeolites from MWW Precursors. *ISRN Chem. Eng.* **2012**, *2012*, 1–35. [[CrossRef](#)]

68. Sardar, M.; Maharana, M.; Manna, M.; Sen, S. 2D Zeolites. In *Layered 2D Advanced Materials and Their Allied Applications*; Inamuddin, Boddula, R., Ahamed, M.I., Asiri, A.M., Eds.; Wiley: Hoboken, NJ, USA, 2020; pp. 193–210. ISBN 978-1-119-65496-4.
69. Guisnet, M.; Ribeiro, F.R. *Zeólitos Um Nanomundo ao Serviço da Catálise*; Calouste Gulbenkian Foundation: Lisbon, Portugal, 2004; ISBN 9723110717.
70. De Souza, V.; Villarroel-Rocha, J.; de Araújo, M.; Sapag, K.; Pergher, S. Basic Treatment in Natural Clinoptilolite for Improvement of Physicochemical Properties. *Minerals* **2018**, *8*, 595. [[CrossRef](#)]
71. Pratti, L.M.; Reis, G.M.; dos Santos, F.S.; Gonçalves, G.R.; Freitas, J.C.C.; de Pietre, M.K. Effects of Textural and Chemical Properties of β -Zeolites on Their Performance as Adsorbents for Heavy Metals Removal. *Environ. Earth Sci.* **2019**, *78*, 553. [[CrossRef](#)]
72. López-Fonseca, R.; de Rivas, B.; Gutiérrez-Ortiz, J.I.; González-Velasco, J.R. Characterisation of the Textural Properties of Chemically Dealuminated Y Zeolites. In *Studies in Surface Science and Catalysis*; Elsevier: Amsterdam, The Netherlands, 2002; Volume 144, pp. 717–722. ISBN 978-0-444-51261-1.
73. Silva, B.J.B.; Sousa, L.V.; Sarmiento, L.R.A.; Carvalho, R.P.; Quintela, P.H.L.; Pacheco, J.G.A.; Fréty, R.; Silva, A.O.S. Effect of Desilication on the Textural Properties, Acidity and Catalytic Activity of Zeolite ZSM-23 Synthesized with Different Structure-Directing Agents. *Microporous Mesoporous Mater.* **2019**, *290*, 109647. [[CrossRef](#)]
74. Saxena, S.K.; Kumar, M.; Viswanadham, N. Studies on Textural Properties of Lanthanum-Exchanged Y Zeolites as Promising Materials for Value Upgradation of Jatropa Oil. *J. Mater. Sci.* **2013**, *48*, 7949–7959. [[CrossRef](#)]
75. Derkowski, A.; Franus, W.; Waniak-Nowicka, H.; Czimerová, A. Textural Properties vs. CEC and EGME Retention of Na-X Zeolite Prepared from Fly Ash at Room Temperature. *Int. J. Miner. Process.* **2007**, *82*, 57–68. [[CrossRef](#)]
76. Sikora, B.J.; Winnegar, R.; Proserpio, D.M.; Snurr, R.Q. Textural Properties of a Large Collection of Computationally Constructed MOFs and Zeolites. *Microporous Mesoporous Mater.* **2014**, *186*, 207–213. [[CrossRef](#)]
77. Price, L.; Leung, K.; Sartbaeva, A. Local and Average Structural Changes in Zeolite A upon Ion Exchange. *Magnetochemistry* **2017**, *3*, 42. [[CrossRef](#)]
78. Shwan, S.; Skoglundh, M.; Lundegaard, L.F.; Tiruvalam, R.R.; Janssens, T.V.W.; Carlsson, A.; Vennestrøm, P.N.R. Solid-State Ion-Exchange of Copper into Zeolites Facilitated by Ammonia at Low Temperature. *ACS Catal.* **2015**, *5*, 16–19. [[CrossRef](#)]
79. Wang, D.; Gao, F.; Peden, C.H.F.; Li, J.; Kamasamudram, K.; Epling, W.S. Selective Catalytic Reduction of NO_x with NH_3 over a Cu-SSZ-13 Catalyst Prepared by a Solid-State Ion-Exchange Method. *ChemCatChem* **2014**, *6*, 1579–1583. [[CrossRef](#)]
80. Morante-Carballo, F.; Montalván-Burbano, N.; Carrión-Mero, P.; Espinoza-Santos, N. Cation Exchange of Natural Zeolites: Worldwide Research. *Sustainability* **2021**, *13*, 7751. [[CrossRef](#)]
81. Ursini, O.; Lilla, E.; Montanari, R. The Investigation on Cationic Exchange Capacity of Zeolites: The Use as Selective Ion Trappers in the Electrokinetic Soil Technique. *J. Hazard. Mater.* **2006**, *137*, 1079–1088. [[CrossRef](#)]
82. Munthali, M.W.; Kabwadza-Corner, P.; Johan, E.; Matsue, N. Decrease in Cation Exchange Capacity of Zeolites at Neutral PH: Examples and Proposals of a Determination Method. *J. Mater. Sci. Chem. Eng.* **2014**, *2*, 1–5. [[CrossRef](#)]
83. Li, W.; Qi, M.; Sun, X.; Chi, M.; Wan, Y.; Zheng, X.; Li, C.; Wang, L.; Dong, B. Novel Dental Adhesive Containing Silver Exchanged EMT Zeolites against Cariogenic Biofilms to Combat Dental Caries. *Microporous Mesoporous Mater.* **2020**, *299*, 110113. [[CrossRef](#)]
84. Chi, M.; Li, N.; Sharma, N.; Li, W.; Chen, C.; Dong, B.; Cheng, L.; Wang, L.; Thieringer, F.M. Positive Regulation of Osteogenesis on Titanium Surface by Modification of Nanosized Ca^{2+} -Exchanged EMT Zeolites. *Mater. Today Commun.* **2022**, *33*, 104874. [[CrossRef](#)]
85. Wiyantoko, B.; Rahmah, N. *Measurement of Cation Exchange Capacity (CEC) on Natural Zeolite by Percolation Method*; AIP Publishing: Malang, Indonesia, 2017; p. 020021.
86. Zijun, Z.; Effeney, G.; Millar, G.J.; Stephen, M. Synthesis and Cation Exchange Capacity of Zeolite W from Ultra-Fine Natural Zeolite Waste. *Environ. Technol. Innov.* **2021**, *23*, 101595. [[CrossRef](#)]
87. Watanabe, Y.; Yamada, H.; Tanaka, J.; Komatsu, Y.; Moriyoshi, Y. Ammonium Ion Exchange of Synthetic Zeolites: The Effect of Their Open-Window Sizes, Pore Structures, and Cation Exchange Capacities. *Sep. Sci. Technol.* **2005**, *39*, 2091–2104. [[CrossRef](#)]
88. Wu, D.; Sui, Y.; Chen, X.; He, S.; Wang, X.; Kong, H. Changes of Mineralogical–Chemical Composition, Cation Exchange Capacity, and Phosphate Immobilization Capacity during the Hydrothermal Conversion Process of Coal Fly Ash into Zeolite. *Fuel* **2008**, *87*, 2194–2200. [[CrossRef](#)]
89. Baek, W.; Ha, S.; Hong, S.; Kim, S.; Kim, Y. Cation Exchange of Cesium and Cation Selectivity of Natural Zeolites: Chabazite, Stilbite, and Heulandite. *Microporous Mesoporous Mater.* **2018**, *264*, 159–166. [[CrossRef](#)]
90. Serrano, D.P.; van Grieken, R. Heterogenous Events in the Crystallization of Zeolites. *J. Mater. Chem.* **2001**, *11*, 2391–2407. [[CrossRef](#)]
91. Liu, X.; Wang, Y.; Cui, X.; He, Y.; Mao, J. Influence of Synthesis Parameters on NaA Zeolite Crystals. *Powder Technol.* **2013**, *243*, 184–193. [[CrossRef](#)]
92. Belviso, C. State-of-the-Art Applications of Fly Ash from Coal and Biomass: A Focus on Zeolite Synthesis Processes and Issues. *Prog. Energy Combust. Sci.* **2018**, *65*, 109–135. [[CrossRef](#)]
93. Grand, J.; Awala, H.; Mintova, S. Mechanism of Zeolites Crystal Growth: New Findings and Open Questions. *CrystEngComm* **2016**, *18*, 650–664. [[CrossRef](#)]
94. Zhang, X.; Tang, D.; Zhang, M.; Yang, R. Synthesis of NaX Zeolite: Influence of Crystallization Time, Temperature and Batch Molar Ratio $\text{SiO}_2/\text{Al}_2\text{O}_3$ on the Particulate Properties of Zeolite Crystals. *Powder Technol.* **2013**, *235*, 322–328. [[CrossRef](#)]

95. Zhao, D.; Armutlulu, A.; Chen, Y.; Wang, Y.; Xie, R. Highly Efficient Removal of Cu(II) Using Mesoporous Sodalite Zeolite Produced from Industrial Waste Lithium-Silicon-Fume via Reactive Oxidation Species Route. *J. Clean. Prod.* **2021**, *319*, 128682. [[CrossRef](#)]
96. Gado, R.A.; Hebda, M.; Łach, M.; Mikuła, J. Alkali Activation of Waste Clay Bricks: Influence of The Silica Modulus, SiO₂/Na₂O, H₂O/Na₂O Molar Ratio, and Liquid/Solid Ratio. *Materials* **2020**, *13*, 383. [[CrossRef](#)]
97. Somerset, V. The Use of X-ray Fluorescence (XRF) Analysis in Predicting the Alkaline Hydrothermal Conversion of Fly Ash Precipitates into Zeolites. *Talanta* **2004**, *64*, 109–114. [[CrossRef](#)]
98. Burriesci, N.; Crisafulli, M.L.; Giordano, N.; Bart, J.C.J. Factors affecting formation of zeolite A from Alumino-silicate gels. *Mater. Lett.* **1984**, *2*, 401–406. [[CrossRef](#)]
99. Kim, Y.C.; Jeong, J.Y.; Hwang, J.Y.; Kim, S.D.; Kim, W.J. Influencing Factors on Rapid Crystallization of High Silica Nano-Sized Zeolite Y without Organic Template under Atmospheric Pressure. *J. Porous Mater.* **2009**, *16*, 299–306. [[CrossRef](#)]
100. Patuwan, S.Z.; Arshad, S.E. Important Synthesis Parameters Affecting Crystallization of Zeolite T: A Review. *Materials* **2021**, *14*, 2890. [[CrossRef](#)] [[PubMed](#)]
101. Zhang, J.; Lu, X.; Wang, Z. Control of Crystallization Rate and Morphology of Zeolite Silicalite-1 in Solvent-Free Synthesis. *Microporous Mesoporous Mater.* **2019**, *283*, 14–24. [[CrossRef](#)]
102. Li, X.; Kita, H.; Zhu, H.; Zhang, Z.; Tanaka, K.; Okamoto, K. Influence of the Hydrothermal Synthetic Parameters on the Pervaporative Separation Performances of CHA-Type Zeolite Membranes. *Microporous Mesoporous Mater.* **2011**, *143*, 270–276. [[CrossRef](#)]
103. Tong, X.; Xu, J.; Xin, L.; Huang, P.; Lu, H.; Wang, C.; Yan, W.; Yu, J.; Deng, F.; Sun, H.; et al. Molecular Engineering of Microporous Crystals: (VI) Structure-Directing Effect in the Crystallization Process of Layered Aluminophosphates. *Microporous Mesoporous Mater.* **2012**, *164*, 56–66. [[CrossRef](#)]
104. Lu, G.; Lu, G.Q.; Xiao, Z.M. Mechanical Properties of Porous Materials. *J. Porous Mater.* **1999**, *6*, 359–368. [[CrossRef](#)]
105. Anderson, R.L.; Ratcliffe, I.; Greenwell, H.C.; Williams, P.A.; Cliffe, S.; Coveney, P.V. Clay Swelling—A Challenge in the Oilfield. *Earth-Sci. Rev.* **2010**, *98*, 201–216. [[CrossRef](#)]
106. Gurevich, S.V. Time-Delayed Feedback Control of Breathing Localized Structures in a Three-Component Reaction–Diffusion System. *Phil. Trans. R. Soc. A* **2014**, *372*, 20140014. [[CrossRef](#)]
107. Kavooosi, N.; Bon, V.; Senkovska, I.; Krause, S.; Atzori, C.; Bonino, F.; Pallmann, J.; Paasch, S.; Brunner, E.; Kaskel, S. Tailoring Adsorption Induced Phase Transitions in the Pillared-Layer Type Metal–Organic Framework DUT-8(Ni). *Dalton Trans.* **2017**, *46*, 4685–4695. [[CrossRef](#)]
108. Rutter, M.D.; Uchida, T.; Secco, R.A.; Huang, Y.; Wang, Y. Investigation of Pressure-Induced Amorphization in Hydrated Zeolite Li-A and Na-A Using Synchrotron X-Ray Diffraction. *J. Phys. Chem. Solids* **2001**, *62*, 599–606. [[CrossRef](#)]
109. Coasne, B.; Haines, J.; Levelut, C.; Cambon, O.; Santoro, M.; Gorelli, F.; Garbarino, G. Enhanced Mechanical Strength of Zeolites by Adsorption of Guest Molecules. *Phys. Chem. Chem. Phys.* **2011**, *13*, 20096. [[CrossRef](#)] [[PubMed](#)]
110. Chapman, K.W.; Halder, G.J.; Chupas, P.J. Guest-Dependent High Pressure Phenomena in a Nanoporous Metal–Organic Framework Material. *J. Am. Chem. Soc.* **2008**, *130*, 10524–10526. [[CrossRef](#)] [[PubMed](#)]
111. Bennett, T.D.; Simoncic, P.; Moggach, S.A.; Gozzo, F.; Macchi, P.; Keen, D.A.; Tan, J.-C.; Cheetham, A.K. Reversible Pressure-Induced Amorphization of a Zeolitic Imidazolate Framework (ZIF-4). *Chem. Commun.* **2011**, *47*, 7983. [[CrossRef](#)]
112. Tse, J.S.; Klug, D.D.; Ripmeester, J.A.; Desgreniers, S.; Lagarek, K. The role of non-deformable units in pressure-induced reversible amorphization of clathrasils. *Nature* **1994**, *369*, 724–727. [[CrossRef](#)]
113. Huang, Y.; Havenga, E.A. Why Do Zeolites with LTA Structure Undergo Reversible Amorphization under Pressure? *Chem. Phys. Lett.* **2001**, *345*, 65–71. [[CrossRef](#)]
114. Tan, J.C.; Bennett, T.D.; Cheetham, A.K. Chemical Structure, Network Topology, and Porosity Effects on the Mechanical Properties of Zeolitic Imidazolate Frameworks. *Proc. Natl. Acad. Sci. USA* **2010**, *107*, 9938–9943. [[CrossRef](#)]
115. Kiely, E.; Zwane, R.; Fox, R.; Reilly, A.M.; Guerin, S. Density Functional Theory Predictions of the Mechanical Properties of Crystalline Materials. *CrystEngComm* **2021**, *23*, 5697–5710. [[CrossRef](#)]
116. Bennett, T.D.; Sotelo, J.; Tan, J.-C.; Moggach, S.A. Mechanical Properties of Zeolitic Metal–Organic Frameworks: Mechanically Flexible Topologies and Stabilization against Structural Collapse. *CrystEngComm* **2015**, *17*, 286–289. [[CrossRef](#)]
117. Ambekar, R.S.; Oliveira, E.F.; Kushwaha, B.; Pal, V.; Machado, L.D.; Sajadi, S.M.; Baughman, R.H.; Ajayan, P.M.; Roy, A.K.; Galvao, D.S.; et al. On the Mechanical Properties of Atomic and 3D Printed Zeolite-Templated Carbon Nanotube Networks. *Addit. Manuf.* **2021**, *37*, 101628. [[CrossRef](#)]
118. Astala, R.; Auerbach, S.M.; Monson, P.A. Density Functional Theory Study of Silica Zeolite Structures: Stabilities and Mechanical Properties of SOD, LTA, CHA, MOR, and MFI. *J. Phys. Chem. B* **2004**, *108*, 9208–9215. [[CrossRef](#)]
119. Göttl, F.; Hafner, J. Structure and Properties of Metal-Exchanged Zeolites Studied Using Gradient-Corrected and Hybrid Functionals. I. Structure and Energetics. *J. Chem. Phys.* **2012**, *136*, 64501. [[CrossRef](#)] [[PubMed](#)]
120. Lin, J.; Shu, X.F.; Dong, J.X. The Experimental Determination of Mechanical Properties of Zeolite Ferrierite Crystal. *Mater. Lett.* **2005**, *59*, 1595–1597. [[CrossRef](#)]
121. Griesinger, A.; Spindler, K.; Hahne, E. Measurements and Theoretical Modelling of the Effective Thermal Conductivity of Zeolites. *Int. J. Heat Mass Transfer* **1999**, *12*, 4363–4374. [[CrossRef](#)]

122. Shimonosono, T.; Hirata, Y.; Nishikawa, K.; Sameshima, S.; Sodeyama, K.; Masunaga, T.; Yoshimura, Y. Thermal Properties of Zeolite-Containing Composites. *Materials* **2018**, *11*, 420. [[CrossRef](#)] [[PubMed](#)]
123. Murashov, V.V.; White, M.A. Thermal Properties of Zeolites: Effective Thermal Conductivity of Dehydrated Powdered Zeolite 4A. *Mater. Chem. Phys.* **2002**, *75*, 178–180. [[CrossRef](#)]
124. Jakubinek, M.B.; Zhan, B.-Z.; White, M.A. Temperature-Dependent Thermal Conductivity of Powdered Zeolite NaX. *Microporous Mesoporous Mater.* **2007**, *103*, 108–112. [[CrossRef](#)]
125. Schnell, S.K.; Vlugt, T.J.H. Thermal Conductivity in Zeolites Studied by Non-Equilibrium Molecular Dynamics Simulations. *Int. J. Thermophys.* **2013**, *34*, 1197–1213. [[CrossRef](#)]
126. Demirkiran, A.Ş.; Artir, R.; Avci, E. Electrical Resistivity of Porcelain Bodies with Natural Zeolite Addition. *Ceram. Int.* **2010**, *36*, 917–921. [[CrossRef](#)]
127. Cruciani, G. Zeolites upon Heating: Factors Governing Their Thermal Stability and Structural Changes. *J. Phys. Chem. Solids* **2006**, *67*, 1973–1994. [[CrossRef](#)]
128. Castro, P.R.d.S.d.; Maia, A.Á.B.; Angélica, R.S. Study of the Thermal Stability of Faujasite Zeolite Synthesized from Kaolin Waste from the Amazon. *Mat. Res.* **2019**, *22*, e20190321. [[CrossRef](#)]
129. Nishu; Liu, R.; Rahman, M.M.; Sarker, M.; Chai, M.; Li, C.; Cai, J. A Review on the Catalytic Pyrolysis of Biomass for the Bio-Oil Production with ZSM-5: Focus on Structure. *Fuel Process. Technol.* **2020**, *199*, 106301. [[CrossRef](#)]
130. Mentzen, B.F.; Letoffe, J.-M.; Claudy, P. Enthalpy Change and Temperature of the Reversible Monoclinic-Orthorhombic Phase Transition in MFI Type Zeolitic Materials. *Thermochim. Acta* **1996**, *288*, 1–7. [[CrossRef](#)]
131. Ardit, M.; Martucci, A.; Cruciani, G. Monoclinic–Orthorhombic Phase Transition in ZSM-5 Zeolite: Spontaneous Strain Variation and Thermodynamic Properties. *J. Phys. Chem. C* **2015**, *119*, 7351–7359. [[CrossRef](#)]
132. Hoff, T.C.; Thilakarathne, R.; Gardner, D.W.; Brown, R.C.; Tessonnier, J.-P. Thermal Stability of Aluminum-Rich ZSM-5 Zeolites and Consequences on Aromatization Reactions. *J. Phys. Chem. C* **2016**, *120*, 20103–20113. [[CrossRef](#)]
133. Wu, D.; Lu, Y.; Kong, H.; Ye, C.; Jin, X. Synthesis of Zeolite From Thermally Treated Sediment. *Ind. Eng. Chem. Res.* **2008**, *47*, 295–302. [[CrossRef](#)]
134. Abdullahi, T.; Harun, Z.; Othman, M.H.D. A Review on Sustainable Synthesis of Zeolite from Kaolinite Resources via Hydrothermal Process. *Adv. Powder Technol.* **2017**, *28*, 1827–1840. [[CrossRef](#)]
135. Feng, S.; Xu, R. New Materials in Hydrothermal Synthesis. *Acc. Chem. Res.* **2001**, *34*, 239–247. [[CrossRef](#)]
136. Hartati; Prasetyoko, D.; Santoso, M.; Qoniah, I.; Leaw, W.L.; Firda, P.B.D.; Nur, H. A Review on Synthesis of Kaolin-based Zeolite and the Effect of Impurities. *J. Chin. Chem. Soc.* **2020**, *67*, 911–936. [[CrossRef](#)]
137. Murayama, N.; Yamamoto, H.; Shibata, J. Mechanism of Zeolite Synthesis from Coal Fly Ash by Alkali Hydrothermal Reaction. *Int. J. Miner. Process.* **2002**, *64*, 1–17. [[CrossRef](#)]
138. Cundy, C.S.; Cox, P.A. The Hydrothermal Synthesis of Zeolites: Precursors, Intermediates and Reaction Mechanism. *Microporous Mesoporous Mater.* **2005**, *82*, 1–78. [[CrossRef](#)]
139. Piccione, P.M.; Yang, S.; Navrotsky, A.; Davis, M.E. Thermodynamics of Pure-Silica Molecular Sieve Synthesis. *J. Phys. Chem. B* **2002**, *106*, 3629–3638. [[CrossRef](#)]
140. Salakhum, S.; Prasertsab, A.; Klinyod, S.; Saenlung, K.; Witoon, T.; Wattanakit, C. Sustainable Transformation of Natural Silica-Rich Solid and Waste to Hierarchical Zeolites for Sugar Conversion to Hydroxymethylfurfural (HMF). *Microporous Mesoporous Mater.* **2021**, *323*, 111252. [[CrossRef](#)]
141. Jiang, H.; Guan, B.; Lin, H.; Huang, Z. Cu/SSZ-13 Zeolites Prepared by in Situ Hydrothermal Synthesis Method as NH₃-SCR Catalysts: Influence of the Si/Al Ratio on the Activity and Hydrothermal Properties. *Fuel* **2019**, *255*, 115587. [[CrossRef](#)]
142. Han, L.; Zhao, X.; Yu, H.; Hu, Y.; Li, D.; Sun, D.; Liu, M.; Chang, L.; Bao, W.; Wang, J. Preparation of SSZ-13 Zeolites and Their NH₃-Selective Catalytic Reduction Activity. *Microporous Mesoporous Mater.* **2018**, *261*, 126–136. [[CrossRef](#)]
143. Mousavi, S.F.; Jafari, M.; Kazemimoghadam, M.; Mohammadi, T. Template Free Crystallization of Zeolite Rho via Hydrothermal Synthesis: Effects of Synthesis Time, Synthesis Temperature, Water Content and Alkalinity. *Ceram. Int.* **2013**, *39*, 7149–7158. [[CrossRef](#)]
144. Mohiuddin, E.; Isa, Y.M.; Mdeleleni, M.M.; Sincadu, N.; Key, D.; Tshabalala, T. Synthesis of ZSM-5 from Impure and Beneficiated Grahamstown Kaolin: Effect of Kaolinite Content, Crystallisation Temperatures and Time. *Appl. Clay Sci.* **2016**, *119*, 213–221. [[CrossRef](#)]
145. Chen, C.-T.; Iyoki, K.; Yonezawa, Y.; Okubo, T.; Wakihara, T. Understanding the Nucleation and Crystal Growth of Zeolites: A Case Study on the Crystallization of ZSM-5 from a Hydrogel System Under Ultrasonication. *J. Phys. Chem. C* **2020**, *124*, 11516–11524. [[CrossRef](#)]
146. Molina, A.; Poole, C. A Comparative Study Using Two Methods to Produce Zeolites from Fly Ash. *Miner. Eng.* **2004**, *17*, 167–173. [[CrossRef](#)]
147. Dere Ozdemir, O.; Piskin, S. A Novel Synthesis Method of Zeolite X From Coal Fly Ash: Alkaline Fusion Followed by Ultrasonic-Assisted Synthesis Method. *Waste Biomass Valorization* **2019**, *10*, 143–154. [[CrossRef](#)]
148. Ojumu, T.V.; Du Plessis, P.W.; Petrik, L.F. Synthesis of Zeolite A from Coal Fly Ash Using Ultrasonic Treatment—A Replacement for Fusion Step. *Ultrason. Sonochem.* **2016**, *31*, 342–349. [[CrossRef](#)] [[PubMed](#)]
149. Naghsh, M.; Shams, K. Synthesis of a Kaolin-Based Geopolymer Using a Novel Fusion Method and Its Application in Effective Water Softening. *Appl. Clay Sci.* **2017**, *146*, 238–245. [[CrossRef](#)]

150. Deng, L.; Xu, Q.; Wu, H. Synthesis of Zeolite-like Material by Hydrothermal and Fusion Methods Using Municipal Solid Waste Fly Ash. *Procedia Environ. Sci.* **2016**, *31*, 662–667. [[CrossRef](#)]
151. Ayele, L.; Pérez-Pariente, J.; Chebude, Y.; Díaz, I. Conventional versus Alkali Fusion Synthesis of Zeolite A from Low Grade Kaolin. *Appl. Clay Sci.* **2016**, *132–133*, 485–490. [[CrossRef](#)]
152. Lee, M.-G.; Park, J.-W.; Kam, S.-K.; Lee, C.-H. Synthesis of Na-A Zeolite from Jeju Island Scoria Using Fusion/Hydrothermal Method. *Chemosphere* **2018**, *207*, 203–208. [[CrossRef](#)] [[PubMed](#)]
153. Miao, Q.; Zhao, B.; Liu, S.; Guo, J.; Tong, Y.; Cao, J. Decomposition of the Potassic Rocks by Sub-Molten Salt Method and Synthesis of Low Silica X Zeolite: Decomposition of the Potassic Rocks and Synthesis of Zeolite. *Asia-Pac. J. Chem. Eng.* **2016**, *11*, 558–566. [[CrossRef](#)]
154. Park, M.; Choi, J. Molten-Salt Method for the Synthesis of Zeolitic Materials I. Zeolite Formation in Alkaline Molten-Salt System. *Microporous Mesoporous Mater.* **2000**, *37*, 9. [[CrossRef](#)]
155. Zhang, X.; Li, C.; Zheng, S.; Di, Y.; Sun, Z. A Review of the Synthesis and Application of Zeolites from Coal-Based Solid Wastes. *Int. J. Miner. Metall. Mater.* **2022**, *29*, 1–21. [[CrossRef](#)]
156. Zhou, H.; Mao, Y.; Wong, S.S. Shape Control and Spectroscopy of Crystalline BaZrO₃ Perovskite Particles. *J. Mater. Chem.* **2007**, *17*, 1707. [[CrossRef](#)]
157. Riley, B.J.; McFarlane, J.; DelCul, G.D.; Vienna, J.D.; Contescu, C.I.; Forsberg, C.W. Molten Salt Reactor Waste and Effluent Management Strategies: A Review. *Nucl. Eng. Des.* **2019**, *345*, 94–109. [[CrossRef](#)]
158. Yang, J.; Li, T.; Bao, X.; Yue, Y.; Liu, H. Mesoporogen-Free Synthesis of Hierarchical Sodalite as a Solid Base Catalyst from Sub-Molten Salt-Activated Aluminosilicate. *Particuology* **2020**, *48*, 48–54. [[CrossRef](#)]
159. Cheng, H.; Zhou, Y.; Liu, Q. Kaolinite Nanomaterials: Preparation, Properties and Functional Applications. In *Nanomaterials from Clay Minerals*; Elsevier: Amsterdam, The Netherlands, 2019; pp. 285–334. ISBN 978-0-12-814533-3.
160. Fernández-Jiménez, A.; de la Torre, A.G.; Palomo, A.; López-Olmo, G.; Alonso, M.M.; Aranda, M.A.G. Quantitative Determination of Phases in the Alkaline Activation of Fly Ash. Part II: Degree of Reaction. *Fuel* **2006**, *85*, 1960–1969. [[CrossRef](#)]
161. Monzón, J.D.; Gonzalez, M.R.; Mardones, L.E.; Conconi, M.S.; Pereyra, A.M.; Basaldella, E.I. The Role of Alkaline Activation in the Structural Transformations of Aluminosiliceous Industrial Wastes towards Zeolite Production. *Mater. Today Commun.* **2019**, *21*, 100624. [[CrossRef](#)]
162. Villa, C.; Pecina, E.T.; Torres, R.; Gómez, L. Geopolymer Synthesis Using Alkaline Activation of Natural Zeolite. *Constr. Build. Mater.* **2010**, *24*, 2084–2090. [[CrossRef](#)]
163. Boycheva, S.; Marinov, I.; Miteva, S.; Zgureva, D. Conversion of Coal Fly Ash into Nanozeolite Na-X by Applying Ultrasound Assisted Hydrothermal and Fusion-Hydrothermal Alkaline Activation. *Sustain. Chem. Pharm.* **2020**, *15*, 100217. [[CrossRef](#)]
164. Chen, Z.; Song, G.; Li, C.; Chen, W.; Li, Z.; Kawi, S. Coal fly ash to Y zeolite of great purity and crystallinity: A new and green activation method of combined in situ microwave and ultrasound. *Solid State Sci.* **2023**, *136*, 107102. [[CrossRef](#)]
165. Li, C.; Sun, H.; Li, L. A Review: The Comparison between Alkali-Activated Slag (Si+Ca) and Metakaolin (Si+Al) Cements. *Cem. Concr. Res.* **2010**, *40*, 1341–1349. [[CrossRef](#)]
166. Panagiotopoulou, C.; Kontori, E.; Perraki, T.; Kakali, G. Dissolution of Aluminosilicate Minerals and By-Products in Alkaline Media. *J. Mater. Sci.* **2007**, *42*, 2967–2973. [[CrossRef](#)]
167. Severo, C.G.S.; Costa, D.L.; Bezerra, I.M.T.; Menezes, R.R.; Neves, G.A. Características, particularidades e princípios científicos dos materiais ativados alcalinamente. *Rev. Eletrônica Mater. Process.* **2013**, *8*, 55–67.
168. Van Jaarsveld, J.G.S.; van Deventer, J.S.J. Effect of the Alkali Metal Activator on the Properties of Fly Ash-Based Geopolymers. *Ind. Eng. Chem. Res.* **1999**, *38*, 3932–3941. [[CrossRef](#)]
169. Palomo, Á.; Alonso, S.; Fernandez-Jiménez, A. Alkaline Activation of Fly Ashes: NMR Study of the Reaction Products. *J. Am. Ceram. Soc.* **2004**, *87*, 1141–1145. [[CrossRef](#)]
170. Tisler, Z. Clinoptilolite Foams Prepared by Alkali Activation of Natural Zeolite and Their Post-Synthesis Modifications. *Microporous Mesoporous Mater.* **2019**, *282*, 169–178. [[CrossRef](#)]
171. Granizo, M.L.; Blanco, M.T. Alkaline activation of metakaolin Na isothermal conduction calorimetry study. *J. Therm. Anal.* **1998**, *52*, 957–965. [[CrossRef](#)]
172. Youssef, H.; Ibrahim, D.; Komarneni, S. Microwave-Assisted versus Conventional Synthesis of Zeolite A from Metakaolinite. *Microporous Mesoporous Mater.* **2008**, *8*, 527–534. [[CrossRef](#)]
173. Tompsett, G.A.; Conner, W.C.; Yngvesson, K.S. Microwave Synthesis of Nanoporous Materials. *Chem. Eur. J. Chem. Phys.* **2006**, *7*, 296–319. [[CrossRef](#)]
174. Li, Y.; Yang, W. Microwave Synthesis of Zeolite Membranes: A Review. *J. Membr. Sci.* **2008**, *316*, 3–17. [[CrossRef](#)]
175. Cundy, C.S. Microwave Techniques in the Synthesis and Modification of Zeolite Catalysts. A Review. *Collect. Czech. Chem. Commun.* **1998**, *63*, 1699–1723. [[CrossRef](#)]
176. Chandrasekhar, S.; Pramada, P.N. Microwave Assisted Synthesis of Zeolite A from Metakaolin. *Microporous Mesoporous Mater.* **2008**, *108*, 152–161. [[CrossRef](#)]
177. Bunmai, K.; Osakoo, N.; Deekamwong, K.; Kosri, C.; Khemthong, P.; Wittayakun, J. Fast Synthesis of Zeolite NaP by Crystallizing the NaY Gel under Microwave Irradiation. *Mater. Lett.* **2020**, *272*, 127845. [[CrossRef](#)]
178. Le, T.; Wang, Q.; Pan, B.; Ravindra, A.V.; Ju, S.; Peng, J. Process Regulation of Microwave Intensified Synthesis of Y-Type Zeolite. *Microporous Mesoporous Mater.* **2019**, *284*, 476–485. [[CrossRef](#)]

179. Bux, H.; Liang, F.; Li, Y.; Cravillon, J.; Wiebcke, M.; Caro, J. Zeolitic Imidazolate Framework Membrane with Molecular Sieving Properties by Microwave-Assisted Solvothermal Synthesis. *J. Am. Chem. Soc.* **2009**, *131*, 16000–16001. [[CrossRef](#)] [[PubMed](#)]
180. Tayraukham, P.; Jantarit, N.; Osakoo, N.; Wittayakun, J. Synthesis of Pure Phase NaP2 Zeolite from the Gel of NaY by Conventional and Microwave-Assisted Hydrothermal Methods. *Crystals* **2020**, *10*, 951. [[CrossRef](#)]
181. Li, X.-Y.; Jiang, Y.; Liu, X.-Q.; Shi, L.-Y.; Zhang, D.-Y.; Sun, L.-B. Direct Synthesis of Zeolites from a Natural Clay, Attapulgitic. *ACS Sustain. Chem. Eng.* **2017**, *5*, 6124–6130. [[CrossRef](#)]
182. Wang, Y.; Li, T.; Li, C.; Lu, J.; Dai, C.; Subhan, F.; Bai, P.; Sun, H.; Feng, R.; Yan, Z. One-Pot Green Synthesis of Fe-ZSM-5 Zeolite Containing Framework Heteroatoms via Dry Gel Conversion for Enhanced Propylene Selectivity of Catalytic Cracking Catalyst. *J. Mater. Sci.* **2021**, *56*, 18050–18060. [[CrossRef](#)]
183. To, J.; Sokol, A.A.; French, S.A.; Catlow, C.R.A.; Sherwood, P.; van Dam, H.J.J. Formation of Heteroatom Active Sites in Zeolites by Hydrolysis and Inversion. *Angew. Chem. Int. Ed.* **2006**, *45*, 1633–1638. [[CrossRef](#)] [[PubMed](#)]
184. Gabelica, Z.; Valange, S. Use of Short Chain Alkylamines as Complexing-Mobilizing Agents: An Alternative to the “Fluoride Route” for the Synthesis of Zeolite Metallosilicate Catalysts. *Res. Chem. Intermed.* **1998**, *24*, 227–258. [[CrossRef](#)]
185. van Bokhoven, J.A.; Lamberti, C. Structure of Aluminum, Iron, and Other Heteroatoms in Zeolites by X-Ray Absorption Spectroscopy. *Coord. Chem. Rev.* **2014**, *277–278*, 275–290. [[CrossRef](#)]
186. Wu, Q.; Xu, C.; Zhu, L.; Meng, X.; Xiao, F.-S. Recent Strategies for Synthesis of Metallosilicate Zeolites. *Catal. Today* **2022**, *390–391*, 2–11. [[CrossRef](#)]
187. Valtchev, V.; Majano, G.; Mintova, S.; Pérez-Ramírez, J. Tailored Crystalline Microporous Materials by Post-Synthesis Modification. *Chem. Soc. Rev.* **2013**, *42*, 263–290. [[CrossRef](#)]
188. Montejo-Valencia, B.D.; Curet-Arana, M.C. DFT Study of the Lewis Acidities and Relative Hydrothermal Stabilities of BEC and BEA Zeolites Substituted with Ti, Sn, and Ge. *J. Phys. Chem. C* **2015**, *119*, 4148–4157. [[CrossRef](#)]
189. Julkapli, N.M.; Bagheri, S. Developments in Nano-Additives for Paper Industry. *J. Wood Sci.* **2016**, *62*, 117–130. [[CrossRef](#)]
190. Rodrigues, M.; Souza, A.; Santos, I. Brazilian Kaolin Wastes: Synthesis of Zeolite P at Low-Temperature. *Am. Chem. Sci. J.* **2016**, *12*, 1–11. [[CrossRef](#)]
191. Sánchez-Soto, P.J.; Eliche-Quesada, D.; Martínez-Martínez, S.; Pérez-Villarejo, L.; Garzón, E. Study of a Waste Kaolin as Raw Material for Mullite Ceramics and Mullite Refractories by Reaction Sintering. *Materials* **2022**, *15*, 583. [[CrossRef](#)] [[PubMed](#)]
192. Sukumar, R.; Menon, A.R.R. Organomodified Kaolin as a Reinforcing Filler for Natural Rubber. *J. Appl. Polym. Sci.* **2008**, *107*, 3476–3483. [[CrossRef](#)]
193. Roy, S.; Kar, S.; Bagchi, B.; Das, S. Development of Transition Metal Oxide–Kaolin Composite Pigments for Potential Application in Paint Systems. *Appl. Clay Sci.* **2015**, *107*, 205–212. [[CrossRef](#)]
194. Prasad, M.S.; Reid, K.J.; Murray, H.H. Kaolin: Processing, Properties and Applications. *Appl. Clay Sci.* **1991**, *6*, 87–119. [[CrossRef](#)]
195. Tan, D.; Yuan, P.; Annabi-Bergaya, F.; Liu, D.; He, H. Methoxy-Modified Kaolinite as a Novel Carrier for High-Capacity Loading and Controlled-Release of the Herbicide Amitrole. *Sci. Rep.* **2015**, *5*, 8870. [[CrossRef](#)]
196. Foroughi, M.; Salem, A.; Salem, S. Characterization of Phase Transformation from Low Grade Kaolin to Zeolite LTA in Fusion Technique: Focus on Quartz Melting and Crystallization in Presence of NaAlO₂. *Mater. Chem. Phys.* **2021**, *258*, 123892. [[CrossRef](#)]
197. Murray, H.H. Traditional and New Applications for Kaolin, Smectite, and Palygorskite: A General Overview. *Appl. Clay Sci.* **2000**, *17*, 207–221. [[CrossRef](#)]
198. Luo, W.; Hu, Q.; Fan, Z.; Wan, J.; He, Q.; Huang, S.; Zhou, N.; Song, M.; Zhang, J.; Zhou, Z. The Effect of Different Particle Sizes and HCl-Modified Kaolin on Catalytic Pyrolysis Characteristics of Reworked Polypropylene Plastics. *Energy* **2020**, *213*, 119080. [[CrossRef](#)]
199. Ukwattage, N.L.; Ranjith, P.G.; Bouazza, M. The Use of Coal Combustion Fly Ash as a Soil Amendment in Agricultural Lands (with Comments on Its Potential to Improve Food Security and Sequester Carbon). *Fuel* **2013**, *109*, 400–408. [[CrossRef](#)]
200. Zou, Y.; Yang, T. Rice Husk, Rice Husk Ash and Their Applications. In *Rice Bran and Rice Bran Oil*; Elsevier: Amsterdam, The Netherlands, 2019; pp. 207–246. ISBN 978-0-12-812828-2.
201. Pinheiro, D.D.R.; Gonçalves, L.R.; Sena, R.L.P.D.; Martelli, M.C.; Neves, R.D.F.; Ribeiro, N.F.D.P. Industrial Kaolin Waste as Raw Material in the Synthesis of the SAPO-34 Molecular Sieve. *Mat. Res.* **2020**, *23*, e20200043. [[CrossRef](#)]
202. Aparicio, P. Mineralogical Interference on Kaolinite Crystallinity Index Measurements. *Clays Clay Miner.* **1999**, *47*, 12–27. [[CrossRef](#)]
203. Menezes, R.R.; Brasileiro, M.I.; Gonçalves, W.P.; Santana, L.N.D.L.; Neves, G.A.; Ferreira, H.S.; Ferreira, H.C. Statistical Design for Recycling Kaolin Processing Waste in the Manufacturing of Mullite-Based Ceramics. *Mat. Res.* **2009**, *12*, 201–209. [[CrossRef](#)]
204. Maia, A.A.B.; Angélica, R.S.; Neves, R.F. Use of Industrial Kaolin Waste from the Brazilian Amazon Region for Synthesis of Zeolite A. *Clay Miner.* **2011**, *46*, 127–136. [[CrossRef](#)]
205. Hildebrando, E.A.; Angélica, R.S.; Neves, R.F.; Valenzuela-Díaz, F.R. Síntese de zeólita do tipo faujasita a partir de um rejeito de caulim. *Cerâmica* **2012**, *58*, 453–458. [[CrossRef](#)]
206. Maia, A.Á.B.; Neves, R.F.; Angélica, R.S.; Pöllmann, H. Synthesis of Sodalite from Brazilian Kaolin Wastes. *Clay Miner.* **2015**, *50*, 663–675. [[CrossRef](#)]
207. Menezes, R.A.; Paz, S.P.A.; Angélica, R.S.; Neves, R.F.; Neumann, R.; Faulstich, F.R.L.; Pergher, S.B.C. Synthesis of Ultramarine Pigments from Na-A Zeolite Derived from Kaolin Waste from the Amazon. *Clay Miner.* **2017**, *52*, 83–95. [[CrossRef](#)]

208. Maia, A.Á.B.; Neves, R.F.; Angélica, R.S.; Pöllmann, H. Synthesis, Optimisation and Characterisation of the Zeolite NaA Using Kaolin Waste from the Amazon Region. Production of Zeolites KA, MgA and CaA. *Appl. Clay Sci.* **2015**, *108*, 55–60. [CrossRef]
209. Da Silva, L.N.; dos Santos Moraes, D.; Santos, S.C.A.; Corrêa, J.A.M. Joint Synthesis of Zeolite A-LDH from Mineral Industry Waste. *Appl. Clay Sci.* **2018**, *161*, 163–168. [CrossRef]
210. Melo, C.C.A.; Melo, B.L.S.; Angélica, R.S.; Paz, S.P.A. Gibbsite-Kaolinite Waste from Bauxite Beneficiation to Obtain FAU Zeolite: Synthesis Optimization Using a Factorial Design of Experiments and Response Surface Methodology. *Appl. Clay Sci.* **2019**, *170*, 125–134. [CrossRef]
211. Kumar, S.; Stewart, J. Evaluation of Illinois Pulverized Coal Combustion Dry Bottom Ash for Use in Geotechnical Engineering Applications. *J. Energy Eng.* **2003**, *129*, 42–55. [CrossRef]
212. Hatt, R.M. Fireside Deposits in Coal-Fired Utility Boilers. *Prog. Energy Combust. Sci.* **1990**, *16*, 235–241. [CrossRef]
213. Federal Highway Administration. Available online: <https://highways.dot.gov> (accessed on 26 March 2022).
214. Sow, M.; Hot, J.; Tribout, C.; Cyr, M. Characterization of Spreader Stoker Coal Fly Ashes (SSCFA) for Their Use in Cement-Based Applications. *Fuel* **2015**, *162*, 224–233. [CrossRef]
215. Koukouzas, N.; Zeng, R.; Perdikatsis, V.; Xu, W.; Kakaras, E. Mineralogy and Geochemistry of Greek and Chinese Coal Fly Ash. *Fuel* **2006**, *85*, 2301–2309. [CrossRef]
216. Van der Merwe, E.M.; Prinsloo, L.C.; Mathebula, C.L.; Swart, H.C.; Coetsee, E.; Doucet, F.J. Surface and Bulk Characterization of an Ultrafine South African Coal Fly Ash with Reference to Polymer Applications. *Appl. Surf. Sci.* **2014**, *317*, 73–83. [CrossRef]
217. Amrhein, C.; Haghnia, G.H.; Kim, T.S.; Mosher, P.A.; Gagajena, R.C.; Amanios, T. Synthesis and Properties of Zeolites from Coal Fly Ash. *Environ. Sci. Technol.* **1996**, *30*, 735–742. [CrossRef]
218. Yao, Z.T.; Ji, X.S.; Sarker, P.K.; Tang, J.H.; Ge, L.Q.; Xia, M.S.; Xi, Y.Q. A Comprehensive Review on the Applications of Coal Fly Ash. *Earth-Sci. Rev.* **2015**, *141*, 105–121. [CrossRef]
219. Bhatt, A.; Priyadarshini, S.; Acharath Mohanakrishnan, A.; Abri, A.; Sattler, M.; Techapaphawit, S. Physical, Chemical, and Geotechnical Properties of Coal Fly Ash: A Global Review. *Case Stud. Constr. Mater.* **2019**, *11*, e00263. [CrossRef]
220. Panda, L.; Dash, S. Characterization and Utilization of Coal Fly Ash: A Review. *Emerg. Mater. Res.* **2020**, *9*, 921–934. [CrossRef]
221. Riehl, A.; Elsass, F.; Duplay, J.; Huber, F.; Trautmann, M. Changes in Soil Properties in a Fluvisol (Calcaric) Amended with Coal Fly Ash. *Geoderma* **2010**, *155*, 67–74. [CrossRef]
222. Jiao, F.; Ninomiya, Y.; Zhang, L.; Yamada, N.; Sato, A.; Dong, Z. Effect of Coal Blending on the Leaching Characteristics of Arsenic in Fly Ash from Fluidized Bed Coal Combustion. *Fuel Process. Technol.* **2013**, *106*, 769–775. [CrossRef]
223. Uzarowicz, Ł.; Zagórski, Z.; Mendak, E.; Bartmiński, P.; Szara, E.; Kondras, M.; Oktaba, L.; Turek, A.; Rogoziński, R. Technogenic Soils (Technosols) Developed from Fly Ash and Bottom Ash from Thermal Power Stations Combusting Bituminous Coal and Lignite. Part I. Properties, Classification, and Indicators of Early Pedogenesis. *Catena* **2017**, *157*, 75–89. [CrossRef]
224. Dai, S.; Zhao, L.; Peng, S.; Chou, C.-L.; Wang, X.; Zhang, Y.; Li, D.; Sun, Y. Abundances and Distribution of Minerals and Elements in High-Alumina Coal Fly Ash from the Jungar Power Plant, Inner Mongolia, China. *Int. J. Coal Geol.* **2010**, *81*, 320–332. [CrossRef]
225. Mendes, B.C.; Pedroti, L.G.; Vieira, C.M.F.; Marvila, M.; Azevedo, A.R.G.; Franco de Carvalho, J.M.; Ribeiro, J.C.L. Application of Eco-Friendly Alternative Activators in Alkali-Activated Materials: A Review. *J. Build. Eng.* **2021**, *35*, 102010. [CrossRef]
226. Terzano, R.; Spagnuolo, M.; Medici, L.; Tateo, F.; Ruggiero, P. Zeolite Synthesis from Pre-Treated Coal Fly Ash in Presence of Soil as a Tool for Soil Remediation. *Appl. Clay Sci.* **2005**, *29*, 99–110. [CrossRef]
227. Koshy, N.; Singh, D.N. Fly Ash Zeolites for Water Treatment Applications. *J. Environ. Chem. Eng.* **2016**, *4*, 1460–1472. [CrossRef]
228. Czurda, K.A.; Haus, R. Reactive Barriers with Fly Ash Zeolites for in Situ Groundwater Remediation. *Appl. Clay Sci.* **2002**, *21*, 13–20. [CrossRef]
229. Berkgaot, V.; Singer, A. High Capacity Cation Exchanger by Hydrothermal Zeolitization of Coal Fly Ash. *Appl. Clay Sci.* **1996**, *10*, 369–378. [CrossRef]
230. Ojha, K.; Pradhan, N.C.; Samanta, A.N. Zeolite from Fly Ash: Synthesis and Characterization. *Bull. Mater. Sci.* **2004**, *27*, 555–564. [CrossRef]
231. Mendoza, T.C. A Review of Sustainability Challenges of Biomass for Energy: Focus in the Philippines. *J. Agric. Technol.* **2016**, *12*, 281–310.
232. Mohamed, R.M.; Mkhaliid, I.A.; Barakat, M.A. Rice Husk Ash as a Renewable Source for the Production of Zeolite NaY and Its Characterization. *Arab. J. Chem.* **2015**, *8*, 48–53. [CrossRef]
233. Chen, H.; Wang, W.; Martin, J.C.; Oliphant, A.J.; Doerr, P.A.; Xu, J.F.; DeBorn, K.M.; Chen, C.; Sun, L. Extraction of Lignocellulose and Synthesis of Porous Silica Nanoparticles from Rice Husks: A Comprehensive Utilization of Rice Husk Biomass. *ACS Sustain. Chem. Eng.* **2013**, *1*, 254–259. [CrossRef]
234. Abbas, A.; Ansumali, S. Global Potential of Rice Husk as a Renewable Feedstock for Ethanol Biofuel Production. *Bioenerg. Res.* **2010**, *3*, 328–334. [CrossRef]
235. Saceda, J.-J.F.; Leon, R.L.D.; Rintramee, K.; Prayoonpokarach, S.; Wittayakun, J. Properties of Silica from Rice Husk and Rice Husk Ash and Their Utilization for Zeolite γ Synthesis. *Quím. Nova* **2011**, *34*, 1394–1397. [CrossRef]
236. Zhang, C.; Li, S.; Bao, S. Sustainable Synthesis of ZSM-5 Zeolite from Rice Husk Ash Without Addition of Solvents. *Waste Biomass Valorization* **2019**, *10*, 2825–2835. [CrossRef]
237. Jaronvechatam, N.; Kongkachuichay, P. SUZ-4 Zeolite Synthesis Derived from Rice Husk Ash. *Chiang Mai J. Sci.* **2013**, *40*, 109–116.

238. Wajima, T.; Kiguchi, O.; Sugawara, K.; Sugawara, T. Synthesis of Zeolite—A Using Silica from Rice Husk Ash. *J. Chem. Eng. Jpn. JCEJ* **2009**, *42*, S61–S66. [[CrossRef](#)]
239. Wittayakun, J.; Khemthong, P.; Prayoonpokarach, S. Synthesis and Characterization of Zeolite NaY from Rice Husk Silica. *Korean J. Chem. Eng.* **2008**, *25*, 861–864. [[CrossRef](#)]
240. Metta, A.; Ginting, S.B. Sintesis ZSM-5 dari Coal Fly Ash (CFA) dengan Sumber Silika Penambah yang Berasal dari Abu Sekam Padi: Pengaruh Rasio SiO₂/Al₂O₃ Terhadap Kristalinitas Produk. *J. Rekayasa Proses* **2014**, *8*, 7.
241. Costa, J.A.S.; Sarmiento, V.H.V.; Romão, L.P.C.; Paranhos, C.M. Synthesis of Functionalized Mesoporous Material from Rice Husk Ash and Its Application in the Removal of the Polycyclic Aromatic Hydrocarbons. *Environ. Sci. Pollut. Res.* **2019**, *26*, 25476–25490. [[CrossRef](#)]
242. Huang, Y.; He, J.; Luan, Y.; Jiang, Y.; Guo, S.; Zhang, X.; Tian, C.; Jiang, B. Promising Biomass-Derived Hierarchical Porous Carbon Material for High Performance Supercapacitor. *RSC Adv.* **2017**, *7*, 10385–10390. [[CrossRef](#)]
243. De Andrade, F.R.D.; Yogi, M.T.A.G.; Gomes, E.B.; Shinzato, M.C. Extent of Zeolite Synthesis via Alkaline Fusion from Tailings Dam Sediments. *Environ. Earth Sci* **2020**, *79*, 379. [[CrossRef](#)]
244. Guan, Q.; Wu, D.; Lin, Y.; Chen, X.; Wang, X.; Li, C.; He, S.; Kong, H. Application of Zeolitic Material Synthesized from Thermally Treated Sediment to the Removal of Trivalent Chromium from Wastewater. *J. Hazard. Mater.* **2009**, *167*, 244–249. [[CrossRef](#)] [[PubMed](#)]
245. Bert, V.; Seuntjens, P.; Dejonghe, W.; Lacherez, S.; Thuy, H.T.T.; Vandecasteele, B. Phytoremediation as a Management Option for Contaminated Sediments in Tidal Marshes, Flood Control Areas and Dredged Sediment Landfill Sites. *Environ. Sci. Pollut. Res.* **2009**, *16*, 745–764. [[CrossRef](#)] [[PubMed](#)]
246. Chen, J.; Huang, R.; Ouyang, H.; Yu, G.; Liang, Y.; Zheng, Q. Utilization of Dredged River Sediments to Synthesize Zeolite for Cd(II) Removal from Wastewater. *J. Clean. Prod.* **2021**, *320*, 128861. [[CrossRef](#)]
247. Akah, A.; Williams, J.; Ghrami, M. An Overview of Light Olefins Production via Steam Enhanced Catalytic Cracking. *Catal. Surv. Asia* **2019**, *23*, 265–276. [[CrossRef](#)]
248. Li, X.; Kant, A.; He, Y.; Thakkar, H.V.; Atanga, M.A.; Rezaei, F.; Ludlow, D.K.; Rownaghi, A.A. Light Olefins from Renewable Resources: Selective Catalytic Dehydration of Bioethanol to Propylene over Zeolite and Transition Metal Oxide Catalysts. *Catal. Today* **2016**, *276*, 62–77. [[CrossRef](#)]
249. Dement'ev, K.I.; Sagaradze, A.D.; Kuznetsov, P.S.; Palankoev, T.A.; Maximov, A.L. Selective Production of Light Olefins from Fischer–Tropsch Synthetic Oil by Catalytic Cracking. *Ind. Eng. Chem. Res.* **2020**, *59*, 15875–15883. [[CrossRef](#)]
250. Corma, A.; Corresa, E.; Mathieu, Y.; Sauvanaud, L.; Al-Bogami, S.; Al-Ghrami, M.S.; Bourane, A. Crude Oil to Chemicals: Light Olefins from Crude Oil. *Catal. Sci. Technol.* **2017**, *7*, 12–46. [[CrossRef](#)]
251. Gholami, Z.; Gholami, F.; Tişler, Z.; Tomas, M.; Vakili, M. A Review on Production of Light Olefins via Fluid Catalytic Cracking. *Energies* **2021**, *14*, 1089. [[CrossRef](#)]
252. Zhu, C.; Zhang, M.; Huang, C.; Han, Y.; Fang, K. Controlled Nanostructure of Zeolite Crystal Encapsulating FeMnK Catalysts Targeting Light Olefins from Syngas. *ACS Appl. Mater. Interfaces* **2020**, *12*, 57950–57962. [[CrossRef](#)] [[PubMed](#)]
253. Guo, L.; Sun, J.; Ge, Q.; Tsubaki, N. Recent Advances in Direct Catalytic Hydrogenation of Carbon Dioxide to Valuable C₂₊ Hydrocarbons. *J. Mater. Chem. A* **2018**, *6*, 23244–23262. [[CrossRef](#)]
254. Su, J.; Zhou, H.; Liu, S.; Wang, C.; Jiao, W.; Wang, Y.; Liu, C.; Ye, Y.; Zhang, L.; Zhao, Y.; et al. Syngas to Light Olefins Conversion with High Olefin/Paraffin Ratio Using ZnCrOx/AlPO-18 Bifunctional Catalysts. *Nat. Commun.* **2019**, *10*, 1297. [[CrossRef](#)]
255. Liu, C.; Su, J.; Liu, S.; Zhou, H.; Yuan, X.; Ye, Y.; Wang, Y.; Jiao, W.; Zhang, L.; Lu, Y.; et al. Insights into the Key Factor of Zeolite Morphology on the Selective Conversion of Syngas to Light Aromatics over a Cr₂O₃/ZSM-5 Catalyst. *ACS Catal.* **2020**, *10*, 15227–15237. [[CrossRef](#)]
256. Su, J.; Liu, C.; Liu, S.; Ye, Y.; Du, Y.; Zhou, H.; Liu, S.; Jiao, W.; Zhang, L.; Wang, C.; et al. High Conversion of Syngas to Ethene and Propene on Bifunctional Catalysts via the Tailoring of SAPO Zeolite Structure. *Cell Rep. Phys. Sci.* **2021**, *2*, 100290. [[CrossRef](#)]
257. Vu, H.X.; Schneider, M.; Bentrup, U.; Dang, T.T.; Phan, B.M.Q.; Nguyen, D.A.; Armbruster, U.; Martin, A. Hierarchical ZSM-5 Materials for an Enhanced Formation of Gasoline-Range Hydrocarbons and Light Olefins in Catalytic Cracking of Triglyceride-Rich Biomass. *Ind. Eng. Chem. Res.* **2015**, *54*, 1773–1782. [[CrossRef](#)]
258. Hussain, A.I.; Palani, A.; Aitani, A.M.; Čejka, J.; Shamzhy, M.; Kubů, M.; Al-Khattaf, S.S. Catalytic Cracking of Vacuum Gasoil over -SVR, ITH, and MFI Zeolites as FCC Catalyst Additives. *Fuel Process. Technol.* **2017**, *161*, 23–32. [[CrossRef](#)]
259. Caeiro, G.; Magnoux, P.; Lopes, J.M.; Ribeiro, F.R.; Menezes, S.M.C.; Costa, A.F.; Cerqueira, H.S. Stabilization Effect of Phosphorus on Steamed H-MFI Zeolites. *Appl. Catal. A Gen.* **2006**, *314*, 160–171. [[CrossRef](#)]
260. Costa, A.F.; Cerqueira, H.S.; Ferreira, J.M.M.; Ruiz, N.M.S.; Menezes, S.M.C. BEA and MOR as Additives for Light Olefins Production. *Appl. Catal. A Gen.* **2007**, *319*, 137–143. [[CrossRef](#)]
261. Numpilai, T.; Cheng, C.K.; Limtrakul, J.; Witoon, T. Recent Advances in Light Olefins Production from Catalytic Hydrogenation of Carbon Dioxide. *Process Saf. Environ. Prot.* **2021**, *151*, 401–427. [[CrossRef](#)]
262. Li, X.; Shen, B.; Guo, Q.; Gao, J. Effects of Large Pore Zeolite Additions in the Catalytic Pyrolysis Catalyst on the Light Olefins Production. *Catal. Today* **2007**, *125*, 270–277. [[CrossRef](#)]
263. Degnan, T.F. The Implications of the Fundamentals of Shape Selectivity for the Development of Catalysts for the Petroleum and Petrochemical Industries. *J. Catal.* **2003**, *216*, 32–46. [[CrossRef](#)]

264. Dugkhuntod, P.; Wattanakit, C. A Comprehensive Review of the Applications of Hierarchical Zeolite Nanosheets and Nanoparticle Assemblies in Light Olefin Production. *Catalysts* **2020**, *10*, 245. [[CrossRef](#)]
265. Rostamizadeh, M.; Eishkooh, P.T.; Hazrati, H. Simulation of Increasing of Light Olefins Production Yield from Methanol Using HZSM-5 Zeolite Catalysis. *J. Appl. Res. Chem.* **2019**, *12*, 77–87.
266. Laredo, G.C.; García-Gutiérrez, J.L.; Pérez-Romo, P.; Olmos-Cerda, E.H. Effect of the Catalyst in the BTX Production by Hydrocracking of Light Cycle Oil. *Appl. Petrochem. Res.* **2021**, *11*, 19–38. [[CrossRef](#)]
267. Qiao, J.; Wang, J.; Frenkel, A.I.; Teng, J.; Chen, X.; Xiao, J.; Zhang, T.; Wang, Z.; Yuan, Z.; Yang, W. Methanol to Aromatics: Isolated Zinc Phosphate Groups on HZSM-5 Zeolite Enhance BTX Selectivity and Catalytic Stability. *RSC Adv.* **2020**, *10*, 5961–5971. [[CrossRef](#)] [[PubMed](#)]
268. Yang, G.; Yang, J.; Huang, D.; Zhou, W.; Yang, L.; Lv, P.; Yi, W.; Sun, Y.; Yan, B. BTX Production from Rice Husk by Fast Catalytic Pyrolysis over a Ga-Modified ZSM-5/SBA-15 Catalyst. *New J. Chem.* **2021**, *45*, 3809–3816. [[CrossRef](#)]
269. Miao, D.; Ding, Y.; Yu, T.; Li, J.; Pan, X.; Bao, X. Selective Synthesis of Benzene, Toluene, and Xylenes from Syngas. *ACS Catal.* **2020**, *10*, 7389–7397. [[CrossRef](#)]
270. Wang, Y.; Tan, L.; Tan, M.; Zhang, P.; Fang, Y.; Yoneyama, Y.; Yang, G.; Tsubaki, N. Rationally Designing Bifunctional Catalysts as an Efficient Strategy To Boost CO₂ Hydrogenation Producing Value-Added Aromatics. *ACS Catal.* **2019**, *9*, 895–901. [[CrossRef](#)]
271. Laredo, G.C.; Pérez-Romo, P.; Escobar, J.; García-Gutiérrez, J.L.; Vega-Merino, P.M. Light Cycle Oil Upgrading to Benzene, Toluene, and Xylenes by Hydrocracking: Studies Using Model Mixtures. *Ind. Eng. Chem. Res.* **2017**, *56*, 10939–10948. [[CrossRef](#)]
272. He, S.; Muizebelt, I.; Heeres, A.; Schenk, N.J.; Bles, R.; Heeres, H.J. Catalytic Pyrolysis of Crude Glycerol over Shaped ZSM-5/Bentonite Catalysts for Bio-BTX Synthesis. *Appl. Catal. B Environ.* **2018**, *235*, 45–55. [[CrossRef](#)]
273. Muraza, O. Peculiarities of Glycerol Conversion to Chemicals Over Zeolite-Based Catalysts. *Front. Chem.* **2019**, *7*, 233. [[CrossRef](#)] [[PubMed](#)]
274. Su, X.; Zan, W.; Bai, X.; Wang, G.; Wu, W. Synthesis of Microscale and Nanoscale ZSM-5 Zeolites: Effect of Particle Size and Acidity of Zn Modified ZSM-5 Zeolites on Aromatization Performance. *Catal. Sci. Technol.* **2017**, *7*, 1943–1952. [[CrossRef](#)]
275. Bandura, L.; Kołodyńska, D.; Franus, W. Adsorption of BTX from Aqueous Solutions by Na-P1 Zeolite Obtained from Fly Ash. *Process Saf. Environ. Prot.* **2017**, *109*, 214–223. [[CrossRef](#)]
276. Bandura, L.; Panek, R.; Rotko, M.; Franus, W. Synthetic Zeolites from Fly Ash for an Effective Trapping of BTX in Gas Stream. *Microporous Mesoporous Mater.* **2016**, *223*, 1–9. [[CrossRef](#)]
277. Kuchinskaya, T.; Kniazeva, M.; Samoilov, V.; Maximov, A. In Situ Generated Nanosized Sulfide Ni-W Catalysts Based on Zeolite for the Hydrocracking of the Pyrolysis Fuel Oil into the BTX Fraction. *Catalysts* **2020**, *10*, 1152. [[CrossRef](#)]
278. Miyake, K.; Hirota, Y.; Ono, K.; Uchida, Y.; Nishiyama, N. Selective Production of Benzene, Toluene and *p*-Xylene (BT *p* X) from Various C₁₋₃ Feedstocks over ZSM-5/Silicalite-1 Core-Shell Zeolite Catalyst. *ChemistrySelect* **2016**, *1*, 967–969. [[CrossRef](#)]
279. Kim, N.S.; Numan, M.; Nam, S.C.; Park, S.-E.; Jo, C. Dynamic Adsorption/Desorption of *p*-Xylene on Nanomorphous MFI Zeolites: Effect of Zeolite Crystal Thickness and Mesopore Architecture. *J. Hazard. Mater.* **2021**, *403*, 123659. [[CrossRef](#)]
280. Gu, X.; Dong, J.; Nenoff, T.M.; Ozokwelu, D.E. Separation of *p*-Xylene from Multicomponent Vapor Mixtures Using Tubular MFI Zeolite Membranes. *J. Membr. Sci.* **2006**, *280*, 624–633. [[CrossRef](#)]
281. Matsufuji, T. Separation of Butane and Xylene Isomers with MFI-Type Zeolitic Membrane Synthesized by a Vapor-Phase Transport Method. *J. Membr. Sci.* **2000**, *178*, 25–34. [[CrossRef](#)]
282. Musilová-Pavlačková, Z.; Zones, S.I.; Čejka, J. Post-Synthesis Modification of SSZ-35 Zeolite to Enhance the Selectivity in *p*-Xylene Alkylation with Isopropyl Alcohol. *Top. Catal.* **2010**, *53*, 273–282. [[CrossRef](#)]
283. Zhao, R.; Zhao, Z.; Li, S.; Parvulescu, A.-N.; Müller, U.; Zhang, W. Excellent Performances of Dealuminated H-Beta Zeolites from Organotemplate-Free Synthesis in Conversion of Biomass-Derived 2,5-Dimethylfuran to Renewable *p*-Xylene. *ChemSusChem* **2018**, *11*, 3803–3811. [[CrossRef](#)] [[PubMed](#)]
284. Kim, T.-W.; Kim, S.-Y.; Kim, J.-C.; Kim, Y.; Ryoo, R.; Kim, C.-U. Selective *p*-Xylene Production from Biomass-Derived Dimethylfuran and Ethylene over Zeolite Beta Nanosponge Catalysts. *Appl. Catal. B Environ.* **2016**, *185*, 100–109. [[CrossRef](#)]
285. Mendoza Mesa, J.A.; Brandi, F.; Shekova, I.; Antonietti, M.; Al-Naji, M. *p*-Xylene from 2,5-Dimethylfuran and Acrylic Acid Using Zeolite in a Continuous Flow System. *Green Chem.* **2020**, *22*, 7398–7405. [[CrossRef](#)]
286. Li, Y.-P.; Head-Gordon, M.; Bell, A.T. Computational Study of *p*-Xylene Synthesis from Ethylene and 2,5-Dimethylfuran Catalyzed by H-BEA. *J. Phys. Chem. C* **2014**, *118*, 22090–22095. [[CrossRef](#)]
287. Nikbin, N.; Feng, S.; Caratzoulas, S.; Vlachos, D.G. *p*-Xylene Formation by Dehydrative Aromatization of a Diels–Alder Product in Lewis and Brønsted Acidic Zeolites. *J. Phys. Chem. C* **2014**, *118*, 24415–24424. [[CrossRef](#)]
288. Purnomo, C.W.; Mellyanawaty, M.; Budhijanto, W. Simulation and Experimental Study on Iron Impregnated Microbial Immobilization in Zeolite for Production of Biogas. *Waste Biomass Valorization* **2017**, *8*, 2413–2421. [[CrossRef](#)]
289. Montalvo, S.; Huiliñir, C.; Borja, R.; Sánchez, E.; Herrmann, C. Application of Zeolites for Biological Treatment Processes of Solid Wastes and Wastewaters—A Review. *Bioresour. Technol.* **2020**, *301*, 122808. [[CrossRef](#)]
290. Shchemelinina, T.N.; Gömze, L.A.; Kotova, O.B.; Ibrahim, J.E.F.M.; Shushkov, D.A.; Harja, M.; Ignatiev, G.V.; Anchugova, E.M. Clay- and Zeolite-Based Biogeosorbents: Modelling and Properties. *Epitoanyag—JSBCM* **2019**, *71*, 131–137. [[CrossRef](#)]
291. Shindo, S.; Takata, S.; Taguchi, H.; Yoshimura, N. Development of Novel Carrier Using Natural Zeolite and Continuous Ethanol Fermentation with Immobilized *Saccharomyces Cerevisiae* in a Bioreactor. *Biotechnol. Lett.* **2001**, *23*, 2001–2004. [[CrossRef](#)]

292. Bhaskar, S.; Anwar Hossain, K.M.; Lachemi, M.; Wolfaardt, G.; Otini Kroukamp, M. Effect of Self-Healing on Strength and Durability of Zeolite-Immobilized Bacterial Cementitious Mortar Composites. *Cem. Concr. Compos.* **2017**, *82*, 23–33. [[CrossRef](#)]
293. Fernández, N.; Montalvo, S.; Fernández-Polanco, F.; Guerrero, L.; Cortés, I.; Borja, R.; Sánchez, E.; Travieso, L. Real Evidence about Zeolite as Microorganisms Immobilizer in Anaerobic Fluidized Bed Reactors. *Process Biochem.* **2007**, *42*, 721–728. [[CrossRef](#)]
294. Montalvo, S.; Guerrero, L.; Borja, R.; Sánchez, E.; Milán, Z.; Cortés, I.; Angeles de la la Rubia, M. Application of Natural Zeolites in Anaerobic Digestion Processes: A Review. *Appl. Clay Sci.* **2012**, *58*, 125–133. [[CrossRef](#)]
295. Badalova, M.; Evstatieva, Y.; Mushekova, L.; Licheva, T.; Nikolova, D.; Savov, V. Natural and modified zeolites as matrices for the immobilization of trichoderma viride sl-45. *Bulg. J. Agric. Sci.* **2014**, *20*, 93–96.
296. Djukić-Vuković, A.P.; Mojović, L.V.; Jokić, B.M.; Nikolić, S.B.; Pejin, J.D. Lactic Acid Production on Liquid Distillery Stillage by Lactobacillus Rhamnosus Immobilized onto Zeolite. *Bioresour. Technol.* **2013**, *135*, 454–458. [[CrossRef](#)] [[PubMed](#)]
297. Ryu, J.C.; Ryu, T.G.; Yoo, S.J.; Hwang, J.Y.; Kim, Y.H.; Yang, H.S. Characteristics of porous ceramic carriers made from fly ash for immobilization of microorganisms. *J. Ind. Eng. Chem.* **2003**, *9*, 735–742.
298. Mardiana, S.; Azhari, N.J.; Ilmi, T.; Kadja, G.T.M. Hierarchical Zeolite for Biomass Conversion to Biofuel: A Review. *Fuel* **2022**, *309*, 122119. [[CrossRef](#)]
299. Taarning, E.; Osmundsen, C.M.; Yang, X.; Voss, B.; Andersen, S.I.; Christensen, C.H. Zeolite-Catalyzed Biomass Conversion to Fuels and Chemicals. *Energy Environ. Sci.* **2011**, *4*, 793–804. [[CrossRef](#)]
300. Perego, C.; Bosetti, A. Biomass to Fuels: The Role of Zeolite and Mesoporous Materials. *Microporous Mesoporous Mater.* **2011**, *144*, 28–39. [[CrossRef](#)]
301. Ennaert, T.; Van Aelst, J.; Dijkmans, J.; De Clercq, R.; Schutyser, W.; Dusselier, M.; Verboekend, D.; Sels, B.F. Potential and Challenges of Zeolite Chemistry in the Catalytic Conversion of Biomass. *Chem. Soc. Rev.* **2016**, *45*, 584–611. [[CrossRef](#)] [[PubMed](#)]
302. Choi, S.-G.; Won, S.-R.; Rhee, H.-I. Oleic Acid and Inhibition of Glucosyltransferase. In *Olives and Olive Oil in Health and Disease Prevention*; Elsevier: Amsterdam, The Netherlands, 2010; pp. 1375–1383. ISBN 978-0-12-374420-3.
303. Gomes, G.J.; Costa, M.B.; Bittencourt, P.R.S.; Zalazar, M.F.; Arroyo, P.A. Catalytic Improvement of Biomass Conversion: Effect of Adding Mesoporosity on MOR Zeolite for Esterification with Oleic Acid. *Renew. Energy* **2021**, *178*, 1–12. [[CrossRef](#)]
304. Jae, J.; Tompsett, G.A.; Foster, A.J.; Hammond, K.D.; Auerbach, S.M.; Lobo, R.F.; Huber, G.W. Investigation into the Shape Selectivity of Zeolite Catalysts for Biomass Conversion. *J. Catal.* **2011**, *279*, 257–268. [[CrossRef](#)]
305. Dijkmans, J.; Dusselier, M.; Gabriëls, D.; Houthoofd, K.; Magusin, P.C.M.M.; Huang, S.; Pontikes, Y.; Trekels, M.; Vantomme, A.; Giebler, L.; et al. Cooperative Catalysis for Multistep Biomass Conversion with Sn/Al Beta Zeolite. *ACS Catal.* **2015**, *5*, 928–940. [[CrossRef](#)]
306. Gallo, J.M.R.; Alonso, D.M.; Mellmer, M.A.; Yeap, J.H.; Wong, H.C.; Dumesic, J.A. Production of Furfural from Lignocellulosic Biomass Using Beta Zeolite and Biomass-Derived Solvent. *Top. Catal.* **2013**, *56*, 1775–1781. [[CrossRef](#)]
307. Limlamthong, M.; Yip, A.C.K. Recent Advances in Zeolite-Encapsulated Metal Catalysts: A Suitable Catalyst Design for Catalytic Biomass Conversion. *Bioresour. Technol.* **2020**, *297*, 122488. [[CrossRef](#)]
308. Sanchez, S.; Demain, A.L. Enzymes and Bioconversions of Industrial, Pharmaceutical, and Biotechnological Significance. *Org. Process Res. Dev.* **2011**, *15*, 224–230. [[CrossRef](#)]
309. Mulinari, J.; Oliveira, J.V.; Hotza, D. Lipase Immobilization on Ceramic Supports: An Overview on Techniques and Materials. *Biotechnol. Adv.* **2020**, *42*, 107581. [[CrossRef](#)]
310. Reis, C.; Sousa, E.; Serpa, J.; Oliveira, R.; Santos, J. Design of immobilized enzyme biocatalysts: Drawbacks and opportunities. *Química Nova* **2019**, *42*, 768–783. [[CrossRef](#)]
311. Datta, S.; Christena, L.R.; Rajaram, Y.R.S. Enzyme Immobilization: An Overview on Techniques and Support Materials. *3 Biotech* **2013**, *3*, 1–9. [[CrossRef](#)]
312. Sheldon, R.A. Enzyme Immobilization: The Quest for Optimum Performance. *Adv. Synth. Catal.* **2007**, *349*, 1289–1307. [[CrossRef](#)]
313. Luckarift, H.R.; Spain, J.C.; Naik, R.R.; Stone, M.O. Enzyme Immobilization in a Biomimetic Silica Support. *Nat. Biotechnol.* **2004**, *22*, 211–213. [[CrossRef](#)] [[PubMed](#)]
314. Fan, J.-Q. A Counterintuitive Approach to Treat Enzyme Deficiencies: Use of Enzyme Inhibitors for Restoring Mutant Enzyme Activity. *Biol. Chem.* **2008**, *389*, 1–11. [[CrossRef](#)] [[PubMed](#)]
315. Xing, G.-W.; Li, X.-W.; Tian, G.-L.; Ye, Y.-H. Enzymatic Peptide Synthesis in Organic Solvent with Different Zeolites as Immobilization Matrixes. *Tetrahedron* **2000**, *56*, 3517–3522. [[CrossRef](#)]
316. Geor Malar, C.; Seenuvasan, M.; Kumar, K.S.; Kumar, A.; Parthiban, R. Review on Surface Modification of Nanocarriers to Overcome Diffusion Limitations: An Enzyme Immobilization Aspect. *Biochem. Eng. J.* **2020**, *158*, 107574. [[CrossRef](#)]
317. Neupane, S.; Patnode, K.; Li, H.; Baryeh, K.; Liu, G.; Hu, J.; Chen, B.; Pan, Y.; Yang, Z. Enhancing Enzyme Immobilization on Carbon Nanotubes via Metal–Organic Frameworks for Large-Substrate Biocatalysis. *ACS Appl. Mater. Interfaces* **2019**, *11*, 12133–12141. [[CrossRef](#)]
318. Homaei, A.A.; Sariri, R.; Vianello, F.; Stevanato, R. Enzyme Immobilization: An Update. *J. Chem. Biol.* **2013**, *6*, 185–205. [[CrossRef](#)]
319. Yagiz, F.; Kazan, D.; Akin, A.N. Biodiesel Production from Waste Oils by Using Lipase Immobilized on Hydrotalcite and Zeolites. *Chem. Eng. J.* **2007**, *134*, 262–267. [[CrossRef](#)]
320. Anderson, D.; Balapangu, S.; Fleischer, H.N.A.; Viade, R.A.; Krampa, F.D.; Kanyong, P.; Awandare, G.A.; Tiburu, E.K. Investigating the Influence of Temperature on the Kaolinite-Base Synthesis of Zeolite and Urease Immobilization for the Potential Fabrication of Electrochemical Urea Biosensors. *Sensors* **2017**, *17*, 1831. [[CrossRef](#)]

321. Lee, S.Y.; Show, P.L.; Ko, C.-M.; Chang, Y.-K. A Simple Method for Cell Disruption by Immobilization of Lysozyme on the Extrudate-Shaped Na-Y Zeolite: Recirculating Packed Bed Disruption Process. *Biochem. Eng. J.* **2019**, *141*, 210–216. [[CrossRef](#)]
322. MacArio, A.; Giordano, G.; Setti, L.; Parise, A.; Campelo, J.M.; Marinas, J.M.; Luna, D. Study of Lipase Immobilization on Zeolitic Support and Transesterification Reaction in a Solvent Free-System. *Biocatal. Biotransform.* **2007**, *25*, 328–335. [[CrossRef](#)]
323. An, N.; Zhou, C.H.; Zhuang, X.Y.; Tong, D.S.; Yu, W.H. Immobilization of Enzymes on Clay Minerals for Biocatalysts and Biosensors. *Appl. Clay Sci.* **2015**, *114*, 283–296. [[CrossRef](#)]
324. Talebi, M.; Vaezifar, S.; Jafary, F.; Fazilati, M.; Motamedi, S. Stability Improvement of Immobilized α -Amylase Using Nano Pore Zeolite. *Iran. J. Biotechnol.* **2016**, *14*, 33–38. [[CrossRef](#)] [[PubMed](#)]
325. Vaidya, L.B.; Nadar, S.S.; Rathod, V.K. Entrapment of Surfactant Modified Lipase within Zeolitic Imidazolate Framework (ZIF)-8. *Int. J. Biol. Macromol.* **2020**, *146*, 678–686. [[CrossRef](#)] [[PubMed](#)]
326. Hwang, E.T.; Gu, M.B. Enzyme Stabilization by Nano/Microsized Hybrid Materials: Enzyme Stabilization by Nano/Microsized Hybrid Materials. *Eng. Life Sci.* **2013**, *13*, 49–61. [[CrossRef](#)]
327. Feng, Y.; Zhong, L.; Bilal, M.; Tan, Z.; Hou, Y.; Jia, S.; Cui, J. Enzymes@ZIF-8 Nanocomposites with Protection Nanocoating: Stability and Acid-Resistant Evaluation. *Polymers* **2018**, *11*, 27. [[CrossRef](#)]
328. Wang, L.; Zhi, W.; Lian, D.; Wang, Y.; Han, J.; Wang, Y. HRP@ZIF-8/DNA Hybrids: Functionality Integration of ZIF-8 via Biom mineralization and Surface Adsorption. *ACS Sustain. Chem. Eng.* **2019**, *7*, 14611–14620. [[CrossRef](#)]
329. Honda, T.; Miyazaki, M.; Nakamura, H.; Maeda, H. Immobilization of Enzymes on a Microchannel Surface through Cross-Linking Polymerization. *Chem. Commun.* **2005**, *40*, 5062. [[CrossRef](#)]
330. Mateo, C.; Palomo, J.M.; van Langen, L.M.; van Rantwijk, F.; Sheldon, R.A. A New, Mild Cross-Linking Methodology to Prepare Cross-Linked Enzyme Aggregates. *Biotechnol. Bioeng.* **2004**, *86*, 273–276. [[CrossRef](#)]
331. Liu, C.; Zhang, L.; Tan, L.; Liu, Y.; Tian, W.; Ma, L. Immobilized Crosslinked Pectinase Preparation on Porous ZSM-5 Zeolites as Reusable Biocatalysts for Ultra-Efficient Hydrolysis of β -Glycosidic Bonds. *Front. Chem.* **2021**, *9*, 677868. [[CrossRef](#)]
332. Ouyang, W.; Zheng, S.; Wu, C.; Hu, X.; Chen, R.; Zhuo, L.; Wang, Z. Dynamic Ammonia Adsorption by FAU Zeolites to below 0.1 Ppm for Hydrogen Energy Applications. *Int. J. Hydrog Energy* **2021**, *46*, 32559–32569. [[CrossRef](#)]
333. Tan, C.; He, C.; Sun, Y.; Dong, H.; Ge, M.; Xia, X. A Layer-like FAU Zeolite with Palladium Particles Embedded in Situ as Catalyst for Hydrogenation of 1,4-Bis(Phenylethynyl) Benzene. *Surf. Interfaces* **2022**, *34*, 102399. [[CrossRef](#)]
334. Koohsaryan, E.; Anbia, M.; Heydar, K.T. Mo-Modified Hierarchical FAU Zeolite: A Catalyst-Adsorbent for Oxidative Desulfurization of Fuel Oil. *J. Solid State Chem.* **2022**, *312*, 123218. [[CrossRef](#)]
335. Ektefa, F.; Towfighi Darian, J.; Soltanali, S. Performance of BEA, FAU, LTL, MFI, and MOR Zeolites in the Removal of Ethyl Mercaptan Traces from Natural Gas by Monte Carlo Molecular Simulation. *Appl. Surf. Sci.* **2022**, *605*, 154833. [[CrossRef](#)]
336. Zaitceva, O.; Louis, B.; Beneteau, V.; Pale, P.; Shanmugam, S.; Evstigneyev, E.I.; Vasiliev, A.V. Post-Modified FAU Zeolites as Efficient Catalysts for the Synthesis of Coumarins. *Catal. Today* **2021**, *367*, 111–116. [[CrossRef](#)]
337. Wang, L.; Liu, J.; Lin, C.; Shang, H.; Yang, J.; Li, L.; Li, J. Effects of Different Alkali Metal Cations in FAU Zeolites on the Separation Performance of CO₂/N₂O. *Chem. Eng. J.* **2022**, *431*, 134257. [[CrossRef](#)]
338. Bolshakov, A.; van de Poll, R.; van Bergen-Brenkman, T.; Wiedemann, S.C.C.; Kosinov, N.; Hensen, E.J.M. Hierarchically Porous FER Zeolite Obtained via FAU Transformation for Fatty Acid Isomerization. *Appl. Catal. B Environ.* **2020**, *263*, 118356. [[CrossRef](#)]
339. Jun, L.Y.; Mubarak, N.M.; Yon, L.S.; Bing, C.H.; Khalid, M.; Jagadish, P.; Abdullah, E.C. Immobilization of Peroxidase on Functionalized MWCNTs-Buckypaper/Polyvinyl Alcohol Nanocomposite Membrane. *Sci. Rep.* **2019**, *9*, 2215. [[CrossRef](#)]
340. Zhang, H.; Jiang, Z.; Xia, Q.; Zhou, D. Progress and Perspective of Enzyme Immobilization on Zeolite Crystal Materials. *Biochem. Eng. J.* **2021**, *172*, 108033. [[CrossRef](#)]
341. Hu, G.; Duan, X.; Yang, J.; Yang, C.; Liu, Q.; Ren, S.; Li, J.; Teng, L.; Liu, W. A Novel Conversion of Ti-Bearing Blast Furnace Slag into Ti-Containing Zeolites: Comparison Study between FAU and MFI Type Zeolites. *Adv. Powder Technol.* **2022**, *33*, 103559. [[CrossRef](#)]
342. Nik, O.G.; Nohair, B.; Kaliaguine, S. Aminosilanes Grafting on FAU/EMT Zeolite: Effect on CO₂ Adsorptive Properties. *Microporous Mesoporous Mater.* **2011**, *143*, 221–229. [[CrossRef](#)]
343. Ullrich, R.; Hofrichter, M. Enzymatic Hydroxylation of Aromatic Compounds. *Cell. Mol. Life Sci.* **2007**, *64*, 271–293. [[CrossRef](#)] [[PubMed](#)]
344. Hamid, M. Khalil-ur-Rehman Potential Applications of Peroxidases. *Food Chem.* **2009**, *115*, 1177–1186. [[CrossRef](#)]
345. Pellegrini, V.D.O.A.; Sepulchro, A.G.V.; Polikarpov, I. Enzymes for Lignocellulosic Biomass Polysaccharide Valorization and Production of Nanomaterials. *Curr. Opin. Green Sustain. Chem.* **2020**, *26*, 100397. [[CrossRef](#)]
346. Regalado, C.; García-Almendárez, B.E.; Duarte-Vázquez, M.A. Biotechnological Applications of Peroxidases. *Phytochem. Rev.* **2004**, *3*, 243–256. [[CrossRef](#)]
347. Juzsakova, T.; Al-Jammal, N.; Cretescu, I.; Sebestyén, V.; Le Phuoc, C.; Domokos, E.; Rédey, Á.; Stan, C. Case Studies for Clean Technology Development in the Chemical Industry Using Zeolite Based Catalysts. *Minerals* **2018**, *8*, 462. [[CrossRef](#)]
348. Travkina, O.S.; Agliullin, M.R.; Kutepov, B.I. State-of-the-Art in the Industrial Production and Use of Zeolite-Containing Adsorbents and Catalysts in Russia. *Catal. Ind.* **2022**, *14*, 56–65. [[CrossRef](#)]
349. Roland, E. Industrial production of zeolites. *Stud. Surf. Sci. Catal.* **1989**, *46*, 645–659. [[CrossRef](#)]
350. Khan, W.; Jia, X.; Wu, Z.; Choi, J.; Yip, A.C.K. Incorporating Hierarchy into Conventional Zeolites for Catalytic Biomass Conversions: A Review. *Catalysts* **2019**, *9*, 127. [[CrossRef](#)]

351. Narkhede, N.; Patel, A. Biodiesel Production by Esterification of Oleic Acid and Transesterification of Soybean Oil Using a New Solid Acid Catalyst Comprising 12-Tungstosilicic Acid and Zeolite H β . *Ind. Eng. Chem. Res.* **2013**, *52*, 13637–13644. [[CrossRef](#)]
352. Nuhma, M.J.; Alias, H.; Tahir, M.; Jazie, A.A. Microalgae Biomass Conversion into Biofuel Using Modified HZSM-5 Zeolite Catalyst: A Review. *Mater. Today Proc.* **2021**, *42*, 2308–2313. [[CrossRef](#)]
353. Munavalli, B.B.; Kariduraganavar, M.Y. Development of Novel Sulfonic Acid Functionalized Zeolites Incorporated Composite Proton Exchange Membranes for Fuel Cell Application. *Electrochim. Acta* **2019**, *296*, 294–307. [[CrossRef](#)]
354. Rosso, I.; Galletti, C.; Saracco, G.; Garrone, E.; Specchia, V. Development of A Zeolites-Supported Noble-Metal Catalysts for CO Preferential Oxidation: H₂ Gas Purification for Fuel Cell. *Appl. Catal. B Environ.* **2004**, *48*, 195–203. [[CrossRef](#)]
355. González, T.; Ureta-Zañartu, M.S.; Marco, J.F.; Vidal, G. Effect of Zeolite-Fe on Graphite Anode in Electroactive Biofilm Development for Application in Microbial Fuel Cells. *Appl. Surf. Sci.* **2019**, *467–468*, 851–859. [[CrossRef](#)]
356. Fujii, S.; Nakagaki, T.; Kanematsu, Y.; Kikuchi, Y. Prospective Life Cycle Assessment for Designing Mobile Thermal Energy Storage System Utilizing Zeolite. *J. Clean. Prod.* **2022**, *365*, 132592. [[CrossRef](#)]
357. Fujii, S.; Kanematsu, Y.; Kikuchi, Y.; Nakagaki, T. Effect of Bagasse Drying on Thermal Energy Storage Utilizing Zeolite Water Vapor Ad/Desorption at a Sugar Mill. *J. Energy Storage* **2022**, *51*, 104495. [[CrossRef](#)]
358. Schaefer, M.; Thess, A. Modeling and Simulation of Closed Low-Pressure Zeolite Adsorbers for Thermal Energy Storage. *Int. J. Heat Mass Transf.* **2019**, *139*, 685–699. [[CrossRef](#)]
359. Xu, S.Z.; Wang, R.Z.; Wang, L.W.; Zhu, J. Performance Characterizations and Thermodynamic Analysis of Magnesium Sulfate-Impregnated Zeolite 13X and Activated Alumina Composite Sorbents for Thermal Energy Storage. *Energy* **2019**, *167*, 889–901. [[CrossRef](#)]
360. Ellis, L.D.; Parker, S.T.; Hu, J.; Zaccarine, S.F.; Stellato, M.J.; Funke, H.H.; Sievers, C.; Pylypenko, S.; Falconer, J.L.; Medlin, J.W. Tuning Gas Adsorption Selectivity and Diffusion Rates in Zeolites with Phosphonic Acid Monolayers. *Cell Rep. Phys. Sci.* **2020**, *1*, 100036. [[CrossRef](#)]
361. Tang, X.; Liu, J.; Shang, H.; Wu, L.; Yang, J. Gas Diffusion and Adsorption Capacity Enhancement via Ultrasonic Pretreatment for Hydrothermal Synthesis of K-KFI Zeolite with Nano/Micro-Scale Crystals. *Microporous Mesoporous Mater.* **2020**, *297*, 110036. [[CrossRef](#)]
362. Zhang, K.; Jiang, H.; Qin, G. Utilization of Zeolite as a Potential Multi-Functional Proppant for CO₂ Enhanced Shale Gas Recovery and CO₂ Sequestration: A Molecular Simulation Study on the Competitive Adsorption of CH₄ and CO₂ in Zeolite and Organic Matter. *Fuel* **2019**, *249*, 119–129. [[CrossRef](#)]
363. Cui, Y.; Xing, Y.; Tian, J.; Su, W.; Sun, F.-Z.; Liu, Y. Insights into the Adsorption Performance and Separation Mechanisms for CO₂ and CO on NaX and CaA Zeolites by Experiments and Simulation. *Fuel* **2023**, *337*, 127179. [[CrossRef](#)]
364. Hong, M.; Yu, L.; Wang, Y.; Zhang, J.; Chen, Z.; Dong, L.; Zan, Q.; Li, R. Heavy Metal Adsorption with Zeolites: The Role of Hierarchical Pore Architecture. *Chem. Eng. J.* **2019**, *359*, 363–372. [[CrossRef](#)]
365. Ibrahim, H.S.; Jamil, T.S.; Hegazy, E.Z. Application of Zeolite Prepared from Egyptian Kaolin for the Removal of Heavy Metals: II. Isotherm Models. *J. Hazard. Mater.* **2010**, *182*, 842–847. [[CrossRef](#)] [[PubMed](#)]
366. Noroozi, R.; Al-Musawi, T.J.; Kazemian, H.; Kalhori, E.M.; Zarrabi, M. Removal of Cyanide Using Surface-Modified Linde Type-A Zeolite Nanoparticles as an Efficient and Eco-Friendly Material. *J. Water Process Eng.* **2018**, *21*, 44–51. [[CrossRef](#)]
367. Abdelrahman, E.A. Synthesis of Zeolite Nanostructures from Waste Aluminum Cans for Efficient Removal of Malachite Green Dye from Aqueous Media. *J. Mol. Liq.* **2018**, *253*, 72–82. [[CrossRef](#)]

Disclaimer/Publisher’s Note: The statements, opinions and data contained in all publications are solely those of the individual author(s) and contributor(s) and not of MDPI and/or the editor(s). MDPI and/or the editor(s) disclaim responsibility for any injury to people or property resulting from any ideas, methods, instructions or products referred to in the content.